Stony Brook University

Dystroglycan is a Novel and Context-Dependent Regulator of Notch in the Postnatal Subventricular Zone

A Dissertation Presented

by

Himanshu Sharma

to

The Graduate School

in Partial Fulfillment of the

Requirements

for the Degree of

Doctor of Philosophy

in

Molecular and Cellular Pharmacology

Stony Brook University

May 2017

Stony Brook University

The Graduate School

Himanshu Sharma

We, the dissertation committee for the above candidate for the

Doctor of Philosophy degree, hereby recommend

acceptance of this dissertation.

Dr. Holly Colognato – *Dissertation Advisor*
Associate Professor
Department of Pharmacological Sciences

Dr. David Talmage – *Thesis Committee Chair*
Professor
Department of Pharmacological Sciences

Dr. Ken-Ichi Takemaru
Associate Professor
Department of Pharmacological Sciences

Dr. Dennis Choi
Professor and Chair
Department of Neurology

This dissertation is accepted by the Graduate School

Charles Taber

Dean of the Graduate School

Abstract of the Dissertation

Dystroglycan is a Novel and Context-Dependent Regulator of Notch in the Postnatal Subventricular Zone

by

Himanshu Sharma

Doctor of Philosophy

in

Molecular and Cellular Pharmacology

Stony Brook University

2017

While the importance of the subventricular zone (SVZ) in brain development and homeostasis has become more well appreciated over the last few decades, many of the mechanisms regulating SVZ development remain unclear. In particular, the role of extracellular matrix (ECM)-mediated signals in shaping the development and function of the postnatal SVZ remain poorly understood, despite the recognized role of ECM in other stem cell niches. We now report that during the first weeks of postnatal development, ECM is reorganized into laminin-rich "hubs" at the interface between neural stem cells and ependymal cells at the ventricular surface. This ECM is of predominantly ependymal cell origin, and the process of hub assembly and organization is regulated by the ECM receptor dystroglycan. Laminin and dystroglycan function in a reciprocal axis wherein dystroglycan, required for appropriate surface laminin assembly, also transmits laminin-mediated signals into the cell. Dystroglycan in the postnatal SVZ helps establish proper niche organization and function. Either genetic removal of dystroglycan or blockade of dystroglycan binding engenders several defects in neural stem cell function in the perinatal SVZ. These include: (i) dysregulation of radial glial proliferation and differentiation, delaying the emergence of progeny ependymal cells that serve as niche support cells in the adult SVZ; (ii) perturbations in ependymal cell polarity and niche organization into pinwheel-like structures; (iii) increased gliogenesis with increases in both the production and proliferation of oligodendrocyte progenitors; and (iv) delayed maturation of oligodendrocyte precursor cells. Furthermore, dystroglycan is identified as a novel regulator of notch signaling, suppressing notch signaling in neural stem cells, ependymal cells, and oligodendrocyte progenitor cells. Finally, we find that dystroglycan appears to play distinct, and at times, opposing roles in neural stem cells and ependymal cells to maintain SVZ neural stem cell homeostasis. In particular, ependymal cell dystroglycan plays both cell-autonomous and non-autonomous roles in regulating SVZ proliferation and the morphology of neural stem cells. These phenotypes occur in spatially distinct domains of the SVZ, highlighting the functional heterogeneity of ECM in the SVZ.

This dissertation is dedicated to my parents, whose constant love, support, and sacrifice have made this work possible

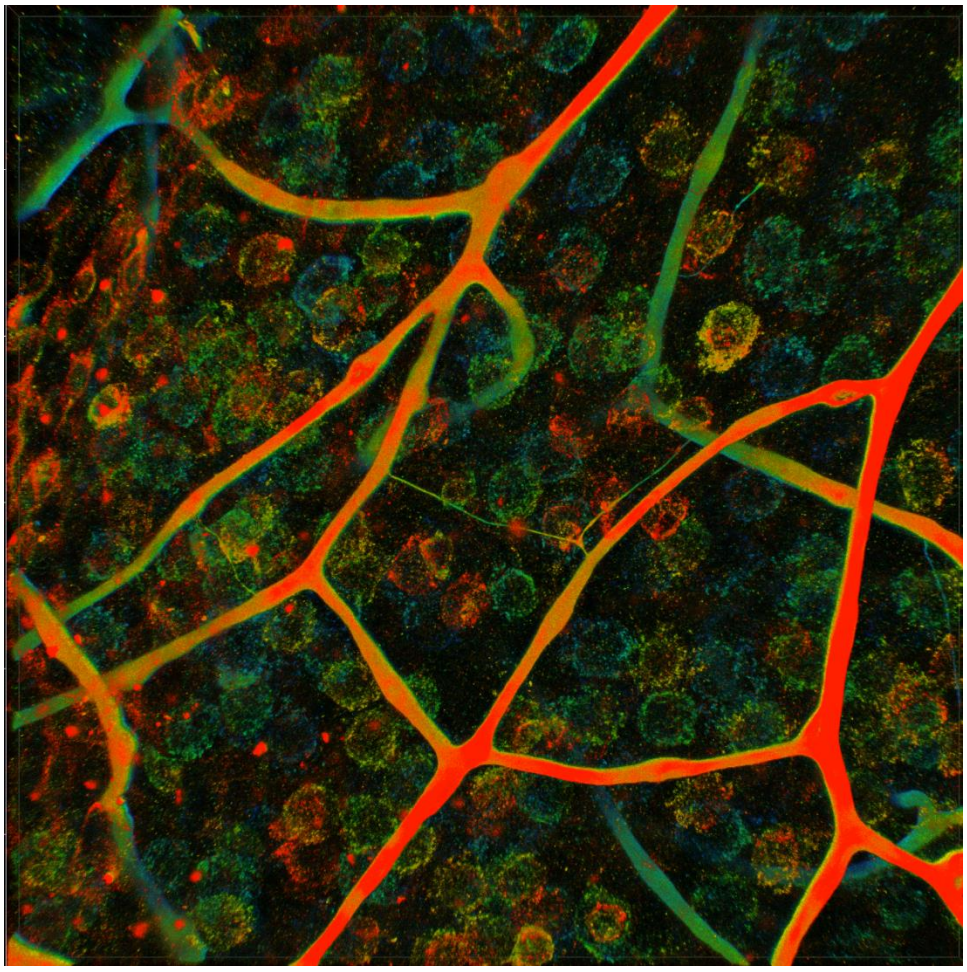

Contents

List of Figures

List of Abbreviations

3D	3 Dimensional
AKT	Protein Kinase B
ANOVA	Analysis of Variance
BB	Basal Body
BLBP	Brain Lipid-Binding Protein
BMP	Bone Morphogenic Protein
CC1	Adenomatous Polyposis Coli
CD (number)	Cluster of Differentiation (number)
CDK	Cyclin-Dependent Kinase
cKO	Conditional Knockout
c-MYB	Myb (myeloblastosis) Proto-Oncogene Protein C
CNP	2',3'-Cyclic-Nucleotide 3'-phosphodiesterase
CNS	Central Nervous System
CRE	Causes Recombination
CSF	Cerebrospinal Fluid
CT	Threshold Cycle
CXCR	CXC Chemokine Receptor
DAG	Dystroglycan
DAPT	N-[N-(3,5-Difluorophenacetyl)-L-alanyl]-S-phenylglycine t-butyl ester
DGC	Dystrophin-Glycoprotein Complex
DNA	Deoxyribonucleic Acid
E (number)	Embryonic Day (number)
EC	Ependymal Cell
ECM	Extracellular Matrix
EGF	Epidermal Growth Factor
EGFR	Epidermal Growth Factor Rceptor
ERK	Extracellular Signal-Regulated Kinase
ERM	Ezrin-Radexin-Moesin
F Actin	Filamentous Actin
FAK	Focal Adhesion Kinase
FGF	Fibroblast Growth Factor
FLOX	Flanked By LoxP Sites
FOXJ1	Forkhead Box J1
FOXO	Forkhead Box O
G Actin	Globular Actin
GC1	GemC1/Lynkeas
GFP	Green Fluorescent Protein
GFAP	Glial Fibrillary Acidic Protein
GLAST	Glutamatergic Astrocyte-Specific Transporter
GLI	Glioma-Associated Oncogene
GM-CSF	Granulocyte-Macrophage Colony Stimulating Factor
GRB2	Growth Factor Receptor-Bound Protein 2
HSPG	Heparan Sulfate Proteoglycan
IGF1	Insulin-Like Growth Factor 1

IgM	Immunoglobulin M
IHC	Immunohistochemistry
IL	Interleukin
IPC	Intermediate Progenitor Cell
kDa	Kilodalton
KIR	Inwardly Rectifying Potassium Channel
MAML	Mastermind-Like
MAPK	Mitogen-Activated Protein Kinase
MASH1	Achaete-Scute Homolog 1
MBP	Myelin Basic Protein
MCI	Multicillin
MDC1A	Merosin-Deficient Congenital Musclar Dystrophy Autosomal Recessive
MEK1	Dual Specificity Mitogen-Activated Protein Kinase Kinase 1
mRNA	Messenger Ribonucleic Acid
NEC	Neuroepithelial Cell
NG2	Neural/Glial Antigen 2
NICD	Notch Intracellular Domain
NOS	Nitric Oxide Synthase
NPC	Neural Progenitor Cell
NSC	Neural Stem Cell
oIPC	Oligodendrogenic Intermediate Progenitor Cell
OL	Oligodendrocyte
OPC	Oligodendrocyte Progenitor Cell
P (number)	Postnatal Day (number) – EXCEPT “P27”
P27	Cyclin-Dependent Kinase Inhibitor 1B
PAX6	Paired Box Protein 6
PCNA	Proliferating Cell Nuclear Antigen
PDGFRα	Platelet-Derived Growth Factor Receptor α
PDL	Poly-D-Lysine
PI3K	Phosphatidylinositol-4,5-bisphosphate 3-kinase
PNS	Peripheral Nervous System
qRT-PCR	Quantitative Reverse Transcription Polymerase Chain Reaction
RAPSYN	Receptor-Associated Protein of the Synapse
RBPJ	Recombining Binding Protein Suppressor of Hairless
RG(C)	Radial Glia(l Cell)
RhoA	Ras Homolog Family Member A
ROCK	Rho-Associated Coiled-Coiled Containing Protein Kinase
SAHM1	Stapled α-Helical Peptide Derived From MAML1
SDF1	Stromal-Derived Factor 1
SH2	Src Homology 2
SH3	Src Homology 3
SHH	Sonic Hedgehog
siRNA	Small Interfering Ribonucleic Acid
SOX	(Sex Determining Region Y)-box
SRF	Serum Response Factor
SVZ	Subventricular Zone

TAP	Transit-Amplifying Progenitor
TGF	Transforming Growth Factor
V/SVZ	Ventricular-Subventricular Zone
VZ	Ventricular Zone
WNT	Wingless-Related Integration Site
WT	Wild-type
ZO-1	Zonula Occludens-1

Acknowledgments

I must first and foremost, acknowledge the incredible support and guidance of my mentor and PI Dr. Colognato. I could not have asked for, nor imagined, a better mentor to guide me through my doctoral work. She not only one of the finest minds I have ever had the honor of coming across, but her patience, kindness, and willingness to allow me to pursue my own path towards becoming a scientist, (with all the vacations and reading time that that entailed!) have allowed me to grow as an independent investigator and as a person over the last four years. Her scientific rigor and sense of integrity will be a guide for me throughout my life.

I must also thank Dr. McClenahan, another brilliant mentor who has played an outsized role in my scientific life. She has laid the groundwork for my dissertation work, in a very real sense she has taught me how to do science, and she has helped me maintain my passion for science even through some of the most difficult and frustrating periods of my life. I would not be the scientist I am today without her sincere and unceasing support.

In the same vein, my thesis committee members have all served as incredible role models and guides. Dr. Talmage has shown me not only what kind of scientific mind I want to develop, but also the sort of person I hope to be as a member of the scientific and larger community. Dr. Takemaru has demonstrated the critical role of following my science wherever it leads as well as the power of taking a closer look at the data right in front of me. Dr. Choi has not only been a tremendous role model as to what a well-trained physician-scientist can accomplish, but also has shown me new ways to approach scientific problems in pragmatic and translatable contexts.

I have been absolutely blessed to be a part of the Pharmacology program, an incredible community that has provided the framework for my education as a scientist. Dr. Garcia-Diaz, Dr. Tsirka, and Ms. Hernandez in particular have been a tremendous source of support and guidance. Throughout my time here, I have had the pleasure of getting to know them not only as consummate professionals, but also as friends. It is my honor to now be able to call them my colleagues. The students in Pharmacology, and throughout Stony Brook have been my constant companions through this process, and through, as with the departmental staff and faculty, those who have had a lasting impact on me are too numerous to name, I would like to thank in particular, Dr. Leiton and Dr. Siller for being a surrogate family to me during my dissertation work. I will never be able to adequately thank you for all you have done for me.

The Stony Brook MSTP has been the other program whose support I am tremendously indebted to. Dr. Frohman, Dr. Seeliger, and Ms. Allen have worked tirelessly to create the perfect environment to foster my, and countless others' development as physician-scientists. I am also grateful for the support of and joy of knowing my MSTP classmates who have provided the light throughout, not simply at the end of, the tunnel.

Finally, my most profound gratitude is to my parents. Everything I have, and will accomplish has been by your grace and love. I hope that I have and continue to make you proud.

Curriculum Vitae

Education

2011 – Present	Stony Brook University School of Medicine, Stony Brook NY Medical Scientist Training (MD/PhD) Program PhD Candidate, Lab of Dr. Holly Colognato Department of Molecular and Cellular Pharmacology Step I: 257
2007 – 2011	Case Western Reserve University, Cleveland OH B.S. in Biology GPA: 3.77; MCAT: 40

Research Experience

Stony Brook University - Stony Brook, NY

Doctoral Candidate *07/13 – Present*

Mentor: **Holly Colognato, PhD;** Associate Professor – Department of Pharmacology

- My current research focuses on understanding the role of the extracellular matrix (ECM) receptor dystroglycan in the developing subventricular zone of the brain. I use *in vitro* and *in vivo* techniques to study the effects of modulating dystroglycan function on ECM formation, cellular architecture and polarity, signaling cascades, and proliferation and differentiation of neural stem cells.

Rotation Student *06/12 – 09/12*

Mentor: **Michael Frohman**, **MD, PhD;** Professor and Chair - Department of Pharmacology

- Examined the effects of mitochondrial phospholipase D on mitochondrial shape, size, and recruitment of p-body associated proteins
- Conducted small molecule inhibitor screen for mitoPLD
- Performed plasmid preps, transfections, confocal microscopy, bacterial culture

Rotation Student *07/11 – 09/11*

Mentor: **Holly Colognato**, **PhD;** Associate Professor - Department of Pharmacology

- Studied the role of matrix metalloproteinases 7, 9, and 14 in the developing and adult SVZ
- Examined expression patterns of MMPs in the SVZ and cleavage of laminin substrates
- Conducted western blotting, RT-PCR, dissections, and developed dissection protocols

Case Western Reserve University – Cleveland, OH

Lab Assistant *01/09 – 05/11*

Mentor: **Jerry Silver, PhD;** Professor – Department of Neuroscience

- Studied spinal cord injury repair using enzymatic treatment and peripheral nerve grafts to overcome the inhibitory environment of the glial scar.
- Performed immunohistochemistry, tissue preparation, perfusions, dissections, suturing

- Involved with experimental design and conducted my own project on determination of cellular changes in the rat spinal cord after injury.

Weill Cornell Medical College – New York City, NY

Lab Assistant *05/05 – 07/05; 05/08 – 08/08*

Mentor: **Brij Saxena, PhD;** Professor – Department of Obstetrics and Gynecology

- Worked on chemical synthesis of a novel anti-cancer compound in treating xeongrafted rats using techniques such as TLC, GC, and HPLC
- Helped determine effective concentrations of an anti-HIV compound in a special formulation for delayed drug release in a contraceptive ring.

Activities and Positions

Stony Brook University – Stony Brook, NY

Course Director, Lecturer: Selected Topics in Pharmacology (BCP 480)	2016 – Present
Translational Pillars Committee (School of Medicine)	2016 – Present
NIH Graduate Fair MSTP Recruitment Representative	2015 – Present
Guest Lecturer: Principles of Pharmacology (BCP 401/501)	2014 – Present
Stony Brook Hypertension Research Project	2014 – Present
Curriculum Committee Student Representative (School of Medicine)	2012 – Present
Student Finance Committee (School of Medicine)	2011 – 2014
Teaching Assistant: Medical Microbiology	2014
SBHome Chart Review Quality Improvement Project	2014
Department of Mathematics Medical Education Consultant	2014
MSTP Admissions Committee	2012 – 2013
Science Mentor (Academy of Inquiry)	2012 – 2013

Academic and Professional Honors

Van Der Kloot Award for Excellence in Research	2016
Discussion Leader, Gordon Research Seminar on Neural Development	2016
GSO Distinguished Travel Award	2016
Provost's Graduate Student Lecture	2016
PhRMA Foundation Predoctoral Fellowship	2015
Stony Brook Pharmacology Best Snapshot Award	2015
BioTechne ISSCR Travel Award	2015
Tufts Idea Competition, Winner	2014
AAAS/Science Program for Excellence in Science	2014 - 2016
President, Student Finance Committee	2012 - 2013
Phi Kappa Theta Academic Excellence Award	2010
Dean's High Honors	2009 - 2011

Memberships in Professional Societies

American Association for the Advancement of Science
American Medical Association
American Medical Student Association
New York Academy of Sciences
International Society for Stem Cell Research

Publications and Presentations

Research Articles

McClenahan FK*, **Sharma H***, Shan X, Eyermann C, Colognato H. Dystroglycan Suppresses Notch to Regulate Stem Cell Niche Structure and Function in the Developing Postnatal Subventricular Zone. Dev Cell August 2016.
*Equal Contributions

Sharma H, Desu H, Colognato H. Ependymal Cell Dystroglycan Regulates Neural Stem Cell and Progenitor Function in Spatially Distinct Domains of the Subventricular Zone. Manuscript in Preparation.

Siller SS, **Sharma H,** Li S, Holdener BC, Holtzman MJ, Winuthayanon W, Colognato H, Li F, Takemaru K. The Distal Appendage Protein CEP164 Coordinates Multiple Steps of Airway Multicilia Formation. Manuscript in Preparation.

Nadesakumaran K, Barkan A, Hall K, Karas J, **Sharma H**, Brathwaite CEM. The Impact of Super Morbid Obesity (preoperative BMI ≥50) on Short Term Postoperative Complications after Bariatric Surgery. Manuscript in Preparation

Reviews and Commentary

Sharma H, Colognato H. An Extracellular Matrix Axis in SVZ Development and Function. Neurogenesis. In Revisions.

Sharma H, Alilain WJ, Sadhu A, Silver J. Treatments to restore respiratory function after spinal cord injury and their implications for regeneration, plasticity, and adaptation. J Experimental Neurology May 2012.

Textbook Chapters

Sharma H, Lang B, Silver J. Effects of the glial scar and extracellular matrix molecules on axon regeneration. In Textbook of Neural Repair and Rehabilitation. Edited by Selzer M, Clarke S, Cohen L, Kwakkel G, and Miller, R. 2014; Chapter 27

Selected Abstracts and Presentations

Sharma H, Desu H, Choi S, Colognato H. Ependymal Cell Dystroglycan Regulates Neural Stem Cell and Progenitor Function in Spatially Distinct Domains of the Subventricular Zone. New York Stem Cell Institute Annual Meeting. 2017

Sharma H, McClenahan FK, Colognato H. A Dystroglycan-Laminin Axis Regulates SVZ Development via Modulation of Notch Signaling. Gordon Research Conference on Neural Development. 2016

Sharma H, McClenahan FK, Colognato H. Dystroglycan: A Novel Notch Regulator in Neural Stem Cell Niche Development and Function. New York Stem Cell Institute Annual Meeting. 2016

Sharma H, Colognato H. Ependymal Cell Dystroglycan Regulates SVZ Neural Stem Cell Niche Development and Function. AAP/ASCI/APSA Joint Annual Meeting. 2016

Sharma H, McClenahan FK, Colognato H. Dystroglycan Regulates the Development, Structure, and Function of the SVZ Neural Stem Cell Niche. International Society for Stem Cell Research Annual Meeting. 2015

Sharma OP, **Sharma H**. Diabetes and Fertility: An Overview. Indian Society for the Study of Reproduction and Fertility Annual Meeting. 2017

Khaing ZZ, Alilain W, **Sharma H**, Silver J, Schmidt JE. Optimized acellular grafts support functional recovery after cervical spinal cord injury. Society for Neuroscience Annual Meeting. 2011

Chapter 1: General Introduction

Stem Cells

Stem cells are undifferentiated cells with the ability to divide and generate two types of progeny cell. They can generate daughter cells that will differentiate into more specialized cell types and/or renew their own population by generating more stem cells identical to themselves in a process known as self-renewal. [1] The ontogeny of stem cells is defined by their 'potency', or ability to generate a variety of different cell types. The earliest stem cell, the fertilized egg, is totipotent, and has the ability to give rise to all embryonic and extra-embryonic tissues. As stem cells progress through development, however, they become more lineage-restricted. Embryonic cells deriving from the blastocyst stage and earlier are pluripotent, meaning that they can produce all differentiated cell types in the body. Fetal and adult stem cells can generate fewer potential lineages, and are classified as either multipotent or unipotent, in the latter case, generating only two cell types – a single differentiated cell type and another unipotent stem cell.

From this definition, it is evident that stem cells fulfill two fundamental mandates – they generate progeny cells to develop or regenerate tissues, and they maintain or expand their own population. By the judicious regulation of these two behaviors, development, homeostasis, and regeneration of cells, tissues, and organs can be maintained throughout life. [2] In order to balance the progeny population appropriately, stem cells have developed the ability to alternate between two different methods of cell division, which can be enacted depending on the needs of the tissue. The first type of division, generating a differentiated cell and another stem cell is termed asymmetric division and gives rise to daughter cells while maintaining the stem cell population. This type of division is often the predominant type of division during tissue homeostasis and later stages of development of a tissue or organ. The second type, termed

symmetric division, usually occurs when the stem cell generates two identical daughter stem cells, effectively doubling the stem cell population. This occurs at a much higher rate during early development, injury, and certain types of disease. [3] There exist variations on these themes, such as division leading to daughter cells with the ability to rapidly divide a fixed number of times to expand their number but are nonetheless lineage-restricted, and whose progeny cells will generate a specific cell type. These rapidly dividing cells are sometimes termed ‘intermediate progenitor cells’ or ‘transit-amplifying cells’. In another variation, symmetric division may also lead to the generation of two differentiated daughter cells, which is also physiological, though does not constitute a significant proportion of stem cell divisions, as it eventually leads to exhaustion of the stem cell pool.

While stem cells have the ability to divide symmetrically or asymmetrically, they may also remain in a state of stasis for extended periods of time, during which they do not divide. This actively maintained, reversible state of non-proliferation is known as quiescence. [4] The reversibility of this state (and concomitant differences in signaling cascades, cellular physiology, and responsiveness to external signals) distinguishes quiescence from irreversible cell-cycle exit, as is seen with terminally differentiated and senescent cells. [5] Originally discovered as a new form of G0 phase that did not constitute an irreversible cell-cycle exit, quiescence is only accessible by cells in early G1 before a restriction point termed the R-point. [6-9] Quiescence can be maintained for prolonged periods of time, and is extremely important for the appropriate balance between stem and progenitor populations. Indeed, dysregulation of quiescence can lead to over-proliferation and stem cell depletion. [10] The scientific consensus on the role of quiescence has shifted in recent decades – viewed less as a default state entered upon nutrient depletion or contact inhibition, it is now widely believed to function as a mechanism allowing

stem cells to persist in the face of metabolic stresses as well as maintain genomic integrity over the lifetime of the organism. [4] Quiescent stem cells employ a host of strategies to achieve these goals, including avoiding reactive oxygen species-mediated damage through FOXO family protein-mediated pathways, [11-13] and adapting their cellular physiology in response to hypoxic metabolic stresses through a variety of response mechanisms. [14, 15] These mechanisms are an integral component of quiescence, and their continued function is a requirement for the maintenance of quiescence. [14, 16] Interestingly, these mechanisms are so potent in their ability to downregulate metabolism and adapt to long-term stasis that viable skeletal muscle stem cells have even been isolated from postmortem tissue. [17]

Thus, the healthy stem cell population as a whole exhibits three general behavioral phenotypes listed in order of their relative predominance during the developmental timeline: symmetric division, asymmetric division, and quiescence. Unlike invertebrate germ stem cells, which constantly cycle unless nutritionally challenged [18], and embryonic stem cells which are often relatively proliferative, adult mammalian stem cells are usually found in a quiescent state, though sometimes coexisting with actively cycling stem cells. [19] The mechanisms by which stem cells decide upon and implement symmetric and asymmetric divisions or enter quiescence are rather complex, multifaceted, and not yet well understood. A complete treatment of the current state of knowledge on this topic is beyond the scope of this introduction. However, several general factors germane to this work have been recognized thus far and will be briefly introduced.

Much of the information gleaned on the mechanisms by which stem cells decide to enter quiescence has been derived in a roundabout fashion. First, quiescent stem cell populations have recently been identified and defined in various tissues through a variety of continually evolving

methods. These methods include cellular and morphological characteristics [20, 21], label retention [22-26], and lineage tracing [27-30]. Next, molecular profiles of these prospectively purified cells are characterized both at the transcriptional [21, 31, 32] and epigenetic levels. [33] Not only have these studies changed our understanding of organogenesis, defined stem cell populations and niches, and revealed the interconvertibility between stem cell activation states in health and disease, they have also identified putative molecular regulators of quiescence. Further studies aimed at validating candidate pathways thus identified are beginning to reveal a bevy of intracellular quiescence regulators including p53 [34], cyclin-dependent kinase inhibitors (CDKIs) [35, 36], Notch [37-39], and many more. The identity of these and other effectors provide clues as to the signals that help the cell decide whether to enter or exit the cell cycle.

One obvious intracellular signal suggested by the involvement of effectors like p53 and cell-cycle checkpoint regulators, for example, is DNA damage, which plays a critical role in determining whether a stem cell will re-enter the cell cycle. [40-42] However, at the population level, extracellular signals from the systemic and local environments play the dominant role in determining cell-cycle rate and quiescence. In Drosophila, for example, stem cell proliferation rates can be modulated four-fold, simply by regulating the proportion of protein in the diet, which controls stem cell proliferation through insulin signaling. [43] In the rodent brain, ischemic injury distant to neural stem cells can also induce proliferation in these cells leading to progeny neurons through factors like insulin-like growth factor-1 (IGF-1) and estradiol. [44-46] On a local level, changes in cell-cell signaling and other factors in the environment are critical to regulating stem cell activation and behavior. In the intestine, niche support cells known as Paneth cells physically signal to neighboring stem cells through a variety of means including Wnt, Notch, Transforming Growth Factor (TGF), and Epidermal Growth Factor (EGF) signaling. [47,

48] Indeed, adhesion [49], secreted factors [50], biophysical properties [51], local oxygen tension [52], and extracellular matrix-mediated signals [53] are only a few of the many environmental factors that are now recognized as regulating the activation, behavior, and fate of stem cells.

It has therefore become clear that for the coordinated generation, homeostasis, and regeneration of tissue, the stem cells' ability to properly integrate a wide variety of environmental cues is absolutely critical. This line of reasoning has led to a closer examination of the anatomical location and environment of stem cells to understand their role in physiology, pathology, and harness these findings in biotechnological pursuits.

Neural Stem Cells – A Historical Perspective

One of the most recently discovered and characterized stem cell populations in the adult vertebrate is the neural stem cell (NSC). By one well-accepted definition, neural stem cells must fulfill three functional criteria in order to be classified as such. First, an NSC must be multipotent – it must have the potential to differentiate into fully functional and mature cells of any of three general neural cell lineages: (i) neuronal (of all classes), (ii) astrocytic, and (iii) oligodendroglial. Second, neural stem cells must have the ability to populate appropriate and permissive CNS regions during development, and/or to repopulate those regions after injury or depopulation. Finally, NSCs must be able to self-renew. In other words, in addition to generating progeny as defined in the first two criteria, they must also be able to maintain their own population as needed by producing daughter cells that remain multipotent and capable of self-renewal. [54]

Almost tautologically therefore, the embryonic neural tissue and developing brain contain neural stem cells that give rise to the cells that will generate the adult brain. The specter of limited to no functional recovery after CNS injury throughout most of the lifespan, however, has

driven inquiry into the *postnatal* maintenance and function of NSCs. In fact, how long embryonic or a similar population of neural progenitors persists in the adult brain and the precise nature of such populations of cells remains a motivating question in neuroscience and stem cell biology to this day. The question of adult repair in the brain has, mirroring the field in general, focused on the ability to generate new neurons, and thus the story of the discovery and characterization of adult NSCs has, until very recently, been the story of the search for the generation of neurons in the postnatal mammalian brain.

For at least 120 years, it has been known (though, for quite some time not well appreciated) that mitosis continues in the CNS of newborn vertebrates such as dogs, rabbits, and rats for at least a few days after birth in both the spinal cord and brain. [55, 56] By the early twentieth century, a more systematic cytological study demonstrated that mitoses in the rat spinal cord and brain parenchyma continue and even increase briefly through the postnatal period, but cease for the most part by the 3rd week of postnatal life (with slight regional variations). [57] However, it was also noted and confirmed over the next several decades that mitosis continues for significantly longer periods of time along the lateral wall of the lateral ventricle [57, 58] – a region known today as the ventricular/subventricular zone (V/SVZ). For the next half-century, however, as further studies failed to identify mitotic neurons in the adult CNS of most higher vertebrates, it was believed that after the generation of the population of post-mitotic neurons during early embryonic development, neurogenesis totally subsided in the adult brain, and the abnormally high mitotic rate in the walls of the lateral ventricle remained understudied, in part due to technical limitations – scientists were unable to follow what happened to these dividing cells over time.

In fact, the failure to identify actively dividing neurons by microscopic techniques seemingly closed the door on hopes of endogenous neurogenesis as a factor in repair after CNS injury. In 1957, however, the technical advancement in radioactive labelling of replicating DNA with tritium-labelled thymidine (which incidentally provided the first evidence for the semi-conservative nature of DNA replication, and laid the ground for the "immortal strand" hypothesis of stem cell replication) [59] enabled neuroscientists to follow the fate of dividing cells in the brain. In a series of seminal reports in the 1960s, Altman and Das used this thymidine-H^3 labelling technique to search for populations of undifferentiated precursor cells that might give rise to new neurons and glia. They found not only evidence for neurogenesis and gliogenesis in the neonatal and adult rat, but elucidated that the SVZ and dentate gyrus of the hippocampus harbor a germinal population of dividing cells, and that cells derived from the SVZ likely migrate to the olfactory bulb and differentiate into neurons there. [60-62] Surprisingly, while these findings should have overturned the paradigm of "no new neurons" in the adult mammalian brain, the prevailing view in the field took some time to significantly change. For many years, the production of new neurons in the adult was still believed to be relatively insignificant after the periods of embryogenesis and the immediate perinatal period [63] even as large numbers of neurons were shown to arise from ventricular zone cells and migrate to other regions of the brain in new species such as the canary [64]**,** and functionally integrate into neural circuitry [65]. Nonetheless, evidence for adult neurogenesis continued to mount through the 70s and 80s, with adult neurogenesis reported across several mammalian species. [66-70]

A major step forward in the identification of cells derived from the neuroepithelium as stem cells came in 1989, when Sally Temple isolated individual blast cells from the septal tissue of E13.5 – E14.5 rat forebrains and allowed them to proliferate i*n vitro.* Three different clonal

populations arise from these cells. The first undergoes limited divisions and differentiate into a single cell type (i.e. glial or neuronal). The second also undergoes few mitotic divisions, but differentiates into both glial and neuronal cell types, indicating multipotency. The third clonal group gave rise to mixed cell types and also a small population of cells that resembled the initial blast cell even after 10 days in culture, indicating a potential self-renewal capability. [71] Three years later, Reynolds and Weiss succeeding in isolating similar stem cells from the *adult* striatum (the region abutting and, in this case, including the SVZ) which could be coaxed into proliferating *in vitro* by the addition of EGF and which could differentiate into neurons or astrocytes. [72] These discoveries spurred a resurgence of interest in adult neurogenesis and stem cells, and it was soon established that a population of neural stem cells reside adjacent to the lateral ventricles (and in the dentate gyrus), subject to both intrinsic and environmental control. Further, these stem cells generate cells that migrate long distances throughout the brain and differentiate into functional neurons and glia at their destinations. [73, 74] In particular, grafted cells from adult donor SVZ explants were able to migrate from the SVZ of recipient mice to the olfactory bulb and differentiate into neurons, [73] which along with the confirmation of adult neurogenesis in the human, [75] elicited enthusiasm for the potential for translational therapies for repairing brain injury in the adult.

One key point that the century-long search for adult neural stem cells illustrates is that while NSCs are highly proliferative during development, in adulthood, when they might be harnessed for repair, NSCs are rare and/or almost entirely quiescent. It wasn't obvious, however, whether the lack of stem cell proliferation in adulthood is due to a loss of NSCs, an intrinsic inability of adult NSCs to proliferate, environmental cues maintaining quiescence and/or senescence, or some combination of the three. Interestingly, while loss of NSCs and cell-intrinsic

factors play a role in the reduction in proliferation in the adult brain, recent work has demonstrated that NSCs that exist in the adult SVZ do continue to maintain a robust ability to proliferate, self-renew, and differentiate *in vitro* and the *in vivo* environment of young mice. [76, 77] Therefore, a significant portion of the fact that neurogenesis in the adult is limited is likely due to environmental regulation of NSCs by factors and cues present *in vivo*. In order to understand what these factors may be, we must examine the microenvironment in which they are found in greater detail.

Stem Cell Niches

In the adult, stem cells are found in specialized microenvironments, termed "niches". This concept was first proposed almost forty years ago by Schofield, in reference to the hematopoietic stem cell niche. He stated:

"[A] hypothesis is proposed in which the stem cell is seen in association with other cells which determine its behaviour. It becomes essentially a fixed tissue cell. Its maturation is prevented and, as a result its continued proliferation as a stem cell is assured. Its progeny, unless they can occupy a similar stem cell 'niche', are first generation colony-forming cells, which proliferate and mature to acquire a high probability of differentiation…" [78]

This definition, over the last several decades has expanded somewhat to include a plethora of factors beyond "other cells" that determine the behavior of the stem cell, but otherwise remains a generally accurate assessment of the prevailing opinion of stem cell niches. A niche has both a specific anatomical location, as well as functional aspects that support and maintain the stem cells it houses as true stem cells. The proper functioning of these niches is critical for the development and maintenance of tissues (e.g. generation of blood during

embryogenesis by the yolk sac, liver, spleen, and bone marrow and the maintenance of blood by bone marrow-localized hematopoietic stem cells), as well as their regeneration (e.g. regeneration of the oligodendrocyte population during demyelinating disease).

Stem cell niches provide an intricately crafted environment that not only regulates endogenous stem cell function, but is necessary for the health and function of these stem cells. Some of these factors include local support cells, physical support and signals, access to local and systemic factors, and extracellular matrix.

Most stem cell niches contain a variety of resident niche "support" cells that create, modify, and maintain the environment along with supporting and signaling to the stem cells. Each niche has a different heterologous set of cell types that work together coordinately create a functional microenvironment, and in most cases, these niche resident cells serve dual functions, contributing to normal physiology as well as signaling to the stem cells. The hematopoietic stem cell niche is one of the best characterized microenvironments in this regard. Immune cells localized to this niche, for example, perform many functions. Regulatory T cells provide active immunosuppression in order to provide stem cells with a relatively immune-privileged site [79], while macrophages maintain other niche support cells and help retain stem cells in the niche, preventing their egress into the circulation. [80] Sympathetic neurons signal to other niche cells to help maintain the niche as well as regulate stem cell mobilization. [81] Osteoblasts [82], vascular cells [83, 84], and progeny cell types such as megakaryocytes [85] are examples of other resident niche cells that work together to maintain the appropriate stem cell pool size, location, division rate, and lineage commitment.

As suggested by the importance of osteoblasts and osteoclasts in regulating the hematopoietic stem cell niche, the physical properties of the niche are also very important in directing stem cell behavior. Some of these effects can be best demonstrated by *in vitro* models showing vastly differing stem behaviors simply by varying the biophysical properties of their substrate. For example, hematopoietic stem cells will more than double their population when grown on more elastic substrates, and respond more robustly to cytokines in this environment. [86] Muscle stem cells also respond much more robustly when grown on substrates that mimic muscle elasticity, and in fact, require substrate of the appropriate elasticity during *in vitro* expansion for proper *in vivo* engraftment. [87] Factors such as sheer stress from blood flow, and, at the single-cell level, contractility mediated by non-muscle myosin II, regulate proliferation and importantly, the balance between symmetric and asymmetric divisions in hematopoietic stem cells. [88, 89] Physical forces and shape in general are such critical factors for stem cells that they can even direct lineage commitment. Mesenchymal stem cells allowed to adhere and spread *in vitro* will become bone, while unspread cells (controlled through micropatterning of substrate) differentiate instead into adipocytes, under the guidance of a RhoA-ROCK-dependent mechanism. [90] Indeed, even altering the geometric shape of the substrate (e.g. growth in lines, circles, with corners, etc.) will alter the fate and ontogeny of mesenchymal stem cells, which can through still unknown mechanisms, determine their distance from edges. [91] Niche physical properties including fluid flow, physical stresses, elasticity, as well as 2- and 3-D organization [92], are therefore all key factors in determining when and how stem cells divide as well as what their progeny cells will be. One of the most important environmental determinants of the physical properties of a niche is a network of proteins and molecules that surround the cells known as the extracellular matrix (ECM).

The Extracellular Matrix

The extracellular matrix is a network of proteins and associated molecules that bind to cells and each other to provide structural support as well as signals to associated cells and tissues. Believed to have originally arisen with the advent of multicellularity, the ECM has evolved into a complex and dynamic network that varies tremendously not only between organisms, but within tissues in a single organism as well. Regulation of its production, remodeling, processing, and degradation is required for normal development, homeostasis, and repair, while dysregulation of the ECM can lead to injury, disease, and death. (Reviewed in [93-97] The ECM is usually found either in a sheet-like form known as a basement membrane (BM) (also known as a basal lamina (BL)), or as interstitial matrix. Basal lamina are often found as sheets that separate and support tissue compartments, and as such, line muscle, fat, epithelial, and endothelial cells among others.

The core constituents of the basal lamina include laminin, type IV collagen, nidogen, and heparan sulfate proteoglycans (HSPG). [98, 99] Every basal lamina consists of at least one laminin, one nidogen, one type IV collagen, and the HSPGs perlecan or agrin. Among these, laminin is the only ECM molecule required for initial assembly of the BL. Basal lamina are initially self-assembled on the surfaces of certain cell types through the interaction between laminin LG domains and their potential binding partners: sulfated glycolipids, integrins, dystroglycan, and heparan sulfates. Only upon initial laminin anchoring do the other components of the basal lamina bind to the laminin scaffold and to each other. [100-104] Cells control the assembly and organization of these components on their surface through a variety of means

including the expression, regulation, and localization of receptors, enzymatic treatment of basal lamina components, and through cytoskeletal dynamics. [105, 106]

Laminins themselves are a family of heterotrimeric proteins that consist of one each of an α, β, and γ chain. Vertebrates are known to express five α, three β, and three γ chains. By combining these chain in different permutations, a wide variety of laminins with unique properties can be generated. These heterotrimers are named by listing the isoform number of each chain in order (e.g. laminin-111 is composed of the α1, β1 and γ1 chains). [107] Within developing organisms, laminin isoforms are expressed in a tissue-specific as well as developmental stage-specific manner. Indeed, varying substrate laminin isoforms for pluripotent stem cells can even help specify and promote lineage progression in a stage-specific manner across different tissue types. [108, 109] Interestingly, *in vitro* work has demonstrated that laminins are some of the most permissive substrates for the support and growth of neural progenitor cells as well as NSCs and other stem cells. [110]

The importance of the role of specific ECM molecules in regulating stem cells was recognized almost thirty years ago, as ECM was shown to promote stem cell function and adsorb granulocyte-macrophage colony stimulating factor (GM-CSF) and interleukin-3 (IL-3) in the hematopoietic stem cell niche. [111, 112] Clearly more than simply a support structure for cells to tether them to their environment, the ECM signals to stem and niche cells in a variety of ways to regulate niche function. In fact, the signals sent to developing cells through the ECM are so important that functional tissues and organs such as the heart and liver have now been reported to be reconstructed by decellularizing cadaveric organs or artificially 3D printing ECM to obtain an ECM scaffold and then re-seeding these scaffolds with appropriate cell types. [113-116]

As the field of niche ECM has expanded greatly in the last several decades resulting in abundance of information on the importance of ECM on stem cell function, only a few examples of how the ECM can regulate stem cells are discussed here. As mentioned above, the properties of the ECM modulate the stiffness and elasticity of local environment. The specific composition of ECM also signals to receptors directly on the cells, triggering intracellular signal cascades such as the PI3K-Akt and MEK1-ERK pathways, which are known to determine stem cell behavior. [117] Additionally, the ECM can also bind to, and present soluble growth factors like Wnt and BMP which are known to be regulators of stem cell fate and activation, effectively raising [118] or lowering [119] the local concentrations of these and other factors in the local environment. Perhaps the best studied mechanism of ECM regulation of stem cell behavior, however, is direct signaling. The major, and most well-described class of ECM receptor is the integrin family [120], though there are several other receptors for the ECM which will be described in greater detail below. The ECM, through integrin signaling, regulates stem cell behavior through a wide variety of mechanisms. For example, in keratinocyte differentiation, cell-ECM adhesions regulate differentiation by regulating actin cytoskeleton assembly, which, through changes in the ratio of G-actin to F-actin, localizes receptors for the growth factor serum response factor (SRF) to the cell surface, altering the cell's competence to detect and respond to locally available cues. [121] On the other hand, epidermal stem cells growing on more elastic substrates differentiate more readily and are less able to maintain their "stemness" as growth on these substrates inhibits integrin clustering, which in turn downregulates ERK MAPK signaling in these cells. [53]

One of the earliest signs that the ECM may be important in regulating neural stem cell behavior was found when ECM glycoprotein tenascin-C was found to be expressed in embryonic

neural stem cells where it regulates neural stem cell number and lineage progression. [122-125] Interestingly, studies in adult neural stem cells find no role of tenascin-C in maintenance or regeneration after injury, indicating that the temporal and developmental context of ECM signals are very important in determining the cellular response. [126] Perhaps the two most critical growth factors in neural stem cell maintenance, fate determination, and proliferation, and migration are EGF and FGF-2, without which NSCs cannot even be maintained *in vitro.* [72, 127-130] The importance of ECM in NSC function has been clearly established by a series of studies demonstrating that NSCs cannot properly respond to EGF or FGF-2 in their environment without the ECM molecules perlecan, anosmin, and the chondroitin sulfate proteoglycan (CSPG) family of proteins. [131-134]

Dystroglycan

One very important ECM receptor functions as a transmembrane receptor component of the dystrophin-glycoprotein complex (DGC), a complex that links the ECM to the actin cytoskeleton of many cells. [135] Originally named ‘cranin’ as it was first isolated from the brain, [136] dystroglycan was shortly thereafter independently identified as part of the DGC, leading to its renaming. [137-139] Dystroglycan, a highly conserved protein across vertebrates, is transcribed as a single gene product (DAG1) and then post-translationally cleaved into α and β subunits, which associate with each other non-covalently. [140]

The extracellular α subunit is extensively glycosylated via both N- and O-linked glycosylation. In particular, O-linked glycosylation at the central mucin domain is critical for proper dystroglycan function, and is required for dystroglycan-laminin binding (unlike N-linked glycosylation). [141, 142] There is significant heterogeneity in dystroglycan glycosylation across

tissues, cell types, and even within individual cell lines [143-145], and the detected size of dystroglycan ranges in size from 156 kDa in skeletal muscle cells [137] to 120 kDa in most of the brain and PNS [136, 146], though isoforms as large as 180 kDa have been found in the Purkinje cells of the cerebellum. [146] The full extent of O-glycosylation of dystroglycan is evident from the fact that predicted molecular mass of the core peptide is only about 40 kDa, and removal of N-linked glycans only reduces the molecular weight of dystroglycan by about 4 kDa. [147] Indeed studies of dystroglycan, its glycosylation, and their impact on ligand binding has revealed unique mechanisms of carbohydrate interactions, glycosylation pathways, post-translational modifications, and sugar structures that have not yet been described elsewhere. [148-152]

The 43 kDa β-dystroglycan is the transmembrane subunit, which interacts with the extracellular α subunit via its N-terminal domain. β-dystroglycan links α-dystroglycan to the actin cytoskeleton either directly [153] or via binding to DGC proteins such as dystrophin and utrophin (reviewed in [154]). The DGC is an important signaling scaffold for pathways not directly regulated by dystroglycan, such as nitric oxide synthase signaling, calcium signaling, and PI3K-Akt-mediated survival. [155-157] β-dystroglycan also serves as a signaling scaffold in its own right, with 19 known functional motifs and over 40 predicted interaction sites. [158] Dystroglycan, for example, can bind to extracellular signal-related kinase (ERK), ezrin-radixin-moesin (ERM), receptor-associated protein of the synapse (Rapsyn), mitogen activated protein (MAP) kinase kinase 2 (MEK2) [159], Grb2 [160], caveolin-3 [161], dynamin-1 [162], and contains Src homology 2 (SH2), SH3 and WW domains. These allow dystroglycan to regulate cellular physiology not simply limited to ECM regulation but also survival, fillapodia formation, and endocytosis. [153, 162, 163] Dystroglycan contains a nuclear localization and export

sequence, and a portion of the β-dystroglycan intracellular domain can translocate to the nucleus where it has been shown to bind the nuclear lamina as well as localize to various bodies throughout the nucleus, though the full repertoire of its functions in the nucleus are still unknown. [164, 165] Of note, however, nuclear targeting of dystroglycan in a prostate cancer cell line alters the transcription of androgen-regulated transcription factors, which suggests a role for transcriptional regulation in those cells at least. [166]

One of the most important functions of dystroglycan is initiating the assembly of laminin on cell surfaces. Dystroglycan is required for the formation of a basement membrane, initiating this process by binding to soluble laminin and organizing it on the cell surface. [167] Upon binding, dystroglycan clusters laminin on the cell surface, at which point integrins, along with perlecan help organize the basement membrane into more complex structures. [168] This process of laminin assembly has been demonstrated in several cell types including embryonic stem cells, myoblasts, and Schwann cells. [169, 170] This process is also important for the expression and localization of other receptors and channels such as acetylcholine receptor aggregation and aquaporins. [171, 172]

Primary mutations in dystroglycan are exceedingly rare in humans, most likely because dystroglycan is required for the formation of Reichert's membrane, a basement membrane formed early during embryogenesis which separates the embryonic and maternal circulations. In mice, therefore, germline knockout of dystroglycan leads to early embryonic lethality before E10.5. [173] Dystroglycan does, nonetheless, play a major role in human health and disease. Mutations in the enzymes that serve to glycosylate dystroglycan alter its affinity for extracellular ligands and lead to a set of diseases collectively known as "secondary dystroglycanopathies". [174] These diseases are characterized by congenital muscular dystrophy, and nearly all of them

occur with developmental brain defects. Specifically, disordered cortical lamination, thickened cortical plates, hydrocephalus, and partial or complete absence of the corpus callosum are all phenotypic components of the dystroglycanopathies. [175, 176] Dystroglycan is important in regulating oligodendrocyte maturation and cells that promote cerebrospinal fluid movement (discussed below). Cortical lamination and cortical plate development defects arise through two mechanisms. First, the pial basal lamina is malformed in the absence of proper dystroglycan functioning. Second, the ability of radial glial cells to bind to the pial basal lamina requires dystroglycan at the radial glial endfeet. Together, these two disruptions lead to detached radial glial basal processes, which no longer serve as appropriate scaffolds for neuroblast migration and cortical development. [176] As the neuroblasts become mislocalized, some migrate through the disrupted glia limitans into the subarachnoid space, leading to a phenotype known as cobblestone lissenecephaly – another feature of the dystroglycanopathies. [176] Dystroglycan can also function as a tumor suppressor, and alterations in dystroglycan binding as well as intracellular function have been described in a variety of cancers including gliomas, but will not be discussed further here. [166, 177-180]

The Subventricular Zone

Early in development, the germinal cells that give rise to the central nervous system (CNS) are found in the neural plate and neural tube. The neural tube is comprised of stem cells known as neuroepithelial cells (NECs) which surround a hollow lumen. These stem cells divide mostly symmetrically at first to increase their population size, thus creating a large enough base of neural progenitor cells to generate the remainder of the nervous system during the latter part of embryogenesis. Around the end of the second week of embryonic development in the mouse, NECs transition into long, bipolar NSCs known as radial glial cells (RGCs). This transition

marks the onset of cortical neurogenesis and a significant increase in the proportion of asymmetric divisions in the NSC population. This transition is also accompanied by the adoption of certain astrocytic features by radial glia. These include the expression of brain lipid binding protein (BLBP), glutamatergic astrocyte-specific transporter (GLAST), and the intermediate filaments nestin and vimentin. [181-184] The radial glia thus generated serve as the neural stem cells of the telencephalon during the remainder of embryogenesis and immediately after birth. [185-187] The newborn neuroblasts generated in the subventricular zone adhere to the radial glial processes that stretch out to the pial basal lamina, and use these processes as scaffolds to migrate radially outwards during the process of corticogenesis.

A brief note on the temporal and spatial expression of dystroglycan during this time: dystroglycan is first expressed in the developing CNS at around E10 along the basolateral surface of NECs, shortly before their transition to RGCs around E13. Here, it mediates the attachment of radial glia to pial basement membrane. [188-190] There is some debate about the extent of dystroglycan expression and localization in radial glial cells after E13.5, however. One report using one α dystroglycan antibody clone (VIA4-1) noted continued expression of α dystroglycan in the SVZ at high levels throughout late embryonic development, while a group using a different clone (clone IIH6C4) found that α dystroglycan levels dropped around E13.5, restricting itself to the basal endfeet of radial glial cells by E15.5. [190, 191] Studies of β-dystroglycan found that protein expression was limited to the basal endfeet of radial glial cells at E15.5, but found high DAG1 mRNA in the VZ at the same time. [192] Whether these differences reflect actual alterations in dystroglycan processing, altered glycosylation at different regions within the same cell, or are an artifact of variations in protocol remain to be determined. Dystroglycan is also found in other regions of the brain at various timepoints such as the cortical

plate at E15, and pyramidal cells in layers II-VI in adulthood as well as on vascular endothelial cells and perivascular astrocytes where it is important in the maturation and maintenance of the blood brain barrier. [172, 188-190, 193-195]

The adult neural stem cells of the SVZ arise from a subpopulation of radial glial embryonic stem cells. After birth, the exuberant neurogenesis that characterizes the embryonic period abates, and most radial glia detach from the pial membrane of the brain as well as the SVZ and differentiate into parenchymal astrocytes. [196, 197] One subpopulation of radial glial cells, however, differentiate instead into relatively quiescent and slowly diving neural stem cells that are localized to the two major neurogenic regions of the adult brain, the SVZ and dentate gyrus of the hippocampus. In the SVZ, these cells continue to share some features with astrocytes (discussed above) such as expression of glutamatergic astrocyte-specific transporter (GLAST) while adding new ones such as expression of the inward rectifying potassium channels Kir2.1 and Kir4.1 and the intermediate filament protein previously used to define astrocytes, glial fibrillary acidic protein (GFAP). [198-200] These neural stem cells have been termed type B cells, and are subdivided into type B1 and B2 cells. B1 cells are neural stem cells, and persist in the SVZ throughout life in all mammalian species examined so far (reviewed in [201, 202]). Like the radial glia, type B1 cells retain their attachment to the ventricular surface, and reattach their basal processes, once contacting the pial surface of the brain, to the ECM basement membrane surrounding the local vasculature. [203-205] B2 cells, unlike the bipolar, radial glial-like B1 cells, have a stellate, astrocytic morphology, and tend to be located further from the ventricular wall, creating a boundary between the SVZ and overlying striatum. [205, 206]

Simultaneously, another subpopulation of SVZ radial glia differentiate into epithelial-like ependymal cells which line the ventricular walls. [207] This subpopulation appears to be

specified towards an ependymal cell fate during embryogenesis, with the majority of ependymal cells specified between E14-E16 in mice (around the same time future type B cells appear to be specified as well). [207] These findings are consistent with older autoradiographic studies of the ependyma of the subcommissural organ showing that most of these ependymal cells undergo their last division between E11 and E13. [208] After specification, however, these future ependymal cells then pause in their maturation, maintaining their radial glial characteristics until birth. At birth, these cells begin to differentiate, increasing their apical surface area, generating their characteristic ciliary patches, and generating the ependymal cell layer. The ependymal cell layer is a simple cuboidal to columnar layer of multicilliated cells, that can be morphologically divided into two subsets: E1 and E2. The former are characterized by patches of approximately 50 long cilia on their apical surface, while the latter have complex basal bodies and 2 long cilia on their apical surface. [205] In the mature ependymal layer, E cells are connected to each other and to intercalating apical processes of type B1 neural stem cells through adherens junctions. In particular, ependymal cell junctions are characterized by high levels of β-catenin, cadherins, occludin, and ZO-1 (though interestingly, tight junctions are not continuous in most parts of the ependymal layer, with a few exceptions such as the circumventricular organs and the choroid plexus [209, 210]). The specific junctional proteins present in the ependyma change during development and differentiation of the ependymal cell layer (for an overview, please see [211])

During the first weeks of postnatal life, the emerging B1 and ependymal cells differentiate and organize themselves into a “pinwheel” architecture that will define the local architecture throughout adulthood. This pinwheel architecture consists of the flat, large surface area ependymal cells arranging themselves around the apical processes of the type B1 stem cells which contact the ventricular surface. [203-205] The ependymal cells display a 2D organization

termed planar cell polarity in the organization of their cilia. This occurs at two levels of organization. The first is translational polarity, wherein the basal bodies from which the cilia protrude are organized in patches that are themselves eccentrically displaced from the center of the cell. These patches are displaced at specific angles which display tissue-level coordination. The second is rotational polarity in which the individual motile cilia are rotated such that their power strokes are all aligned. [212] Translational polarity is already organized in ependymal cells around the time they are specified, but rotational polarity develops after the docking of the basal bodies at the apical surface during the first days of postnatal life, and is driven by hydrodynamic forces. [213] Ependymal cilia, differentially polarized based on their location along the SVZ, coordinately beat to propel cerebrospinal fluid (CSF) across the ventricular surface. This is proposed to help circulate CSF which clears toxins, delivers secreted signals (e.g. growth factors, morphogens), and acts as a mechanical and thermal buffer for the brain. Functional CSF movement is critical for proper brain homeostasis; disruptions in EC activity can lead to hydrocephalus and concomitant brain dysfunction. [214-216] The directional movement of CSF across the walls of the lateral ventricle in particular has been proposed to help guide the directional movement of neuroblasts along their physiological trajectory in the rostral migratory stream [217], though whether ependymal cilia can generate this type of bulk flow directional movement in larger mammals is unclear (Joanne Conover, personal communications).

After embryogenesis, the SVZ generates mostly glial cells, including astrocytes and oligodendrocytes. In fact, the third major wave of oligodendrogenesis originates during the postnatal period, during which SVZ stem cells give rise to the majority of oligodendrocytes that will go on to myelinate the adult forebrain. [218] However, stem cells of the postnatal SVZ also give rise to transit amplifying precursors which differentiate into neuroblasts that migrate along

the rostral migratory stream, eventually reaching the olfactory bulb, where they differentiate into several different types of local interneurons. [73, 199, 219, 220]

SVZ Extracellular Matrix

The SVZ is characterized by an enrichment of extracellular matrix molecules and structures, some of which are unique to this region. While relatively little is known about the role and function of SVZ ECM in the development, maintenance, and regulation of the niche, recent findings have begun to elucidate some of the characteristics of niche ECM and highlight its importance in both physiology as well as pathology.

The SVZ is highly vascularized, and the vascular basal lamina serves as an important source of ECM in the niche. A key set of findings demonstrating the importance of direct ECM-cell interactions in the SVZ population examined the role of the largest family of laminin receptors, the integrins. Integrins at the basal processes of NSCs in the adult stem cell niche contact the basement membrane of the local vasculature, [203, 204, 221] where α6β1 integrin receptors mediate attachment of NSCs and neural progenitors to vasculature-associated laminin. Analysis of the dynamics of stem cell activation has demonstrated that upon NSC activation, stromal cell-derived factor 1 (SDF-1) and CXC chemokine receptor 4 (CXCR4) act together to upregulate α6β1 integrin (along with EGFR) in activated NSCs and transit amplifying progenitors (TAPs), presumably to facilitate TAP interaction with the vascular basement membrane. [222] Blockade of this receptor leads to detachment of progenitors from the vasculature, aberrant progenitor proliferation, and precocious neuronal differentiation. [204, 222, 223] Recent studies *in vitro* suggest that these interactions may be important in helping maintain the stemness of SVZ-derived cells as well. [224] Thus, integrin-laminin interactions are

important in maintaining the appropriate balance between quiescence and proliferation in the adult niche.

One of the relatively unique features of the SVZ is the presence of fractal-like processes of extracellular matrix extending outwards from the vascular basal lamina in long branched structures termed ‘fractones’. These thin, laminin-rich processes contact all of the various cell types in the SVZ through their highly branched stems which terminate in bulbs immediately subjacent to the ependymal layer. [225] Actively dividing NSCs and NPCs are localized particularly close to both the vascular basal lamina and the fractones that arise from it. [203, 204] Further analysis of the fractone structures has demonstrated the presence of a variety of other ECM molecules including nidogen and collagen-I and IV. One component of particular note is the heparin sulfate proteoglycan (HSPG) perlecan, which is largely restricted to the fractones themselves, and not found in most of the local vascular basal lamina. [226, 227] Dividing cells are preferentially enriched in apposition to these HSPG+ fractones. Indeed, it has been recently shown that perlecan, which binds to the diffusible factor fibroblast growth factor 2 (FGF-2), traps and activates FGF-2, presenting it to local SVZ cells thereby stimulating their proliferation. [227] This mechanism has also been hypothesized to regulate Bone Morphogenic Protein 7 (BMP-7), as loss of HSPGs abrogates the ability of BMP-7 to inhibit SVZ proliferation. [228] Similar results have been demonstrated with BMP4 [229], which is of particular interest, as type B and type C cells express BMP4 and its receptor, while B cells and ependymal cells express the BMP inhibitor Noggin. [230] [231, 232] Thus, balanced BMP signaling may be orchestrated by the interplay of cellular and ECM components of the niche. The SVZ ECM therefore modulates the presentation of growth factors in order to both promote expansion of, and constrain the progenitor pool upon stem cell activation.

Fractone composition and morphology change throughout the lifespan, becoming much larger in aged mice with alterations in the expression of specific HSPG epitopes. [233] The fact that ECM regulates neural precursor proliferation, combined with observations that neurogenesis and neural stem cell number decline with age [234-236] despite relatively similar intrinsic progenitor proliferation dynamics and kinetics across the lifespan [77] suggest that changes in ECM may be a key regulatory factor in stem cell dynamics in development across the lifespan though this hypothesis remains to be rigorously tested. Recently, a few studies have begun to examine the correlation between disease states and SVZ ECM. Studies of human tissue have demonstrated that the SVZs of autistic individuals have structural abnormalities in SVZ laminin and heparin sulfate in young and mature (but not elderly) patients. [237] These results corroborate data from the BTBR mouse model of autism, where in addition to behavioral deficits and structural alterations in the brain (including an absent corpus callosum, a phenotype found in many dystroglycanopathies as mentioned above), the SVZ and its fractones are much smaller and contain less HSPGs and laminin. [238, 239] On the other hand, mechanical disruptions leading to hydrocephalus lead to a significant increase in the size of SVZ fractones through unknown mechanisms. [240]

One of the least well-understood ECM features of the adult SVZ was first described nearly a decade ago with the advent of the SVZ wholemount technique. Hitherto undescribed ECM aggregates were found at the ventricular surface of the SVZ. They were noted to consist of laminin α5 and β1 chains, and stain positive for nidogen, suggesting a similar composition to the basement membrane expressed by postnatal capillary endothelial cells. [204, 241] Beyond the fact that these aggregates were described as associated with the apical tips of GFAP+ processes (Type B1 stem cells), nearly nothing is known about their source, development, and function. It

is unclear whether the role of ventricular ECM is simply to promote adhesion to the ventricular surface or whether it has other, unexplored roles in regulating stem cell behavior. Recent work demonstrating that laminin 511 is one of the most permissive and beneficial isoforms in the maintenance of pluripotency in induced and embryonic stem cells [242, 243] and can protect neurons from excitotoxin-induced death in the hippocampus [244] raise the possibility that these structures may play a role in communicating with, and regulating NSCs.

As discussed above, one of the most dramatic changes in NSC function across the entire lifespan occurs at birth, when SVZ NSCs downregulate their proliferation, dramatically change their morphology, adopt astrocytic characteristics, give rise to the major wave of oligodendrogenesis for the postnatal forebrain, as well as to niche ependymal cells, and organize into the adult SVZ configuration. Since niche environmental factors such as ECM are critical in regulating NSC behavior, we hypothesized that understanding the role of ECM-receptor interactions during this transitional period is likely to be very instructive in understanding the various roles that the ECM plays in regulating SVZ NSC development and function.

Chapter 2: Dystroglycan Regulates Postnatal SVZ Organization, Development, Cellular Output, and ECM

NB: *Some of the results presented in figures below were generated by my colleague, Dr. Freyja McClenahan. I have included these data in this text for the sake of coherency, rationale, and completeness. I would be remiss if I did not once again mention that I am indebted to her work for laying the foundation for much of this dissertation.*

The ECM, as discussed in Chapter 1, is a network of proteins and molecules that serves as a key regulatory factor in stem cell niche function. The ECM's many roles in modulating cellular function include: providing physical support and cues to stem and niche support cells, directly signaling to these cells, and potentiating or abrogating other extracellular cues. As discussed earlier, not only are the neurogenic regions of the brain (i.e. the SVZ and dentate gyrus) enriched in ECM, but the SVZ also houses unique ECM structures such as highly branched ECM fractones, [225] and laminin hubs at the ventricular surface. Despite local ECM enrichment, the role of ECM in the regulation of the SVZ remains understudied. Interestingly, the ventricular surface of the adult SVZ is characterized by specialized ECM aggregates that associate with the apical processes of NSCs but whose origins and function remain unknown. [204]

VZ Laminin is Organized into Hubs in the Postnatal SVZ

Extracellular matrix (ECM) proteins in the adult SVZ neural stem cell niche are uniquely arranged, and can be found in both vascular basal lamina and extra-vascular structures [203, 204]. However, how niche ECM organization is adopted and the factors regulating its development remain unknown. To better understand the cell-extracellular matrix interactions that

might help orchestrate the transition to the adult SVZ, we used whole mount IHC to track cell and ECM relationships in the SVZ during the immediate postnatal period when the SVZ niche is first established.

At birth, the vascular plexus, as visualized by laminin immunoreactivity, is morphologically similar to, but denser than, that of the adult mouse (Fig. 1A). Additionally, fractones, thin ECM structures that project from the vascular basal lamina in the adult SVZ [225], are already present at birth (arrowheads and inset, Fig. 1B). At the ventricular surface, laminin is present at birth in a diffuse pattern, but laminin-rich aggregates begin to appear between P3 and P8 (arrows, Fig. 1B). At P3, laminin is diffusely distributed on or near the apical (ventricle-adjacent) surface of immature ependymal cells, which can be identified by an apical surface area several-fold larger than that of neural stem cells (Fig. 1C). However, between P3 and P8, large laminin aggregates, or "hubs" begin to coalesce at the ventricular surface of these cells, concurrent with a reduction in diffuse ependymal cell-associated laminin (P8, arrowheads). By the end of the third postnatal week, ventricular surface laminin is largely restricted to hubs (P21, arrowheads) with many such hubs found at the interface of ependymal cells and adult neural stem cells within niche pinwheels (P21, arrows). The final location of these laminin aggregates led us to term them "hubs" – their location at the center of the characteristic pinwheels endows them with proximity to both NSCs as well as ECs.

At P21, many hubs appear to be connected via tethers, even across cell borders (Fig. 1D, inset, arrow), suggestive of coordinated grouping and/or merging of hub structures. This process could help explain the phenomenology of how diffuse surface laminin at P0 and P3 gives rise to larger aggregates and hub structures over the first weeks of life. Closer examination of VZ surface laminin revealed that laminin structures at any single time during the postnatal period

appear to be in various stages of “merging” (Fig. 1E). These structures can broadly be grouped into two general categories of putative process. In the first, hub-like structures in close apposition may directly merge with each other, eventually becoming one larger structure (Fig. 1F). In the second, hubs may first extend and connect to each other by thin, tendril-like tethers and then move towards each other in order to merge. (Fig. 1G). It must be stated, however, that whether these processes are in fact how hubs form and grow remains a matter of speculation in the absence of some form of time-lapse imaging, which would allow for definitive description of the dynamics of hub formation and which remains a future direction for this study.

Overall, these results show that laminin is present at birth on the VZ surface in a diffuse manner, and during the first week of life, is enriched on the surface of nascent ependymal cells. Over time, the laminin organizes into small aggregates which then continue to merge into larger structures which are themselves transposed to the interface between stem and ependymal cells. These laminin hubs take several weeks to form, appear to be the result of a complicated and coordinated process involving two cell types (i.e. neural stem cells and ependymal cells), and form simultaneously with the development, maturation, and organization of these cells. The complexity of this process and the tightly coordinated timing of surface laminin aggregation led us to hypothesize that ventricular surface laminin plays an important role in the development and/or function of the SVZ. As no studies thus far had engaged in an in-depth characterization of surface ECM in the SVZ using the wholemount technique, it was unclear whether the surface ECM characterized here is a new facet of the previously described vascular ECM structures that may project to the ventricular surface, or a separate ECM structure entirely. We therefore decided to reconstruct in 3D the V/SVZ ECM to understand its spatial and temporal relationship to the neonatal vascular ECM.

Ependymal and Vascular ECM Form Distinct Compartments in the V/SVZ

Z-projections of optical stacks at P8 indicate that these VZ surface laminin aggregates are distinct from the vascular basal lamina by the end of the first postnatal week (Fig. 1B, lower panels, arrows, ventricle surface at the top). However upon examination of development during the first week, 3D reconstructions of V/SVZ laminin revealed that at P3, ventricular surface laminin is, in fact, often contiguous with the vascular basal lamina, either directly (Fig. 2A, P3, arrowheads) or via "tethers" (arrows). Nonetheless, by P8, two distinct classes of laminin aggregates have emerged: (i) laminin hubs, visible at the surface (P8, arrowheads) and (ii) fractone "bulbs" that appear to be fractone termini, which lie beneath the developing ependymal layer (P8, arrow). These two niche ECM elements, spatially distinct at P8, remain so throughout the remainder of development. At P21, laminin hubs and blood vessel-associated basal lamina have formed totally separate ependymal and vascular elements, with the ependymal ECM consisting predominantly of laminin hubs. These two morphologically distinct elements can also be distinguished by their distance from the ventricular surface as illustrated by Z-projections at P21 co-stained for the ventricular surface adherens junctions (Fig. 2B), and depth-coded whole mount images stained for laminin (Fig. 2C, left panel). Interestingly, adult type B1 GFAP+ neural stem cells span the distance between the ventricular surface, characterized by adherens junctions and laminin hubs, and the vascular basal lamina. (Fig. 2C, middle panel). In fact, superposition of depth-coded GFAP and laminin IHC shows that these neural stem cells contact both vascular basal lamina as well as the laminin hubs at the surface (Fig. 2C, right panel and see below, Fig. 3E) – with the breakdown of adherens junctions at the interface of surface hubs. We

also confirmed that type B1 NSCs continue to contact both vascular basal lamina (Fig. 2D) and ventricular surface laminin hubs (Fig. 2E) in the aged animal.

These results suggest that SVZ neural stem cells, at least, maintain an important relationship with their environmental ECM, as they contact specialized laminin structures with both their apical and basal processes. Furthermore, apical contacts with the laminin hubs are present not only during development, but are maintained throughout life. As discussed in greater depth later, the ependymal and vascular ECM elements are not redundant in their functional effects on NSCs, but rather exhibit stark differences, particularly in terms of the receptors that mediate NSC-laminin binding and the functional effects that arise from this contact. Further evidence towards a specialized role of surface ECM comes from findings to be presented later in this chapter showing that disruption of some of the cellular machinery responsible for ventricular surface laminin hub formation has no appreciable effect on vascular laminin.

Laminin Hubs are Likely Formed and/or Assembled by Ependymal Cells

These results highlighting the predominantly ependymal localization of developmental laminin (Figs. 1C, 2A) stand in contrast to earlier findings in the *adult* SVZ that showed that "specks" of laminin were usually associated with GFAP+ adult neural stem cell processes [204], as well as our own observations of GFAP+ processes contacting surface laminin hubs. One possible explanation of this discrepancy is that VZ laminin may be of ependymal cell origin, but the hubs may be then translocated to the centers of the pinwheels where they would be near apical NSC processes as seen in (Fig 1C).

Therefore, to confirm that the laminin-positive cells we observed during the immediate postnatal period were indeed ependymal cells, we used FoxJ1-GFP reporter mice to label

ependymal cells during development. In these mice, developing ependymal cells are labelled by GFP upon expression of FoxJ1, a transcription factor expressed relatively early in multicilliated cell development. Both en face views and 3D reconstructions over the first postnatal week confirmed that (i) cell-associated laminin is almost exclusively restricted to immature ependymal cells, strongly suggesting an ependymal cell origin of surface laminin and (ii) laminin tethers beneath the apical surface serve as bridges, connecting immature ependymal cells to the vascular basal lamina during niche construction (Fig. 3A).

Furthermore, at P21, depth-coded high gain images of intra- and extracellular laminin from the same field showing actively merging hubs (See Fig. 1E) show that presumptive apical processes of neural stem cells coincide with laminin-sparse regions, while intracellular laminin-rich regions appear to be restricted to ependymal cells (Fig. 3B). These data further support the idea that the majority of VZ laminin is of ependymal cell origin, at least after the first week of postnatal life. We also found that niche pinwheel arrangement is nearly complete by P21. At this point, many laminin hubs are central on the apical surfaces of ependymal cells (Fig. 3C, arrow), while some are transposed to the center of pinwheels (closed arrowhead), and others appear to be in transit, protruding into the center of a pinwheel while retaining attachment to an ependymal cell (open arrowhead). By adulthood, however, virtually all pinwheels contain one or more laminin hubs, localized to the interface between ependymal cells and neural stem cell apical processes, in agreement with, and further clarifying earlier reports of laminin immunoreactivity at the VZ surface [204] and (Fig. 3D). Once these hubs do find their way to the centers of pinwheels, they are positioned so that they are able to contact both ependymal cells as well as neural stem cells (Fig. 3E). High magnification images show that they are in fact in direct physical contact with both cell types, and that adherens junctions at the laminin hub site, may

actually break down at these regions as indicated by a gap in β-catenin immunoreactivity in this region, which is reasonable as the hubs themselves are unable to interact with adherens junctions (Insets).

Taken together, our observations indicate that in the early postnatal V/SVZ, extravascular laminin is concentrated around immature ependymal cells, becoming restricted with niche maturation, and eventually achieving an adult configuration of discrete laminin hubs at the interfaces between neural stem cells and ependymal cells. These results also bolster the conclusion in the previous section that NSC – ECM contacts are likely important to the proper function of SVZ NSCs, as the loss of adherens junctions at the interface of the laminin hubs indicates a specialized contact region. The nature of these contacts, both on the ependymal and stem cell side is an ongoing area of research in the lab. For example, as laminin binding proteins such as dystroglycan can directly and indirectly localize a host of signaling and structural proteins (e.g. FAK, filamentous actin, nitric oxide synthase), we are trying to determine what complement of molecules may be specially localized to these cell-ECM contact regions.

Dystroglycan Regulates Surface Laminin

Intrigued by the extensive reorganization of V/SVZ laminin during niche development, we sought to understand the effect of surface laminin mediated signals on SVZ development. We hypothesized that laminin-receptor interactions may regulate aspects of niche construction and function. The two major classes of laminin receptors are the integrin family of receptors, and a phylogenetically unrelated receptor, dystroglycan. [245] Dystroglycan has been little appreciated as a "signaling receptor" for ECM but has been reported to regulate basement membrane formation in general, and the assembly, endocytosis, and degradation of laminin in particular

[167, 169, 246, 247]. Indeed, dystroglycan is best known as a member of the dystrophin-glycoprotein complex in skeletal muscle, where it bridges the actin cytoskeleton via dystrophin, with the muscle sarcolemmal basement membrane via laminin. The loss of dystroglycan function thus leads to a subset of muscular dystrophies termed “dystroglycanopathies”. Intriguingly, dystroglycanopathies also present with a wide range of structural abnormalities of the brain and cognitive deficits whose underlying etiology remains unclear (Reviewed in [248]). Furthermore, in several types of cells, the laminin receptor dystroglycan is required for initial laminin clustering on cell surfaces [167-169, 247, 249, 250] giving it a potential role not only in the detection and transmission of laminin-mediated cells, but also, reciprocally, in the generation and organization of extracellular laminin structures.

Examination of laminin and dystroglycan in the V/SVZ using wholemount IHC (Fig. 4A) revealed that in the newborn VZ, laminin and dystroglycan are localized mainly to radial glial cell (RGC) adherens junctions at the cell-cell junctions (Fig. 4A). Emerging ependymal cells, identified by their large apical surface areas, have more cell surface laminin by P3, and this increase is generally paralleled by an increase in surface dystroglycan. At P8, however, cell-associated laminin becomes more restricted, and dystroglycan immunoreactivity is even more limited, with dual laminin- and dystroglycan-positive hubs now appearing at the ventricular surface. To more carefully examine the relationship between dystroglycan and ependymal cell maturation, and to confirm that dystroglycan is indeed enriched at ependymal cell surfaces, we turned to our *in vitro* SVZ-derived ependymal cell cultures (Fig. 4B). Using SVZ cells from P0 FoxJ1-GFP mice (wild type for dystroglycan), we found that, in agreement with our *in vivo* observations, dystroglycan level is tightly correlated with ependymal cell maturation (Fig. 4C),

and reaches its highest expression in mature, multicilliated ependymal cells relative to immature ependymal cells or non-ependymal cells.

We therefore next investigated dystroglycan's functional role in the developing SVZ neural stem cell niche by comparing *nestin-cre;DAG*$^{Flox/Flox}$ (DAG cKO) mice, which lack dystroglycan in neural stem cells and their progeny (with Cre enzyme driven under the control of the type VI intermediate filament nestin promoter), to *nestin-cre*$^{-/-}$;*DAG*$^{Flox/Flox}$ (WT) littermates. These mice have been previously characterized to have total absence of β-dystroglycan immunoreactivity in the brain by E13.5. [251] Having confirmed the loss of dystroglycan protein in DAG cKOs by IHC (Fig. 4D), and western blot (Fig. 4E), we examined SVZ RGC density at birth and found that DAG cKO and WT mice have similar BLBP+ cell densities ($45.1 \pm 4.2 \times 10^5$ cells/mm^3 vs. $44.6 \pm 2.3 \times 10^5$ in WT). The apical processes of nestin+ RGCs make contact with laminin-positive puncta at the ventricular surface at birth, but fewer VZ laminin puncta are present in DAG cKO mice and the association of RGC apical processes with laminin puncta is diminished in the dystroglycan-deficient SVZ (Data not shown). It should be noted, however, that laminin immunoreactivity in the vascular basal lamina appears normal in DAG cKO mice, with typical contacts between RGC basal processes and blood vessel basal lamina, indicative of normal physical adhesion between radial glia and the vascular laminin (Data not shown). Additionally, qRT-PCR revealed that the expression of a panel of laminin genes in the DAG cKO SVZ is largely unchanged (not shown) indicating that large deficits in apical surface laminin (i.e., laminin hubs) reflect either a failure of laminin recruitment/organization on cell surfaces, or, a highly localized loss of expression.

To gain a more detailed spatiotemporal understanding of VZ laminin dynamics, we examined en face views of the ventricular surface from SVZ wholemounts during early niche

development (Fig. 4G). As expected, at P0 the density of RGCs at the apical surface of the lateral ventricle appears normal in DAG cKO mice, with laminin immunoreactivity diminished compared to that seen in the wild type. By P3, developing ependymal cells are readily apparent in both WT and DAG cKO mice, but the dystroglycan-deficient VZ has a marked decrease in pericellular laminin associated with developing ependymal cells (Fig. 4G, center panels). Interestingly, at P8, cells at the ventricular surface of DAG cKO mice have *increased* cell-associated laminin, surpassing levels seen in wildtype littermates (Fig. 4G, right panels). By P21, however, when laminin immunoreactivity is largely confined to hubs, DAG cKO mice display a more than 30-fold reduction in the number of laminin hubs per 1000 μm^2 (Figs. 4 H, I). Additionally, we found a trend towards a reduction in mean hub size in DAG cKO wholemounts (Fig. 4I; 1.45±0.19 μm2 in WT vs. 0.54±0.25 μm2 in DAG cKO). As we noted that some weakly immunoreactive hubs were eliminated by intensity thresholding, we also adjusted the image intensity to visualize some very weakly immunoreactive hubs in the DAG cKO (Fig. 4H, right panels). However even upon inclusion of *all* weakly positive hubs, DAG cKO wholemounts contained almost two-fold fewer laminin hubs. Further indications that it is dystroglycan's ability to bind to laminin that leads to the dysregulation of surface laminin came from our SVZ cultures. In these cultures, we noted that application of dystroglycan blocking antibody *in vitro*, led to fewer and more disorganized laminin fibrillary structures normally present on the surface of ependymal cells (data not shown).

As expected, these data indicate that laminin recruitment and/or retention at ependymal cell surfaces is aberrant in the absence of dystroglycan, and, even in ependymal cells of the same genotype, laminin surface organization is perturbed by blocking dystroglycan's ability to bind

ECM proteins. It is therefore evident that dystroglycan-laminin interactions are crucial for the appropriate formation and retention of laminin hubs at the ventricular surface.

The pattern of laminin abundance at the ventricular surface over the first weeks of postnatal life remains an intriguing point of inquiry. At birth, laminin at the ventricular surface is present at low levels in a diffuse distribution, and along cell-cell borders. The findings that vascular ECM is often contiguous with surface ECM at P3 in the wildtype mouse may indicate that P0 surface laminin is part of, or derived from, the vascular ECM network. Potentially, as ependymal cells emerge, they begin to take over responsibility for regulating surface laminin, expressing it at much higher levels on their surface, which is dysregulated in the absence of dystroglycan. In the knockout, as surface laminin drops rapidly, ECs may increase localized production or externalization of laminin to compensate (or perhaps are unable to partake in dystroglycan-mediated internalization if internalization is dystroglycan's predominant contribution to surface laminin at this time). This would result in an overabundance of laminin at the surface by P8. Why this laminin drops off by P21, however, is unexplained. One possibility is that surface laminin simply cannot be maintained in the long run in the absence of dystroglycan. Alternately it is possible that surface laminin structures can only be maintained in the long run when it has reached a critical size and/or complexity (perhaps in complex with other ECM molecules). One hint that this may be the case comes from findings to be presented in Chapter 4. These results show that when dystroglycan is removed in the first few days after birth from ependymal cells, initial total laminin coverage is unchanged, but the laminin clusters present are more fragmented and smaller in the knockout at P8. By P21, there is a reduction in the total number of hubs and the amount of laminin per hub in this model. Thus, if a critical size threshold is required for laminin clusters to generate more complex structures, a reduced ability

to generate laminin clusters of the appropriate size early in development could lead to the phenotypes seen here.

We next wondered what, if any, functional effects dystroglycan plays in the emergence of the cellular components of the SVZ niche during the postnatal period. As ependymal cells develop during this period and appeared to be central to the production and regulation of ventricular surface ECM, we first wondered whether the loss of dystroglycan might impact ependymal cell generation.

Dystroglycan Regulates Ependymal Cell Maturation and Organization

Early in SVZ stem cell niche construction, a subset of RGCs transform into ependymal cells. [207, 252] As ECM interactions can regulate cell differentiation in the adult stem cell niche, [203, 204, 227, 228] we decided to test if dystroglycan might regulate the maturation of RGCs into ependymal cells. Despite having equivalent RGC densities at birth (Fig. 5A), P3 DAG cKO mice have fewer CD24+ ependymal cells than wildtype littermates ($3.01\pm0.23 \times 10^3$ cells/mm^2 vs. $4.82\pm0.34 \times 10^3$ in WT; Fig. 5B) and slightly more BLBP+ RGCs than WT littermates ($44.2\pm2.16 \times 10^5$ cells/mm^3 vs. $38.2\pm2.05 \times 10^5$ in WT; Fig. 5C). Indeed, while the RGC population as detected by BLBP in WT mice decreases from birth to P3, it does not change in the DAG cKO SVZ. Together, our findings of decreased ependymal cell densities concurrent with elevated RGC densities suggest a delayed differentiation of RGCs into ependymal cells. As ependymal cells mature, they increase their apical surface area and acquire large patches of multiple cilia that can be visualized using γ-tubulin IHC to detect ciliary basal bodies. [253] By these measures, DAG cKO SVZs also exhibit lower levels of ependymal cell maturation through the third postnatal week (Fig. 5D), with a significantly lower percentage of apical surface

coverage by multiciliated ependymal cells both at P8 (39.8±2.3% of total area vs. 62.0±3.1% in WT; Fig. 5E) and P21 (41.5±3.0% of total area vs. 61.8% ± 5.0% in WT; Fig. 5F). Dystroglycan loss also disrupts the ability of ependymal cells to arrange into pinwheels. At P8 (Fig. 5G) and P21 (Fig. 5H), ependymal-NSC pinwheel clusters are smaller in the DG cKO SVZ (P8: 7.5±0.3 $x10^2$ μm^2 vs. 11.3±0.6 $x10^2$ in WT; P21: 8.3±1.0 $x10^2$ μm^2 vs. 13.9±1.4 $x10^2$ in WT), and have a disorganized appearance (Fig. 5D, insets).

The size and polarity of ependymal cell ciliary basal body patches, normally tightly regulated and essential for proper CSF flow and neural stem cell function [253], are also abnormal in the DAG cKO SVZ at P21 (Fig. 5I). The fractional basal body (BB) patch displacement (Fig. 5K; also Methods) is significantly increased in DAG cKO ependymal cells (Fig. 5K; 0.42±0.01 vs. 0.30±0.01 in WT). This change reflects an increase in BB patch displacement itself, as the absolute distance of BB patch displacement increases, while the average cell radius does not (Fig. 3L). Additionally, BB patches are smaller in DAG cKO ependymal cells (Fig. 5M; 0.111±0.004 vs. 0.156±0.004 in WT). Measurements of the BB patch angle, a readout for ependymal cell translational polarity (with each cell's BB patch angle normalized to the average BB patch angle per field) displayed a trend towards a greater variability of BB patch angle in DAG cKO ependymal cells relative to WT, though this trend was not statistically significant (Fig. 5N).

Thus, the loss of dystroglycan delays the emergence and maturation of the ependymal cell population despite the fact that these cells have already been specified embryonically. This phenomenon, beginning with the delayed loss of the stem-marker BLBP and acquisition of the ependymal marker CD24 within a few days of postnatal life, eventually leads to lower numbers of ependymal cells as measured by acquisition of cilia as late as the third week. Surprisingly, this

also results in disorganization of pinwheel structures in the knockout, which may suggest a critical period during early development during which ependymal cell maturation is required in order for stem and ependymal cells to arrange themselves appropriately.

Additionally, the loss of dystroglycan appears to affect the polarization of the basal bodies on the apical surface of ependymal cells. In the dystroglycan-deficient SVZ, the patches of cilia on the surface of ependymal cells are smaller and more eccentrically displaced towards the edges of each individual cell. There are at least two potential explanations for these observations. On one hand, this may represent a dysregulation of the normal polarity mechanisms underlying basal body localization and packing in a 2D plane. [212, 213, 215, 254] The results could also be a result of a reduction in the number of basal bodies which are then localized from the outside edge of the cell inwards, giving the appearance of more eccentric basal body localization. While the resolution of wholemount images taken thus far has largely precluded a rigorous analysis of basal body number and packing, this work is ongoing in the lab. Additionally, a reduction in the transcript levels of a key transcription factor involved in the generation of basal bodies provides circumstantial evidence that a reduction in basal body number may be at least partially responsible for the observed phenotype.

Dystroglycan Regulates Postnatal SVZ Gliogenesis

As perinatal DAG cKO RGCs are defective in their ability to transform into ependymal cells and establish a normal SVZ stem cell niche, we wanted to determine if these disturbances impacted the niche's ability to produce progenitor cells. The principal wave of dorsal oligodendrogenesis begins perinatally and extends into the second postnatal week. [218] During this time, oligodendrogenic intermediate progenitor cells (oIPCs) are specified from neural stem-

and transit amplifying cells. oIPCs, as they transition into oligodendrocyte progenitor cells (OPCs), proliferate and migrate out of the SVZ into the overlying white matter.

We examined oIPC/OPC production and proliferation in DAG cKO mice and their WT littermates at P0 and P3 (Fig 6A). At birth, oligodendrogenesis has begun in DAG cKO mice, although to a slightly lesser extent than seen in WT littermates (10.6±1.8 $x10^5$ PDGFR+ cells/mm^3 vs. 15.1±3.6 x 10^5 in WT; Fig. 6B). By P3, however, DAG cKO oligodendrogenesis not only catches up, but far surpasses that seen in the WT, with an SVZ oIPC/OPC density of more than double that of their WT littermates (30.6±3.1 $x10^5$ cells/mm^3 vs. 14.0±1 $x10^5$ in WT; Fig. 6B). DAG cKO SVZ oIPC/OPC densities remain elevated over WT levels until the beginning of the second postnatal week (not shown). Interestingly, however, the changes in niche output during this period appear to be limited to gliogenic lineage cells. We did not observe similar disturbances in neurogenesis, with the density of Pax6+ neuronal IPCs being unchanged (44.4±3.7 $x10^5$ cells/mm^3 vs. 44.2±4.3 $x10^5$ in WT; not shown).

It was unclear at this point, however, whether the increase in oIPC/OPC population was due to an increase in the proliferation within this population. We therefore sought to characterize the proliferative profile of the DAG cKO SVZ. Surprisingly, at birth, DAG cKO mice exhibit significantly *decreased* SVZ cell proliferation (38.8±3.6 $x10^5$ PCNA+ cells/mm^3 vs. 63.1±2.1 $x10^5$ in WT littermates; Fig. 6C). However, while proliferation sharply declines in the WT SVZ between P0 and P3 as the niche becomes more quiescent, proliferation in the DG cKO SVZ remains relatively constant between P0 and P3, resulting in a slight elevation in proliferation over WT levels by P3 (44.2±8.4 $x10^5$ cells/mm^3 vs. 28.7±4.2 $x10^5$ in WT; Fig. 6C). Additionally, while WT NSC/NPC proliferation is concentrated mainly in the VZ, proliferative Sox2+ cells (NSC/IPCs) are mislocalized throughout the DAG cKO SVZ; further from the ventricle on

average at birth, but then closer at P3 (not shown). To determine which cell types contribute to altered proliferation, we examined the radial glial marker BLBP in conjunction with PCNA. At birth, the percentage of proliferating RGCs is significantly lower in DAG cKO mice (36.1% ± 3.5% vs. 64.8% ± 1.9% in WT; Fig. 6D), mirroring the phenotype observed in the general V/SVZ population (Fig. 6B). However, while WT mice undergo the typical decrease in RGC proliferation between P0 and P3, RGC proliferation levels remain constant in DAG cKO mice between P0 and P3, again resulting in RGC proliferation levels being slightly higher by P3 (34.4% ± 1.9% vs. 27.8% ± 1.8% in WT littermates; Fig. 6D). The loss of dystroglycan does not alter proliferation of the oIPC/OPC population at P0 (65.6% ± 8.6% vs. 67.6% ± 5.7% in WT; Fig. 6E), but by P3, the DAG cKO SVZ oIPC/OPCs proliferate at a much greater rate than their WT counterparts (57.7% ± 2.8% vs. 39.3% ± 5.3% in WT; Fig. 6E). In fact, an analysis of the total proliferation at P3 shows that while the increase in RGC proliferation does contribute to the increase in overall SVZ proliferation, the increase in oIPC/OPC proliferation is the predominant driver of this phenotype in the dystroglycan-deficient SVZ (Fig. 6F).

To rule out the possibility that embryonic loss of dystroglycan leads to global alterations in the NSC developmental profile, which then indirectly alters oIPC/OPC production, we used the nestin-CreERT2 to generate an inducible dystroglycan conditional knockout mouse in which postnatal tamoxifen injections drive the loss of dystroglycan gene expression in NSCs and their progenitors (iDAG cKO; Fig. 6G). Following 3 days of tamoxifen injections beginning at birth, we then analyzed oIPC/OPC density in the SVZ at P8 (Fig. 6H), and found a significant increase in PDGFRα+ cell density in the iDAG cKO SVZ relative to the densities in control (*cre*-/-) littermates (25.5±1.9 $X10^5$ mm^3 vs. 18.4±1.4 $X10^5$ mm^3; Fig. 6I, J). These findings suggest that

eliminating dystroglycan expression specifically in perinatal RGCs is sufficient to drive oIPC/OPC overproduction.

Thus, both the RGC and oIPC/OPC populations displayed an increase in proliferation, which could contribute to the increase in oIPC/OPC numbers. However, these results did not rule out the possibility that an increase in oIPC/OPC production by RGCs could be the source of increased oIPC/OPCs which then also happened to proliferate more rapidly. To determine whether the increases in SVZ oIPC/OPC density in the DAG cKO mice arise from increased generation of these cells from RGCs, or from increased oIPC/OPC proliferation, we developed a strategy to acutely disrupt dystroglycan-ligand interactions in wild type rodents and track SVZ cell phenotypes shortly thereafter. Here, we injected either control IgM or α-dystroglycan-blocking (clone IIH6) antibodies into the lateral ventricles of P2 rats, followed by analysis at either 6 or 24 hours post-injection (Fig. 6K). By visualizing laminin and β-catenin in SVZ wholemounts obtained 6 hours post-injection, we observed that ventricular surface laminin is found mainly in aggregates on the surface of immature ependymal cells in controls. These aggregates, however, are lost in rats injected with dystroglycan-blocking antibodies, with laminin immunoreactivity appearing more diffuse (not shown). Indeed, these results indicate that abrogation of laminin-dystroglycan binding is sufficient to disrupt nascent laminin cluster formation, and additionally provide supporting evidence that the dystroglycan-blocking antibody is able to outcompete at least some laminin binding to dystroglycan. At 24 hours post-injection of dystroglycan-blocking antibodies, however, laminin immunoreactivity recovers, likely due to antibody clearance from the lateral ventricles.

We then examined coronal sections from antibody-injected rodents for oIPC/OPCs (PDGFαR+), proliferating cells (PCNA+) and NSC/IPCs (Sox2+) within the SVZ. We found that

dystroglycan blockade increases the oIPC/OPC population twofold by just 6 hours post-injection (Fig. 6L) ($14.30\pm2.33x10^5$ cells/mm^3 vs. $6.96\pm1.94x10^5$ in controls; Fig. 6M), concomitant with approximately a 50% increase in Olig2+ cell densities ($6.15\pm0.21x10^5$ cells/mm^3 vs. $4.33\pm0.30x10^5$ cells/mm^3 in controls; not shown), supporting PDGFαR immunoreactivity as a means to identify oIPC/OPCs. Critically, this increase is *not* explained by greater oIPC/OPC proliferation as PCNA immunoreactivity within the oIPC/OPC population is similar between control and treated groups at this time (25.5±11.7% vs. 36.3±9.7% in controls; Fig. 6N). To confirm increased oIPC/OPC densities were indeed the result of *de novo* gliogenesis, we assessed PDGFαR expression within the Sox2+ NSC/IPC population. Six hours post-injection of dystroglycan-blocking antibodies, the proportion of Sox2+ cells co-expressing PDGFαR is nearly *fourfold* that of controls (38.2±8.3% vs. 9.6±4.4% in controls; Fig. 6O), a result consistent with an acute pro-gliogenic effect on neural stem- and/or uncommitted progenitor cells. PDGFαR+ cell populations within the SVZ returned to control levels by 24 hours post-injection, suggesting that the population of newly-formed oIPC/OPCs seen at 6 hours post-injection has exited the SVZ. In contrast, dystroglycan blocking antibodies have no effect on the density of cells expressing Pax6 ($26.3\pm2.87x10^5$ cells/mm^3 vs. $25.2\pm2.44x10^5$ in controls; Fig. 6P), a transcription factor that represses Olig2 to promote neuronal fate in postnatal SVZ progenitors [255, 256]. Additionally, dystroglycan blockade leads to a twofold increase in Sox2+ cell proliferation (32.6±2.0% vs. 15.7±1.7% in controls; Fig. 6Q), although this effect is not observed until 24 hours post-injection. These findings suggest that detachment from dystroglycan ECM ligands deregulates the proliferation and maturation of Sox2+ stem/progenitors and drives rapid oligodendroglial production without an intermediate transit-amplifying (i.e., proliferation) step.

As discussed in the previous sections, removal of dystroglycan dysregulated surface laminin deposition within the first week after birth. However, intriguingly, here we found that many changes in NSC/progenitor cell phenotypes in the dystroglycan-deficient SVZ *preceded* the substantial dysregulation of laminin levels. For instance dystroglycan-mediated signals regulate NSC proliferation during the immediate postnatal period. NSCs are quite proliferative at birth, but then dramatically downregulate their proliferation over the first few days of postnatal life as they transition into adult NSCs. In the dystroglycan cKO, however, NSC proliferation at birth is significantly lower than normal, despite a normal density of NSCs within the SVZ. Furthermore, these dystroglycan-deficient NSCs also fail to undergo the normal postnatal reduction in proliferation, and instead maintain their newborn proliferation levels at P3. Dystroglycan-deficient proliferating cells are furthermore aberrantly localized throughout the SVZ rather than being constrained to the VZ as is typical [223]. As a result, by P3, the conditional dystroglycan knockouts have slightly *higher* levels of NSC proliferation compared to controls. These findings indicate that laminin and dystroglycan function in a reciprocal axis, wherein dystroglycan mediates the transmission of laminin signals to regulate NSC proliferation but also regulates the presence of cell-surface laminin.

When we examined the major progeny population of SVZ NSCs during the early postnatal period, the oligodendrocyte progenitor pool, we found that, while the dystroglycan-deficient SVZ has slightly fewer OPCs at birth, by P3, it is home to double the number of OPCs relative to wildtype littermates, despite no apparent defects in OPC migratory capacity. The predominant contributor to this increase is an increased proliferation of oligodendrocyte lineage cells themselves. Again, in the dystroglycan-deficient SVZ, the proliferation of OPCs over the first three days of postnatal life does not undergo the expected decrease, such that the

proliferative profile of OPCs, while normal at birth, remains aberrantly high at P3, leading to an increased OPC density within the SVZ. Thus, it is reasonable to conclude that either dystroglycan-mediated signals help downregulate both NSC and OPC proliferation immediately after birth.

Short-term application of dystroglycan-blocking antibodies *in vivo* revealed that the loss of dystroglycan signal directly drives NSC acquisition of an OPC phenotype *first*, which is then followed by a burst of proliferation in Sox2+ cells, presumably to replenish the NSC and/or intermediate progenitor cell (IPC) population. As a result of this overproduction of OPCs, by the end of the first postnatal week, dystroglycan-deficient mice have an overabundance of OPCs and oligodendrocytes in the corpus callosum, a major white matter tract immediately dorsal to the SVZ. The speed with which the NSC to OPC phenotype acquisition occurs is not only unexpectedly rapid, but places temporal constraints on the mechanism that might be responsible for this phenomenon. The induction of NSC reprogramming with concomitant chromatin and epigenetic modification to drive the acquisition of an OPC genetic signature followed by protein translation is unlikely to occur within 6 hours. Rather, I believe it is more likely that a subset of NSCs, already epigenetically primed to become OPCs are held in check by some unknown factors preventing the active transcription and translation of OPC-specific genes similar to mechanisms similarly described recently in stem cell genomic control in other models. [257-259] The loss of dystroglycan signaling removes the block on lineage progress, allowing cells to rapidly acquire an OPC phenotype.

Conclusions

At birth, the ECM molecule laminin is present in a diffuse pattern upon the ventricular surface of the SVZ. Over the first few weeks of postnatal life, this surface laminin undergoes a dramatic reorganization, initially forming small puncta that later appeared to coalesce into much larger “hubs”. These hubs are then transposed to the centers of the nascent pinwheels where, by adulthood, they simultaneously contact both ependymal cells and NSC apical processes. This process takes weeks to occur and appears to be regulated by the coordinated merging of smaller laminin puncta into larger ones. Laminin is enriched on the emerging ependymal cell population which help generate and assemble the laminin hubs through the laminin receptor dystroglycan.

Dystroglycan also plays a key role in the lineage progression of ependymal cells as well as their ability to organize themselves into pinwheel structures with properly localized cilia. This indicates a reciprocal axis for dystroglycan and laminin, as dystroglycan helps mediate laminin-based signals into the cell while simultaneously organizing and maintaining laminin at the apical surface. Additionally, dystroglycan in the postnatal SVZ is a key regulator of neural stem cell maintenance and gliogenesis. Dystroglycan helps regulate NSC proliferation at birth, entry of these NSCs into the oligodendrogenic lineage, and proliferation within the oligodendrogenic progenitor pool.

Figure II-1

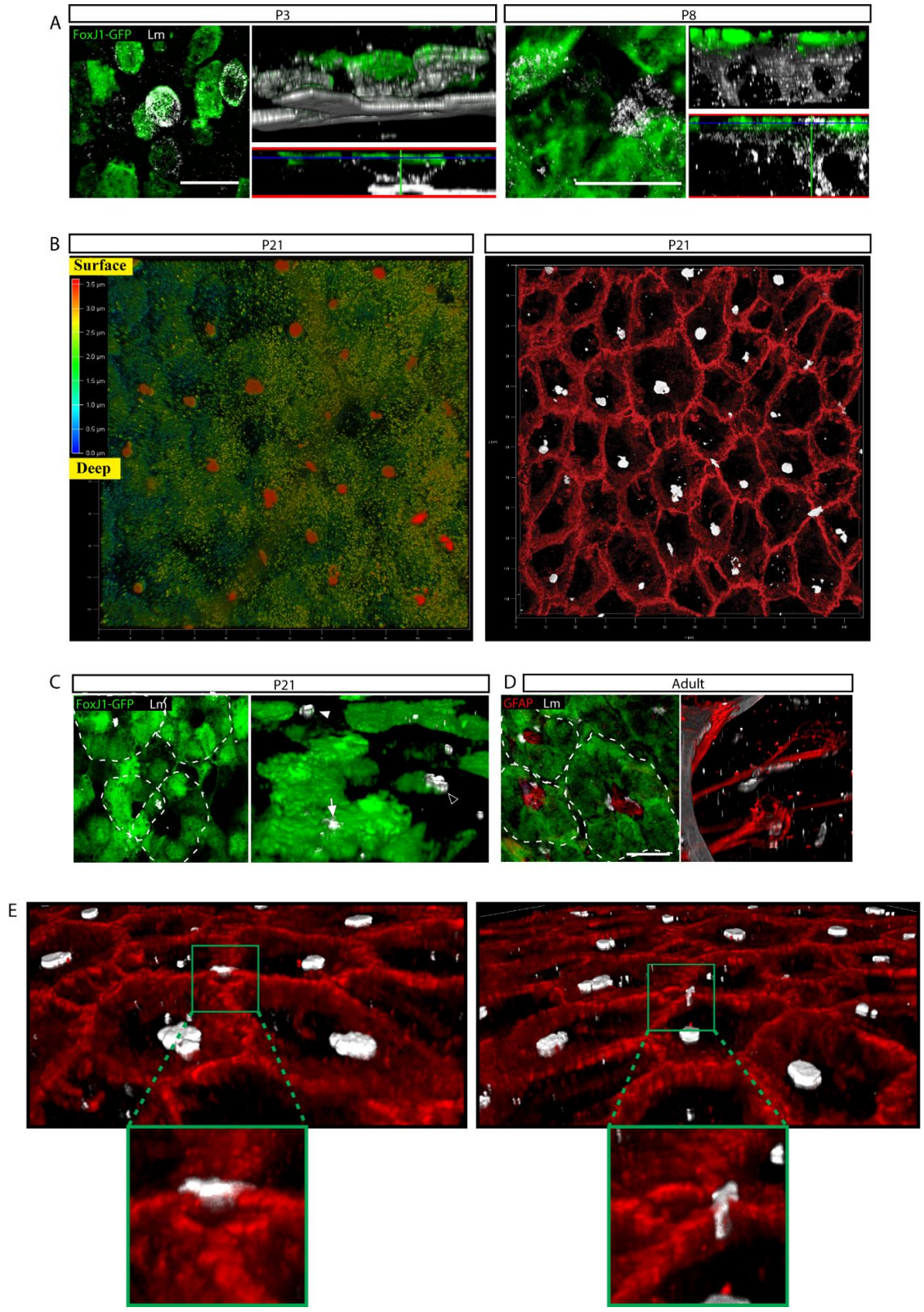
A
P3
FoxJ1-GFP Lm
P8
B
P21
Surface
Deep
P21
C
P21
FoxJ1-GFP Lm
D
Adult
GFAP Lm
E

Figure II-1: Laminin-rich ECM Structures Develop at the Ventricular Surface During the Early Postnatal Period.

(A) Laminin immunoreactivity defines the vascular basal lamina in a SVZ wholemount from a WT postnatal day 0 (P0) mouse. Box denotes anterior-dorsal area used for wholemount analysis. A, *anterior*; P, *posterior*.
(B) Confocal stack projections from WT wholemounts over the first postnatal week highlighting vascular and extra-vascular laminin. Extensive blood vessel-fractone networks (arrowheads) and ECM "hubs" (arrows) are visible by P8. Bottom panels: XZ projections, with ventricular surface at top.
(C) En face views of laminin and β-catenin immunoreactivity in WT wholemounts illustrate the dramatic ECM reorganization from P3 to P21. Ventricular surface laminin is enriched on emerging ependymal cells, and has begun the process of forming larger aggregates by P8. Ependymal-cell associated laminin is localized to hubs by P21 (arrowheads), with many hubs at the interface between stem and ependymal cells (arrows)
(D) 3D reconstructions of ventricular surface laminin and β-catenin in the WT V/SVZ at P21 illustrating ventricular surface laminin hubs. Bottom panels: In some instances, tethers appear to bridge laminin hubs, even across cell boundaries.
(E) Overhead view of region projected in D. In this representative field, laminin aggregates of various sizes can be seen in various stages of merging. Some hubs are still at the surface of ependymal cells, while others have translocated to the centers of the pinwheels.
(F) Proposed order of laminin hub assembly from smaller aggregates. Laminin hubs appear to first be brought into close proximity with each other. Next, hubs contact each other before but are still visible as two distinct structures, before beginning to merge with each other. Finally, a single larger hub is formed as the two aggregates coalesce.
(G) Some hubs appear to contact and merge with each other through thin, tendril-like laminin structures that may follow tortuous paths before connecting the two hubs.

Figure II-2

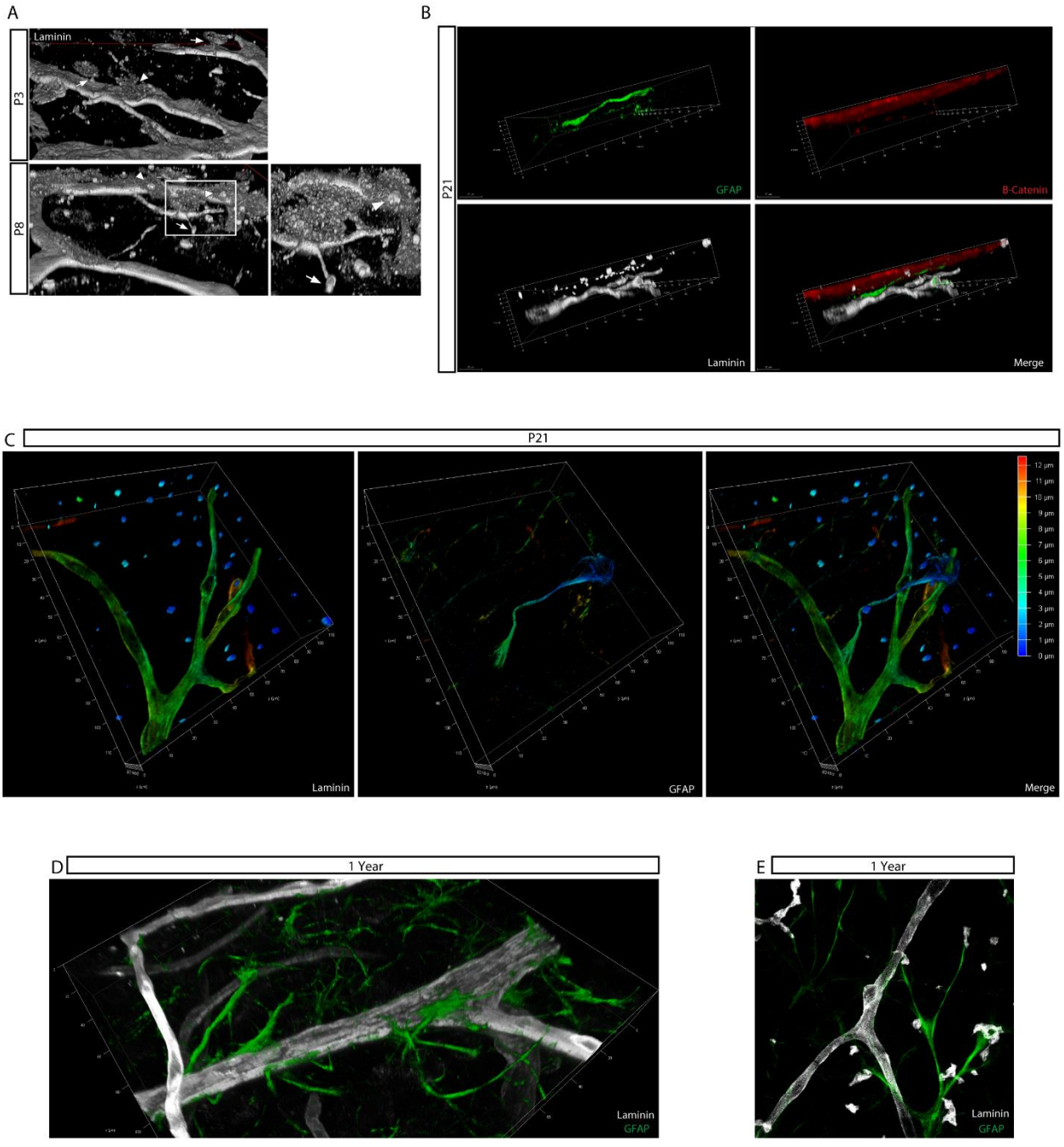
A
Laminin
P3
P8
B
P21
GFAP
B-Catenin
Laminin
Merge
C
P21
Laminin
GFAP
Merge
12 µm
11 µm
10 µm
9 µm
8 µm
7 µm
6 µm
5 µm
4 µm
3 µm
2 µm
1 µm
0 µm
D
1 Year
Laminin
GFAP
E
1 Year
Laminin
GFAP

Figure II-2: Ependymal and Vascular ECM Form Distinct Compartments in the V/SVZ

(A) 3D reconstructions of confocal stacks showing laminin immunoreactivity in the wild-type V/SVZ. At P3, ventricular surface cell-associated laminin is contiguous with the blood vessel basal lamina either directly (arrowheads) or via "tethers" (arrows). At P8, ventricular surface "hubs", (arrowheads) and "bulbs", deeper in the SVZ at fractone termini (arrows), are also observed.
(B) Transverse view of a 3D construction of the WT V/SVZ as visualized by GFAP, β-catenin, and laminin immunoreactivity. Ventricular surface towards the top left. The apical region is marked by extensive adherens junctions (red), co-localizing in the Z-axis with laminin hubs (white). Deeper beneath the surface, the vasculature can be visualized by its basal lamina (white). Adult neural stem cells seen here in green, inhabit the region between these two ECM elements.
(C) 3D reconstruction of the WT V/SVZ as visualized by laminin (left panel), GFAP (middle panel), and both (right panel). In these images, antigens are color-coded based on their depth in the SVZ, with blue representing the ventricular surface, and red representing the deepest structures. Surface and vascular laminin are distinguishable by their morphology and depth. The GFAP+ neural stem cell contacts both vascular ECM as well as surface laminin hubs.
(D) 3D reconstruction of the SVZ of a 1 year old mouse. In the aged WT V/SVZ, GFAP+ neural stem cells continue to maintain extensive contact with the vascular basal lamina.
(E) En face view of a 1 year old WT mouse wholemount. At this age, neural stem cells continue to maintain contact with surface laminin hubs. Some laminin hubs in the aged animal now display a convoluted elongated morphology, while others maintain a "donut hole" at their center.

Figure II-3

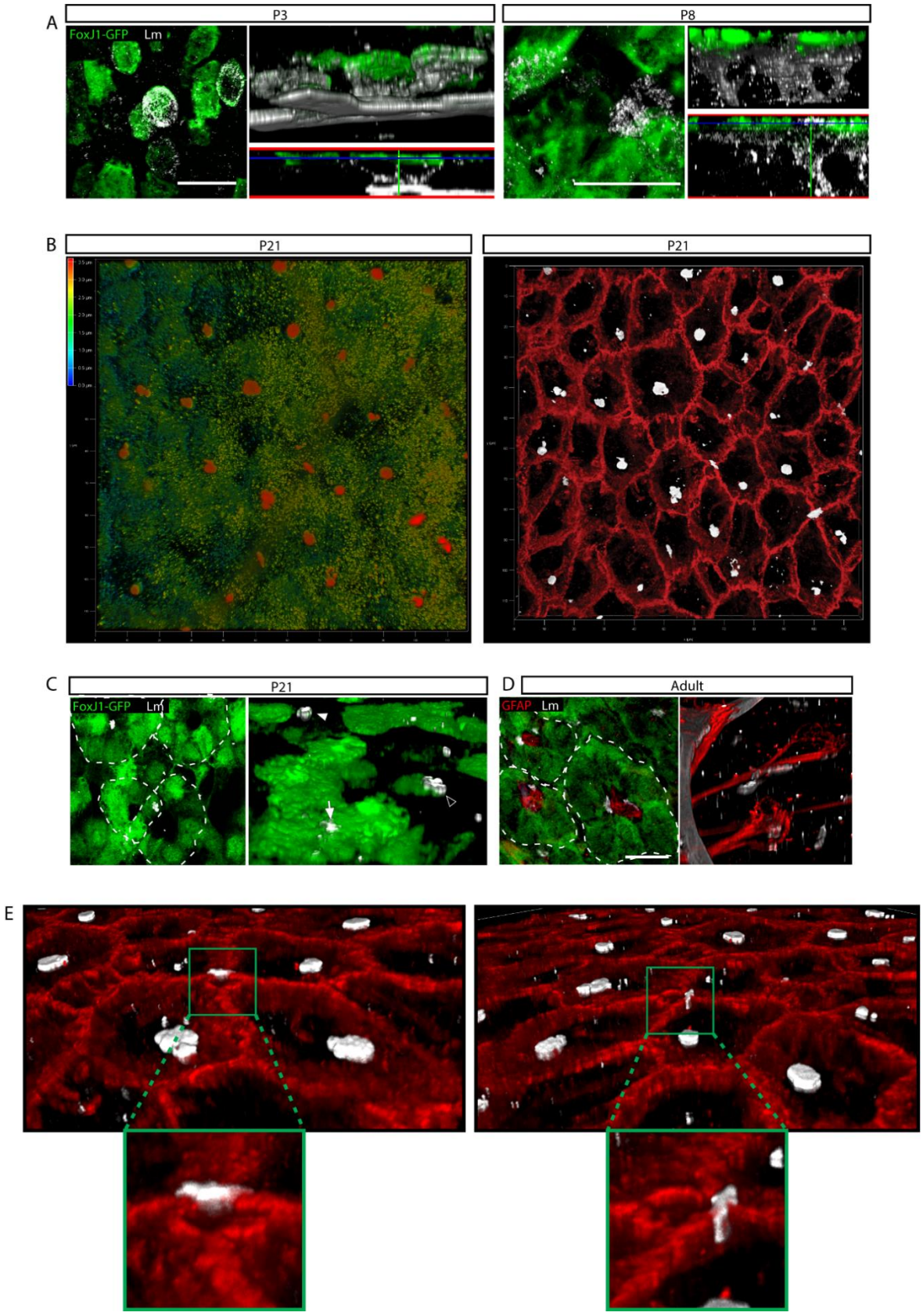

Figure II-3: Laminin Hubs Form on Ependymal Cell Surfaces And Translocate to Pinwheeel Centers

(A) IHC for GFP and laminin in P3 and P8 FoxJ1-GFP mice. Left panels: en face view of P3 and P8 wholemounts showing emerging ependymal cells (green) and surface-associated laminin (white) at the apical surface of these cells. Top right panels: 3D reconstructions of confocal stacks showing laminin tethers connecting immature ependymal cells to the vasculature basal lamina. Bottom right panels: orthogonal slices through the top panel.
(B) Left panel: High-gain depth-coded en face view of laminin in a WT P21 wholemount, with red indicating laminin at the ventricular surface and green and blue indicating laminin below the apical surface. Hubs can be seen as red dots. Right panel: en face view of the same region with β-catenin in red and laminin in white. Putative regions of neural stem cell processes at the centers of pinwheels colocalize with relatively laminin-sparse regions in the left panel.
(C) Left panel: en face view of a P21 wholemount from a FoxJ1-GFP mouse, with dashed lines delineating individual pinwheels. Right panel: 3D reconstruction of the same field. At P21, VZ laminin is largely restricted to hubs, associated with ependymal cell surfaces (arrow), relocated to the center of pinwheels (closed arrowhead), or in the process of relocating (open arrowhead).
(D) Left panel: en face view of an adult FoxJ1-GFP wholemount. In the adult mouse, most laminin hubs are localized to the centers of pinwheels at the interface between the apical processes of type B GFAP+ stem cells (red) and ependymal cells (green). Right panel: 3D reconstruction.
(E) 3D reconstructions of the right panel in (B). Some laminin hubs have already translocated to the centers of pinwheels and positioned themselves at the NSC-EC interface by P21. Left panel: view of laminin hub from a vector leading away from the apical stem cell process. Apical processes of stem cells directly contact laminin hubs, with absence of adherens junctions at this point. Right panel: rotated view of laminin hub from the ependymal cell side showing direct ependymal cell-laminin hub interaction here as well.

Figure II-4

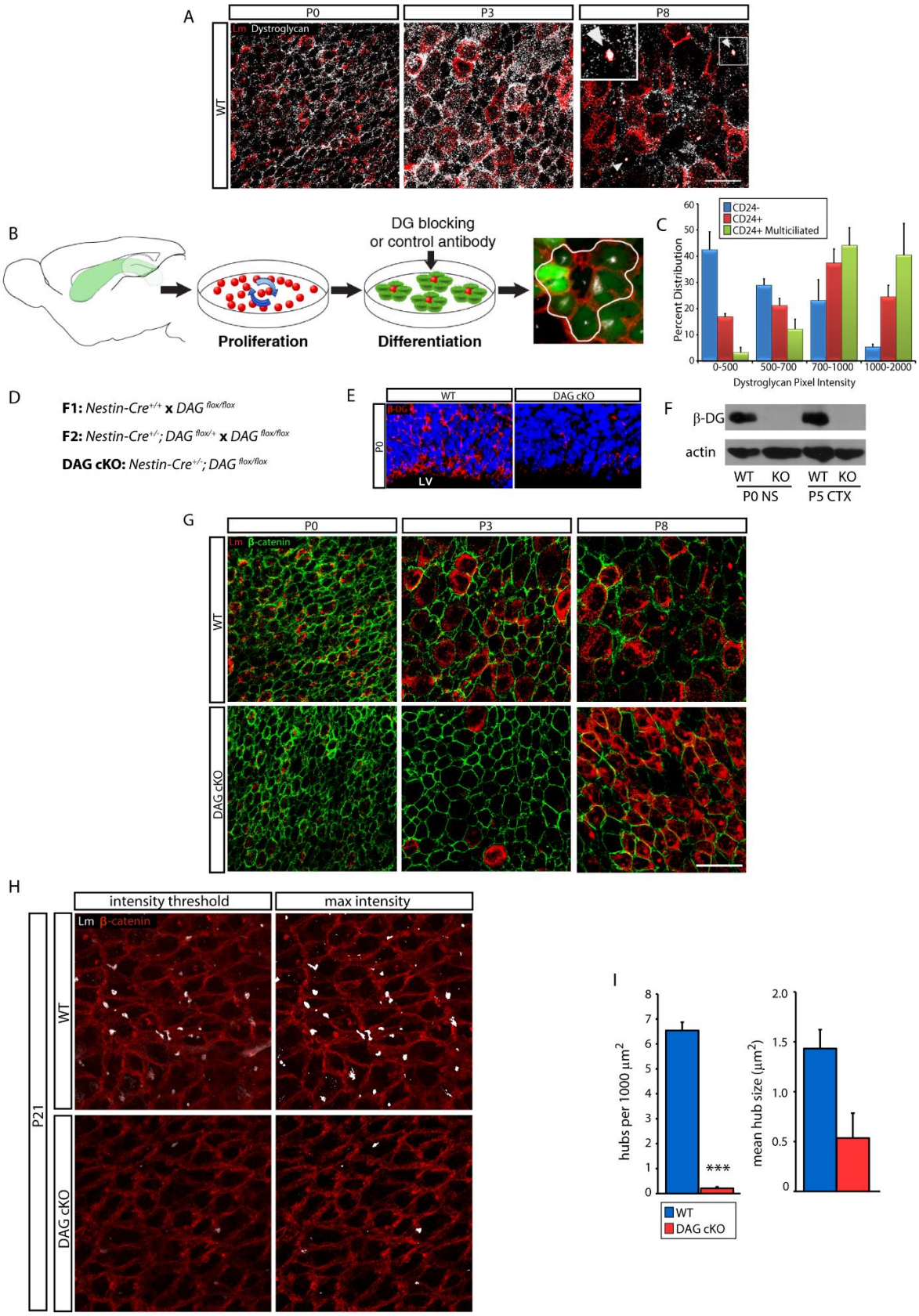
A
P0
P3
P8
Lm Dystroglycan
WT
B
DG blocking
or control antibody
Proliferation
Differentiation
C
CD24-
CD24+
CD24+ Multiciliated
Percent Distribution
0-500
500-700
700-1000
1000-2000
Dystroglycan Pixel Intensity
D
F1: Nestin-Cre+/+ x DAG flox/flox
F2: Nestin-Cre+/-; DAG flox/+ x DAG flox/flox
DAG cKO: Nestin-Cre+/-; DAG flox/flox
E
WT
DAG cKO
β-DG
P0
LV
F
β-DG
actin
WT KO WT KO
P0 NS
P5 CTX
G
P0
P3
P8
Lm β-catenin
WT
DAG cKO
H
intensity threshold
max intensity
Lm β-catenin
P21
WT
DAG cKO
I
hubs per 1000 µm2
***
mean hub size (µm2)
WT
DAG cKO

Figure II-4: Dystroglycan Regulates Ventricular Surface Laminin Accumulation and Retention

(A) En face views of laminin and dystroglycan IHC in WT SVZ whole mounts reveals developmental upregulation on ependymal cell surfaces. By P8, laminin- and dystroglycan-positive hubs are apparent (arrowheads, inset)
(B) Schematic of SVZ ependymal cell cultures. SVZ cells were isolated from P0 mice, dissociated, and allowed to proliferate for 3-4 days until confluent. Upon confluence, cells were switched to low-serum media and allowed to differentiate. A typical ependymal cell cluster at 7 days in differentiation media is outlined (far right; GFP, green; b-catenin, red; g-tubulin, white)
(C) Quantification of dystroglycan intensity in CD24-, CD24+, and CD24+ multiciliated cells in SVZ ependymal cell cultures at 7 days differentiation.
(D) Breeding scheme used generate DAG cKO mice
(E) IHC against β-dystroglycan in coronal sections taken from P0 WT and DAG cKO mice. LV: lateral ventricle.
(F) Western blotting against β-dystroglycan on lysates taken from i) second passage neurospheres isolated from P0 WT and DAG cKO mice and ii) cortices from P5 WT and DAG cKO mice.
(G) En face views of laminin and β-catenin in WT and DAG cKO wholemounts taken at P0, P3, and P8. DAG cKO mice display substantial dysregulation of laminin immunoreactivity at the ventricular surface throughout the first week of postnatal life.
(H) Laminin and β-catenin IHC in WT P21 SVZ whole mounts to detect laminin+ ECM hubs. Images with Vertical pairs of images have matched intensity thresholds
(I) Left Graph: Quantification of laminin hubs per 1,000 μm2. ***$p < 0.001$, Student's t test. Right Graph: Quantification of mean hub size.

Figure II-5

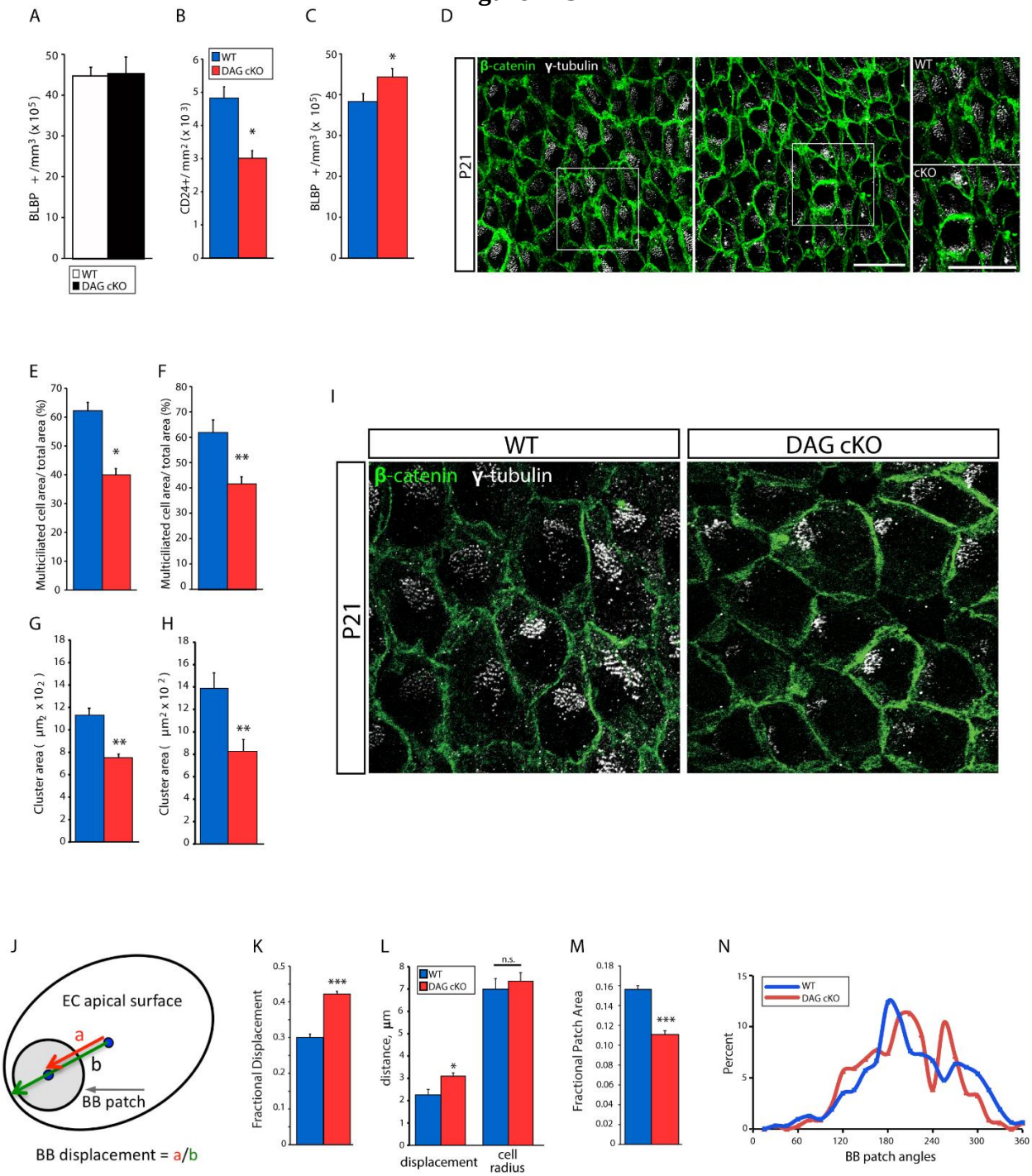
A
B
C
D
BLBP +/mm³ (x 10⁵)
WT
DAG cKO
CD24+/ mm² (x 10 ³)
β-catenin γ-tubulin
P21
WT
cKO
E
F
Multiciliated cell area/ total area (%)
G
H
Cluster area (µm² x 10 ²)
I
WT
DAG cKO
β-catenin γ-tubulin
P21
J
EC apical surface
a
b
BB patch
BB displacement = a/b
K
Fractional Displacement
L
distance, µm
displacement
cell radius
n.s.
M
Fractional Patch Area
N
Percent
BB patch angles

Figure II-5: Dystroglycan Regulates Ependymal Cell Maturation and Planar Cell Polarity

(A) Quantification of BLBP+ cell density at P0 in WT and DAG cKO mice.
(B) Quantification of ventricular surface CD24+ cells at P3. *$p < 0.05$, Student's t test.
(C) Quantification of BLBP+ cells in the dorsal SVZ at P3. *$p < 0.05$
(D) β-Catenin and γ-tubulin IHC in P21 SVZ whole mounts (higher magnification inset, right panels).
(E) Quantification of relative surface area coverage of multiciliated cells in P8 WT and DAG cKO whole mounts (*$p < 0.05$, Student's t test)
(F) Quantification of relative surface area coverage of multiciliated cells in P21 WT and DAG cKO whole mounts (**$p < 0.01$, Student's t test)
(G) Quantification of average cluster size in P8 SVZ whole mounts. **$p < 0.01$, Student's t test.
(H) Quantification of average cluster size in P21 SVZ whole mounts. **$p < 0.01$, Student's t test.
(I) Higher-magnification view of β-catenin and γ-tubulin IHC in P21 whole mounts highlights basal body (BB) patches.
(J) Schematic depicting BB patch analysis on ependymal cell apical surfaces. BB displacement is the length from the apical surface center to the BB patch center (''a''), over the length from the apical surface center to the cell perimeter (''b''), with b being measured along the vector of a.
(K) Quantification of fractional displacement of BB patches (***$p<0.001$; n = 337 cells from three mice per genotype).
(L) Absolute distance measurements of BB patch displacement (*$p<0.05$) and cell radii ($p = 0.432$; n = 3). n.s., not significant
(M) Quantification of fractional patch area (n = 315 [WT] or n = 337 [KO] cells from three mice per genotype; ***$p < 0.001$).
(N) Distribution of BB patch angles (each BB patch angle normalized to the average BB patch angle per field). n = 315 (WT) or n = 337 (DAG cKO) cells from three mice per genotype, $p = 0.0860$, Watson's U2 test.

Figure II-6

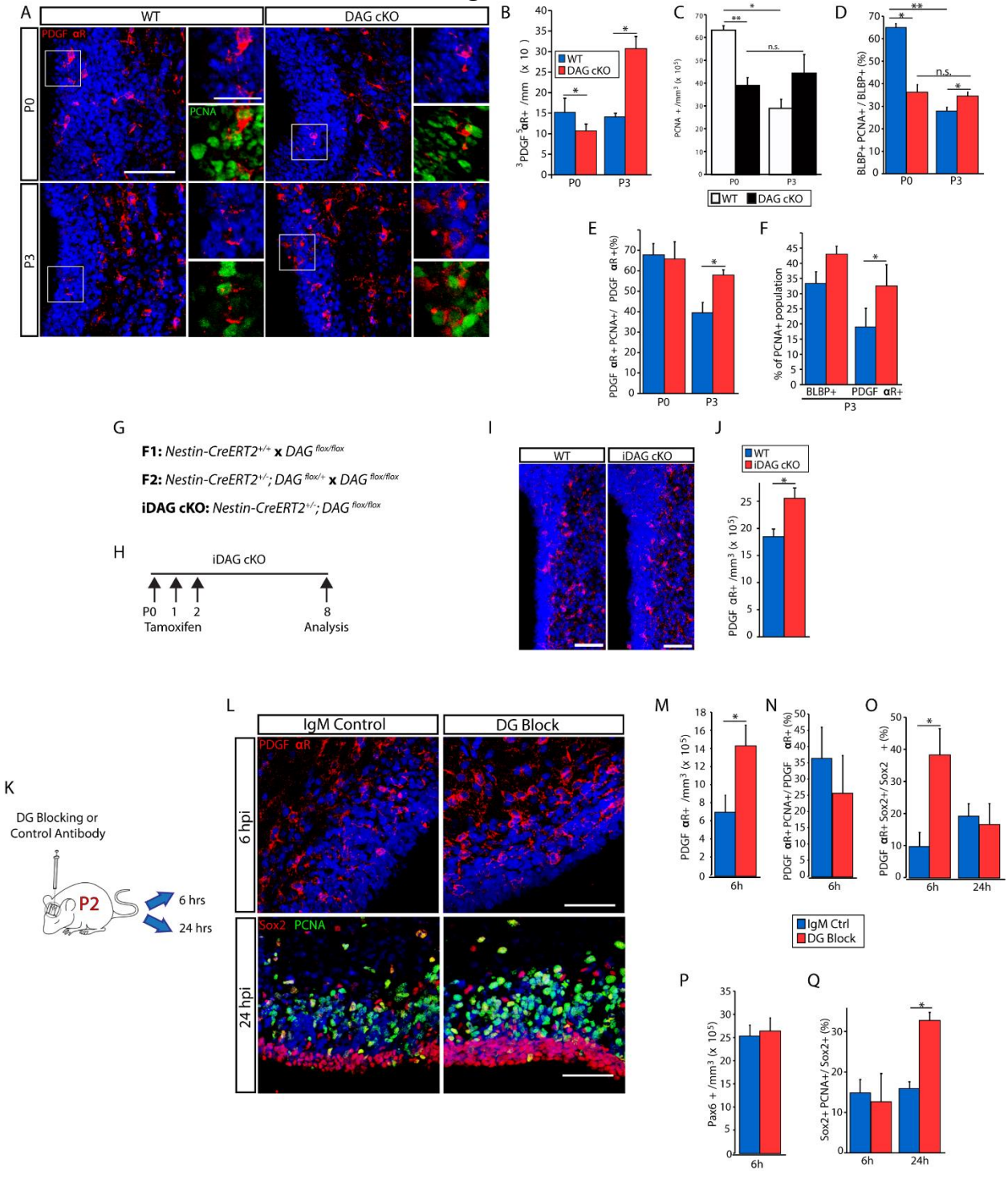
A
WT
DAG cKO
PDGF αR
PCNA
P0
P3
B
WT
DAG cKO
P0
P3
C
P0
P3
WT
DAG cKO
n.s.
D
n.s.
P0
P3
E
P0
P3
F
BLBP+
PDGF αR+
P3
G
F1: Nestin-CreERT2+/- x DAG flox/flox
F2: Nestin-CreERT2+/-; DAG flox/+ x DAG flox/flox
iDAG cKO: Nestin-CreERT2+/-; DAG flox/flox
H
iDAG cKO
P0 1 2
Tamoxifen
8
Analysis
I
WT
iDAG cKO
J
WT
iDAG cKO
K
DG Blocking or
Control Antibody
P2
6 hrs
24 hrs
L
IgM Control
DG Block
6 hpi
24 hpi
PDGF αR
Sox2 PCNA
M
6h
N
6h
O
6h
24h
IgM Ctrl
DG Block
P
6h
Q
6h
24h

Figure II-6: Dystroglycan Regulates Postnatal SVZ Gliogenesis

(A) PDGFRα IHC staining of the dorsal SVZ in coronal sections from P0 and P3 WT and DAG cKO mice. OPC proliferation is indicated by PCNA co-IHC (insets). Gliogenesis is delayed in the DAG cKO SVZ, with fewer OPCs present at P0 (top panels) but no decrease in OPC proliferation (insets). At P3 (bottom panels), OPC numbers in DAG cKO mice far exceed those of WT littermates and newborn DAG cKO OPCs are more proliferative.
(B) Quantification of PDGFRα+ cell densities in the SVZ of P0 and P3 WT and DAG cKO mice (*$p < 0.05$, Student's t test)
(C) Quantification of PCNA+ cell density in the SVZ of WT and DAG cKO mice at P0 and P3 (*$p < 0.05$, **$p < 0.01$, Student's t-test)
(D) Quantification of BLBP+ cell proliferation (i.e., PCNA+) at P0 and P3 in WT and DAG cKO mice (*$p < 0.05$, **$p < 0.01$, Student's t test).
(E) Quantification of PDGFRα+ cell proliferation (i.e., PCNA+) in P0 and P3 WT and DAG cKO mice (*$p < 0.05$, Student's t test).
(F) Quantification of BLBP+ and PDGFRα+ cells within the PCNA+ population in P3 WT and DAG cKO mice (*$p < 0.05$, Student's t test).
(G) Breeding scheme used generate iDAG cKO mice
(H) Time line of tamoxifen injections and cellular analysis for inducible dystroglycan conditional knockout mice (iDAG cKO).
(I) PDGFRα IHC in the dorsal-lateral SVZ in coronal sections from P8 WT and iDAG cKO mice.
(J) Quantification of PDGFRα+ cell density in the SVZ of P8 WT and iDAG cKO mice (*$p < 0.05$, Student's t test).
(K) Schematic of dystroglycan blocking antibody injections into the lateral ventricles
(L) Upper panels: IHC to detect PDGFRa in the dorsal SVZ in coronal sections taken from control or dystroglycan-blocking antibody-injected rats at 6 hpi. Lower panels: IHC to detect Sox2 and PCNA at 24 hpi.
(M) Quantification of PDGFRα+ OPC densities in the SVZ 6 hpi of control or DG-blocking antibodies (*$p < 0.05$, Student's t test).
(N) Quantification of PDGFRα+ OPC proliferation in the SVZ at 6 hpi with control or DG-blocking antibodies.
(O) Quantification of PDGFRα expression within Sox2+ cells (NSC/IPCs) at 6 and 24 hr post antibody injection (*$p < 0.05$, Student's t test).
(P) Quantification of Pax6+ neuronal progenitor densities in the SVZ 6 hpi of control or DG-blocking antibodies.
(Q) Quantification of Sox2+ cell proliferation (PCNA+) at 6 and 24 hr post antibody injection (*$p < 0.05$, Student's t test).

Chapter 3: Dystroglycan Modulates Notch Signaling to Regulate Ependymal and Oligodendrogenic Maturation

Dystroglycan Suppresses Notch to Promote Ependymal Cell Maturation

Recent work into the transcriptional control underlying the development and maturation of ependymal cells has demonstrated that a complicated cascade of signals are involved in coordinating the timely emergence of these cells. Mcidas (also known as multicillin, (MCI)) and GemC1/Lynkeas (GC1) are two of the earliest known factors involved in this process. These coiled-coil proteins are expressed in periventricular cells around E16, just as ECs are specified from radial glia, and their expression follows the same spatio-temporal organization pattern as the emergence of ependymal cells (posterior to anterior, ventral to dorsal). [207, 260] MCI and GC1 are necessary and sufficient for RGC fate commitment to the ependymal lineage, and mediate their actions through a pathway involving, among others, the downstream effectors c-Myb and FoxJ1. FoxJ1, in particular, is a transcription factor and master regulator of ependymal cell maturation essential for regulating ciliary biogenesis and centriolar docking to the apical cell surface in all multiciliated cells, including ependymal cells. [261-264]

To explore whether dystroglycan's effects on ependymal development are due to modulation of FoxJ1 expression, we applied dystroglycan-blocking or control IgM antibodies to SVZ cultures of FoxJ1-GFP neonates, allowing us to assess FoxJ1 activation within each cell (Schematic, Fig. 1A, and Fig. 1E, top panels). In agreement with ependymal cell deficits seen in DAG cKO mice, after 7 days in differentiation-promoting medium, dystroglycan blockade *in vitro* significantly reduces the percentage of FoxJ1+ ependymal cells (49.4±5.5% of total cells vs. 71.5±5.1% in controls; Fig. 1B, top and bottom panels, 1E), as well as the proportion of FoxJ1+ cells that became multiciliated (17.5±2.2% vs. 31.8±3.1% in controls; Fig. 1C).

Additionally, dystroglycan-blocking antibodies antagonize the ability of GFP+ cells to arrange into pinwheel-like clusters, reducing cluster areas by over 50% (2.48±0.08 $x10^3$ μm^2 vs. 5.62±0.75 $x10^3$ in controls; Fig. 1D). These results indicate that blockade of dystroglycan-ligand binding impedes ependymal cell differentiation before and after FoxJ1 expression as well as organization at the multicellular level.

To further probe dystroglycan's effects on the ependymal differentiation program, we assessed *FoxJ1* expression along with that of its upstream regulators in ependymal cells – *Mcidas* (*MCI*) and *c-Myb* – in SVZ cultures treated with dystroglycan-blocking antibodies under long-term conditions (Fig. 1E). During the cell expansion phase, when SVZ cultures are proliferating, *MCI, Myb,* and *FoxJ1* mRNA levels are unchanged in the short-term (at 6 and 24 hours; data not shown). However, by the onset of maturation (when cultures are confluent), expression of *c-Myb* and *FoxJ1* are both significantly suppressed by dystroglycan blockade (0.08±0.03 fold and 0.43±0.09 fold control, respectively (Fig. 1F)). Unfortunately, at this time point, *MCI* was not reliably detectable, which made accurate determination of CT difficult (not shown). However, by day 5 in ependymal cell maturation medium, *MCI* levels were detectable and significantly lower (0.73±0.07 fold) in the dystroglycan-blocking condition compared to control. *FoxJ1* mRNA levels, while rebounding somewhat closer to wildtype levels, also remain significantly reduced at this time (0.71±0.04 fold control). Interestingly, however, *Myb* expression at this time is indistinguishable from controls (0.91±0.10 fold control) (Fig. 1F). This is consistent with previous reports indicating that during the ciliogenic program, in contrast with *FoxJ1*, *Myb* is only transiently upregulated during the differentiation process [265].

The signaling receptor Notch is a master cell fate regulator in many tissues including the brain [266] that is known to downregulate expression of *MCI, Myb*, and *FoxJ1* in ependymal

[260] and bronchial airway cells [265, 267], and suppresses acquisition of a multiciliated phenotype. [268-272] In the context of the results above, we therefore wondered whether dystroglycan regulates ependymal cell development by influencing Notch activation.

We first tested this hypothesis by treating SVZ cultures with dystroglycan blocking antibody, lysing the cells, and examining Notch Intracellular Domain (NICD) levels by western blot (Fig. 1G). Semi-quantitative densitometry analysis of the blots using a LICOR system revealed that dystroglycan blockade increased NICD levels, indicating increased activation of the Notch signaling pathway under these conditions (Fig. 1H). However, NICD levels alone are not always sufficient to determine activity of the pathway, and endogenous NICD detection in tissue can be extremely difficult due to low overall levels. A more direct measurement of Notch pathway activity is measuring the transcriptional activity of direct Notch response genes, such as those in the Hes and Hey family. [273] We therefore, decided to measure expression levels of these proteins to confirm that notch signaling was enhanced by dystroglycan loss-of-function.

Surprisingly, under long-term treatment conditions (i.e., at the onset of maturation), despite higher NICD, canonical Notch-regulated gene expression as measured by *Hes1* and *Hey1* was not significantly changed by dystroglycan blockade (1.13±0.24 and 1.16±0.13 fold control respectively). Indeed, longer-term cultures in differentiation media also showed no significant changes in *Hes1* and *Hey1* transcript levels (data not shown). As Notch signaling is upstream of *Myb* and *FoxJ1*, we wondered if notch activity might change acutely but temporarily upon dystroglycan blockade. In this set of experiments, we also examined the less commonly-used Notch target gene *HeyL,* as it had been reported to be involved in differentiation of neural cells in a non-redundant role as compared with *Hes* and *Hey* factors. [274, 275] Acute treatment with dystroglycan-blocking IIH6 antibody at this time point does indeed lead to small but significant

increases in canonical Notch-regulated gene expression, as measured by *Hes1* (1.15±0.09 fold control), *Hey1* (1.14±0.04 fold control), and *HeyL* (1.46±0.17 fold control), at 6 hours post-dystroglycan blocking antibody treatment (Fig. 1I). Of note, these changes are transient, however, as transcription of *Hes1, Hey1,* and *HeyL* returns to control levels within 24 hours (Fig. 1I and not shown). Furthermore, these effects are not mediated by changes in Notch receptor or ligand expression, as at both 6 and 24 hours, none of Notch 1-4, Jag1, 2, DLL 1, 3, 4, expression levels are significantly different from control. (Fig. 2A and B) Additionally, the Notch negative regulator Numb expression levels are unchanged from control at 6 hrs and during long-term treatment (data not shown). These data do not rule out the possibility that Notch and/or its receptors are rapidly regulated at the protein level by a number of potential mechanisms (e.g. internalization, degradation, compartmentalization, cleavage, etc.), and this possibility remains an active area of investigation in our lab.

One interesting piece of data that emerged from analysis of Notch regulation in long-term differentiating ependymal cell cultures, however, is the anomalous behavior of another downstream Notch target, Hes5. Hes5, unlike the more widely used targets Hes1 and Hey1, did not move in lockstep with the other battery of Notch effectors tested in our ependymal cell cultures. At 6 and 24 hours, Hes5 expression was not significantly changed in treatment compared to control in ependymal cultures (0.81± 0.09 and 0.95± 0.03 fold control respectively) (Fig. 2C), but by differentiation onset, Hes5 expression had plunged four-fold (0.25±0.04 fold control) (Fig. 2D). By the third day of differentiation culture, Hes5 expression had recovered, and remained unchanged compared to control by the fifth day in differentiation conditions, the last day tested (0.95±0.05 and 1.10±0.05, respectively) (Fig. 2D).

At the time of these experiments, while the Notch/MCI/Myb/FoxJ1 cascade had been described in parts in other models, whether this pathway was also the regulator of ependymal differentiation in brain development had not yet been fully explored. As such, we next wanted to test whether this putative pathway was indeed downstream of Notch signaling and sufficient to rescue the deficiencies in ependymal cell differentiation genes, (e.g., *MCI*) seen with dystroglycan loss-of-function. We therefore used the γ-secretase inhibitor DAPT, which prevents the S3 Notch cleavage event and therefore its activation. First, we confirmed that DAPT treatment significantly blocks canonical notch gene expression by 6 hours post-treatment and for at least 24 hours post-treatment, and does so both in the presence and absence of dystroglycan-blocking antibodies (Fig. 3B, C). We then sought to develop a timeline of the effect of dystroglycan blockade in the differentiation pathway. At 6 hours, dystroglycan blockade, while upregulating notch downstream target expression (Fig. 1I), had not yet affected *MCI or Myb* expression (data not shown). At 24 hours, however, the change in *Hes1, Hey1*, and *HeyL* expression had normalized, but as with longer-term cultures (Fig. 1F), we found that dystroglycan block decreased *MCI* expression (0.81±0.02 fold control, Fig. 3D). Conversely, DAPT alone increases *MCI* expression (1.27±0.05 fold), and the addition of DAPT to dystroglycan blocking antibodies fully rescues the dystroglycan loss-of-function effect (1.03±0.05 fold control), indicating Notch activation is required for the dystroglycan loss-of-function phenotype. While dystroglycan blockade for 24 hours had not yet significantly affected *Myb* expression (0.94±0.04 fold control) (which was not significantly reduced until 72 hours (Fig. 1F), we did find that DAPT treatment significantly increased *Myb* and *MCI* expression and that, interestingly, the addition of dystroglycan blocking antibodies returns *Myb* and *MCI* expression in DAPT-treated cells to control levels, indicating that dystroglycan likely also

regulates *MCI/Myb* expression independent of Notch. Finally, we checked to see whether DAPT application had an effect on dystroglycan expression, which might indicate a feedback regulation mechanism active in this system. Under the differentiation conditions discussed here, DAPT treatment increased dystroglycan expression (1.45±0.07 fold control) at 6 hours, but this effect disappeared by 24 hours, (0.80±0.48 fold control) and despite high variability at this time point, there was no trend towards increased dystroglycan expression at this time (Fig. 3E). There was no significant difference in proliferating cultures at either 6 or 24 hours (1.04±0.03 fold control and 1.14±0.13 fold control respectively) (Fig. 3E).

We next examined whether the effects of DAPT could rescue the ability of dystroglycan blocking antibodies to suppress ependymal cell differentiation and *FoxJ1* expression. Dystroglycan-blocking antibodies significantly reduce the percentage of multiciliated cells at day 3 (3.20±0.76% vs. 6.80±0.55% in control; Fig. 3F, G), consistent with the results of longer-term blockade. Conversely, DAPT treatment to block Notch activation *increases* the percentage of multiciliated cells (9.59±0.61% vs. 6.80±0.55 in control). Finally, treating with both DAPT and dystroglycan blocking antibody engenders a "rescue" of the dystroglycan loss-of-function phenotype such that the percentage of multiciliated cells is no longer different from that in control cultures (6.43±0.8% vs. 6.80±0.55% in control). Additionally, DAPT plus dystroglycan block (6.43±0.80%) leads to significantly fewer multicilliated cells compared with DAPT treatment alone (9.59±0.61). However, two factors remained potential confounding factors in the interpretation of these results. First, DAPT, as a γ-secretase inhibitor, can have off-target effects on other signaling pathways that rely on γ-secretase activity. Additionally, after cleavage, the NICD fragment can function through both canonical and non-canonical pathways to exert its effects. We therefore used the peptide inhibitor SAHM1, to specifically disrupt the Notch-RBPJ-

MAML1 transcriptional activator complex, and observed similar results in a set of experiments conducted with vehicle control, DAPT, and SAHM1 with and without IIH6 administration (Data not shown), giving us greater confidence that these phenotypic effects on ependymal cell maturation are mediated specifically by modulation of canonical Notch signaling. Furthermore, 2-way ANOVA of the effect of dystroglycan blockade and notch inhibition (with both DAPT and SAHM1 datasets) in these cultures indicated that both blocking dystroglycan signaling and inhibition of notch had a significant effect on the differentiation of ependymal cells ($p=0.001$ and $p=0.004$ respectively), with no significant interaction between the two factors ($p=0.11$).

We also found that DAPT increases the percentage of FoxJ1+ cells (35.46±3.95% versus 22.56±1.46% in control; Fig. 3H), a phenotype that is blocked by concurrent administration of both DAPT and dystroglycan blocking antibodies (13.64±5.78%; Fig. 3H). As we performed DAPT rescue experiments on SVZ ependymal cultures that were not fully mature (day 3 in maturation medium), we modified our cluster analysis criteria and scored the percentage of *solo* FoxJ1+ cells versus those that were adjacent to one or more FoxJ1+ cells, as a rough indicator of the degree of nascent clustering. As ependymal cells turn on FoxJ1 expression and begin to differentiate, they tend to do so in clusters; less than 15% of FoxJ1+ cells and less than 3% of multicilliated cells are found without another adjacent FoxJ1+ or multicilliated cell, respectively. Dystroglycan blocking antibody, however, significantly enhances the percentage of solo (i.e., non-clustered) FoxJ1+ cells at day 3 (9.06±1.39% versus 2.68±0.37% in the control; Fig. 3I). Interestingly, however, DAPT alone does *not* alter the fraction of solo FoxJ1+ cells (4.33±0.98%), and has no effect on the ability of the dystroglycan block to increase the percentage of solo FoxJ1+ cells. These data indicate that dystroglycan regulates pinwheel/cluster formation through a Notch-independent mechanism.

In summary, in developing ependymal cells, dystroglycan blockade (*in vitro)* or dystroglycan loss (*in vivo)* leads to upregulation of notch effector genes such as the *Hes* and *Hey* family of transcription factors as well as the expected phenotypic effects of increased Notch activation. These phenotypic effects of delayed differentiation in the ependymal lineage are due to the ability of Notch to suppress the downstream effectors multicillin, c-myb, and FoxJ1 which coordinately function to drive maturation and adoption of a multicilliated phenotype in ependymal cells. As such, these results indicate that dystroglycan normally acts to suppress Notch activation and promote ependymal cell maturation in the early postnatal SVZ. Indeed, the enrichment of dystroglycan on ependymal cells may function as a feed-forward mechanism, helping promote the timely emergence of ependymal cells after birth while simultaneously helping to generate laminin hubs.

Further, Notch activation is necessary for dystroglycan loss-of-function's effects on many aspects of ependymal cell maturation as shown by the fact that delayed ependymal maturation in the absence of dystroglycan can be rescued by simultaneous suppression of the Notch signaling pathway by DAPT. Many of the phenotypic effects of dystroglycan activity in ependymal cells are due to its suppression of canonical Notch signaling in particular, as specific inhibition of the Notch-RBPJ-MAML1 transcriptional activator complex can rescue the effect of dystroglycan blockade. The fact that DAPT treatment transiently increases dystroglycan expression indicates that Notch normally suppresses dystroglycan expression, just as dystroglycan suppresses Notch activity. This may mean that the two function in a self-reinforcing and transient "switch", wherein activation of dystroglycan suppresses Notch, which may allow for further dystroglycan expression. This switch activity appears to be reset between 6 and 24 hours after activation, however, as expression of dystroglycan is indistinguishable from control at this time. The

mechanism of how regulatory feedback loop may be enacted, however remains unknown, but may involve Hes5 paralleling recent findings of Hes5 activity in notch signaling in the spinal cord (Bennett Novitch, personal communication). It should also be noted here that dystroglycan is almost certain to also act via Notch-independent mechanisms to affect ependymal cell maturation, for instance, by regulating ependymal cell spatial organization into pinwheels, as this phenotype is not rescued by suppression of Notch signaling in dystroglycan loss-of-function.

Dystroglycan Suppresses Notch to Regulate Gliogenesis

To determine whether changes in Notch activation also occur concurrent to altered gliogenesis, we evaluated NICD levels in the P8 and P21 DAG cKO SVZ, but pilot studies by IHC did not show consistent changes in NICD levels (data not shown). In light of the transient changes observed in NICD signaling *in vitro*, however, we next decided to analyze the iDAG cKO SVZ in an attempt to understand whether there were transient changes in SVZ Notch signaling *in vivo* after dystroglycan loss of function. Given the timescale of recombination and the knowledge that dystroglycan is a relatively long-lived protein species *in vivo*, taking 2 – 3 days to be eliminated (Kevin Wright, personal communication), we decided to induce recombination over the first 3 days of postnatal life and assess for phenotypic changes at the end of the first week of postnatal life (Fig. 4A). In this model, we did in fact observe increased NICD immunoreactivity in cells lining the lateral ventricle (Fig. 4B). We also observed decreased γ - tubulin immunoreactivity along the ventricle wall (indicative of fewer maturing, multiciliated ependymal cells, confirming the reduction in multiciliated ependymal cells seen in the DAG cKO, (Fig. 3F, G). Unexpectedly, we also observed increased coverage of GFAP+ immunoreactivity within the iDAG cKO SVZ (Fig. 4B lower panels, C), with cells exhibiting a

radial glial phenotype (broad endfeet at the ventricle surface), in keeping with the persistence of the extended RGC phenotype observed in DAG cKO. Evaluating changes in Notch target gene expression in the SVZ at P3 (Fig. 4D), we found elevated levels of *Hes1* (1.91±0.28 fold control) and *HeyL* (2.05±0.29 fold control; Fig. 4E). We also observed increases in mRNA levels for *Hes5* and *Hey1* (2.19±0.49 and 1.90±0.44 fold control, respectively), as well as in pro-oligodendrogenic transcription factors stimulated by Notch activation, *Olig2* and *Sox9* (1.36±0.18 and 1.27±0.19 fold control, respectively), though these increases were variable and did not reach statistical significance.

As changes in Notch signaling in NSCs themselves might be dampened by other cellular constituents when evaluating the entire SVZ (e.g. by endothelial cells, microglia, etc.), we next generated neurospheres from the P0 wild type SVZ, treated freshly-plated dissociated NSCs with dystroglycan-blocking or control antibodies for 6 hours, and evaluated mRNA levels of Notch target genes (Fig. 4F). We found that dystroglycan block in NSCs significantly increases mRNA levels for *Hes1* (1.49±0.14 fold control), *Hey1* (1.42±0.13 fold), *Hes5* (1.72±0.22 fold), and *HeyL* (1.73±0.22 fold). Furthermore, we reasoned that changes in pro-oligodendrogenic transcription factors may be further dampened in the SVZ *in vivo* as nascent OPCs rapidly migrate out of the SVZ, whereas the neurosphere assay *in vitro* would allow us to capture this population of cells. In accordance with this hypothesis, we found significantly elevated levels of *Sox9* mRNA (1.57±0.16 fold control), a pro-oligodendrogenic transcription factor that is directly stimulated by Notch signaling [276], and, along with Sox10, responsible for expression of PDGFRα and thus PDGF-responsiveness and lineage progression in OPCs. [277] Of note, changes in notch target gene expression in dissociated neurospheres are transient, and in many cases return to normal after longer-term treatment of neurosphere cultures with dystroglycan-

blocking antibodies. Together, these data suggest that both *in vitro* and *in vivo*, dystroglycan loss-of-function acutely increases Notch-regulated gene expression. In an attempt to uncover how exactly dystroglycan regulates Notch activation, we also tested the possibility that dystroglycan loss-of-function rapidly alters the expression of Notch ligands, but did not detect any changes in Notch ligands or Numb in the neurosphere assay (not shown).

Dystroglycan Suppresses Notch and Promotes Timely Maturation in OPCs

Newly-produced OPCs migrate dorsally and tangentially out of the SVZ into the overlying corpus callosum, where they differentiate into oligodendrocytes (OLs) that myelinate axons. To determine if dystroglycan loss affected OL lineage cells *after* they exited the SVZ, we examined PDGFαR, Sox2, and CC1 (a marker for mature OL cell bodies) in coronal sections from DAG cKO and WT mice at P3 and P8 (Fig. 5A). While WT and DAG cKO mice exhibit similar numbers of OPCs in the corpus callosum at P3 (Fig 5B), dystroglycan-deficient OPCs appeared less mature, with a higher proportion co-expressing the NSC/IPC marker Sox2 (36.0±3.9% vs. 22.1±5.4% in WT; Fig. 5C). By P8, DAG cKO callosa contain more OPCs and OLs than those of WT littermates ($39.6\pm1.2x10^4$ PDGFαR+ and $30.5\pm1.2x10^4$ CC1+ cells/mm^2 vs. $22.1\pm4.2x10^4$ PDGFαR+ and $15.2\pm0.8x10^4$ CC1+ in WT; Fig. 5D), though the OPC:OL ratio does not differ significantly (not shown). Furthermore, WT and DAG cKO OPC proliferation in the corpus callosum is similar (29.9±5.7% vs. 34.7±3.4% in WT), indicating that the OPC surplus in DAG cKO white matter is the result of SVZ overproduction, and not due to increased OPC proliferation *within* the white matter. These data also suggest that OPCs produced in the DAG cKO SVZ migrate effectively to the overlying corpus callosum. We then examined MBP immunoreactivity at P8 and P21 to assess oligodendrocyte myelination capacity in DAG cKO white matter. Despite higher densities of mature OLs (Fig. 5D), MBP immunoreactivity was

surprisingly *reduced* in the DAG cKO corpus callosum at P8 relative to WT (Fig. 5E). Similarly, despite normal densities of mature OLs by P21 (not shown), MBP immunoreactivity remained lower in the DAG cKO corpus callosum than in WT littermates (Fig. 5E). Furthermore, western blots of cerebral cortices revealed lower levels of MBP protein in the DAG cKO cortex at P21 compared to that in WT littermates (not shown). By 3 months, however, MBP levels in DAG cKO cerebral cortices normalize (not shown), indicating that dystroglycan loss delays, but does not prevent, myelination by DAG cKO OLs.

To understand the effects of dystroglycan loss on oligodendrogenesis and OL lineage progression independent of niche alterations, we isolated SVZ cells from WT and DAG cKO mice at P0, cultured them as neurospheres, dissociated the cells, and allowed them to differentiate for 3 or 7 days (Fig. 5F). By detecting Sox2 (NSC/IPC), PDGFαR, NG2 (OPCs), CNPase (OLs) and MBP (myelinating OLs) we found that, in line with our *in vivo* observations, more PDGFRα+ oIPC/OPCs from DAG cKO neurospheres retain Sox2 expression than those derived from WT neurospheres (59.6±6.1% vs. 25.0±3.5% in WT; Fig. 5G), indicating a higher oIPC:OPC ratio. Dystroglycan-deficient cultures also contain higher percentages of NG2+ OPCs (56.1±4.5% vs. 39.7±2.7% in WT; Fig. 5H) and, although only a small number of CNP+ OLs had begun to differentiate from WT OPCs by day 3, almost no OLs were observed in DAG cKO cultures (1.1±0.3% vs. 4.5±1.4% in WT; Fig. 5H). After 7 days of differentiation, a significantly higher percentage of DAG cKO cells are OPCs (43.2±5.1% vs. 25.1±2.6% in WT; Fig. 5I), while the percentage of CNP+ OLs is significantly lower (5.2±1.8% vs. 12.3±3.2% in WT; Fig. 5I).

These results suggest that dystroglycan loss perturbs the timely differentiation of OL lineage cells in a niche-independent manner. We did not, however, observe any significant proliferative changes in OPCs derived from dystroglycan-deficient neurospheres (not shown),

indicating that increased oIPC/OPC proliferation in the DAG cKO SVZ is likely a result of disruption to the SVZ niche itself, e.g., loss of normal niche cellular architecture or ability to respond to niche-specific signals. Together these results suggest that from gliogenesis to myelination, dystroglycan is critical to the timely production of a competent OL pool. Furthermore, our *in vitro* results suggest that dystroglycan continues to regulate OL lineage progression outside of the SVZ stem cell niche, and thus is likely to play a role in OL maturation in white matter tracts (as is seen in the corpus callosum; Fig. 5E). In accordance with this hypothesis, we observed delayed myelination in the corpus callosum of *CNP-cre*$^{+}$*:DAG*$^{fl/fl}$ mice (DG OL-cKO), which lack dystroglycan expression specifically in myelinating glia (Fig. 5J). In DG OL-cKO mice, myelin basic protein levels are reduced in the corpus callosum at P21 (Fig. 5K-M) but reach normal levels by adulthood (not shown), suggesting that OL-specific loss of dystroglycan delays, but does not prevent myelination. In support of this, *in vitro* studies using siRNA-mediated loss of dystroglycan expression in primary OPCs result in delayed OL maturation. [278-280] These findings revealed that OPCs born in the dystroglycan-deficient brain are delayed in their maturation, and that dystroglycan deficiency specifically in OPCs leads to delayed myelination.

As Notch activation is known to enhance OPC production while delaying OL maturation [281-283], mirroring the effects of dystroglycan loss-of-function we observed, we hypothesized that loss of dystroglycan function would engender aberrant activation of the Notch signaling pathway in OPCs during their differentiation progress. We plated OPCs from neonatal rat cerebral cortices in OL-differentiation-permissive medium (Sato with T3) in the presence of dystroglycan-blocking or control antibodies (Fig. 5N). At 6 hours, dystroglycan-blocking antibodies robustly increase Notch activation, as evidenced by elevated levels of *Hes1* and *Hey1*

mRNA (2.27±0.12 and 4.24±0.76 fold control, respectively; Fig. 5O). However other Notch-regulated genes were unaffected, including *HeyL*, *Hes5*, *Olig2*, *Sox9*, and *Mash1*, in contrast to dissociated neurospheres and SVZ ependymal cell cultures, both of which show elevated *HeyL* mRNA at 6 hours following dystroglycan loss-of-function (Fig. 4B, 5K). By 24 hours both *Hes1* and *Hey1* mRNA levels return to near control levels (Fig. 5P), whereas *HeyL* mRNA levels are now significantly increased (2.02±0.20 fold control; Fig. 5P). *Mash1* mRNA levels are also significantly elevated at 24 hours following dystroglycan loss-of-function (2.81±0.50 fold control, while *Olig2* and *Sox9* mRNA levels remained unchanged. These results are consistent with delayed oligodendroglial differentiation, as among *Olig2*, *Sox9*, and *Mash1*, only *Mash1* is known to sharply decrease in expression as OPCs begin to differentiate into OLs. [284]

The results here explain the surprising findings that developmental myelination is not accelerated in the dystroglycan-deficient brain despite increased OPC production by the SVZ by demonstrating that dystroglycan loss also delays oligodendrocyte lineage maturation. The proportion of OPCs in the corpus callosum expressing the NSC/IPC marker Sox2 is increased in dystroglycan-deficient mice compared with littermate controls indicating a significant stall in differentiation. The stall in differentiation is so marked that even as these developing white matter tracts are populated with higher than normal densities of OPCs and OLs, developmental myelination in these dystroglycan-deficient mice actually lags behind wildtype. These results are consistent with previous work from our group that has shown that, at least in cultured oligodendroglia, dystroglycan regulates proliferation, maturation, and myelination (but not survival). [278-280, 285] The data in our new study, however, extend these results by showing that in OPCs, dystroglycan normally suppresses Notch signaling and specific downstream transcriptional targets of notch such as Hes and Hey genes as well as Mash1 (Ascl). Thus, in the

absence of dystroglycan function, these Notch-regulated genes remain elevated, stalling differentiation. The results taken together also confirm that OL maturation delay due to dystroglycan deficiency is niche-independent, and not due to the loss of dystroglycan in surrounding cells in the white matter tracts for example.

The fact that dystroglycan-ECM interactions promote oligodendrocyte maturation helps to resolve an open question as to how extracellular matrix regulates myelination. When LAMA2, the gene for the α2 subunit of the ECM protein laminin, is mutated or lost (as occurs in a form of muscular dystrophy known as MDC1A), patients present with white matter abnormalities, and in mouse models, oligodendrocyte differentiation and myelination is reduced. [286, 287] However, many of the phenotypes present in the LAMA2 knockout mice are not recapitulated by oligodendrocyte loss of integrin β1, a subunit of the only integrin receptor in oligodendrocytes. [288, 289] In the current study we show that the loss of dystroglycan from either neural stem cells or oligodendrocyte lineage themselves leads to delayed myelination, indicating that dystroglycan plays a distinct and non-redundant role from integrins in oligodendrocyte maturation. We postulate that dystroglycan helps oligodendroglia interact with extracellular laminin to regulate maturation and myelination through several mechanisms including suppression of Notch signaling [290] and the ability to respond to other extracellular signals including growth factors. [279, 285]

Open and Ongoing Questions in Dystroglycan Signaling

As NICD has an Ankyrin domain which are important for and regulate its function [291], and dystroglycan has the ability to bind to Ankyrin3 [292], we next hypothesized that dystroglycan may directly bind notch to regulate its activation. As protein levels of dystroglycan

and NICD obtained from mice and primary cell culture proved relatively low for these analyses, we switched to cell line models for this analysis. We expressed a GFP-tagged construct of the dystroglycan intracellular domain and either a Myc/6xHis-tagged full-length Notch1 or empty vector in HEK293T cells, and pulled down Notch1 to test whether any dystroglycan was bound. We did not find any evidence for direct binding, however, making this possibility less likely (FIG 6A, B). It is nonetheless possible, though, that this model system is simply not appropriate to study binding as HEK293T cells may simply not utilize dystroglycan in the same way that neural progenitor cells do. It is also possible that interaction between Notch and dystroglycan requires specialized glycosylation steps for Notch (or, less likely, for the dystroglycan intracellular domain) not normally carried out in these cells. Muscle cells endogenously express dystroglycan, and so we next transfected the C2C12 myoblast line with the intracellular domain of dystroglycan and full-length Notch1, and found no evidence of direct binding in this set of experiments either, though the transfection efficiency in this cell line was significantly lower than in the HEK293T cells, and therefore, conditions may require further refinement. (Data not shown) As such, further studies in this vein are warranted and ongoing.

While dystroglycan's ability to regulate notch signaling does appear to be critical for many of its effects, other signaling pathways are likely involved in mediating dystroglycan's phenotypic effects. Indeed, our data on pinwheel formation *in vitro* show that some of these defects cannot be rescued by globally suppressing Notch activation in these cells. We therefore blocked dystroglycan binding *in vitro* and looked for changes in other various candidate signaling pathways not only to identify signaling pathways modulated by dystroglycan, but also to understand the global changes in cell-signaling machinery taking place upon dystroglycan loss of function.

As discussed earlier, dystroglycan has a variety of binding partners that may be involved in transducing its signals into the cell, including ERK and Focal Adhesion Kinase (FAK). Additionally, we have shown that in oligodendrocytes, dystroglycan mediates responsiveness to insulin-like growth factor1 (IGF1). [279] We thus sought to understand whether these pathways were involved in dystroglycan signaling in the SVZ. We began by treating SVZ cultures with either IIH6 blocking antibody or IgM control antibody under both proliferating and differentiation conditions and performing western blot analyses. There were no changes in total protein levels of extracellular regulated kinase (ERK), pERK, or IGFR1 under proliferation or differentiation conditions (thought there were trends for an increase in IGFR1 levels upon dystroglycan block). (Proliferation: 0.90±0.16, 0.88±0.08, 1.24±0.11; Differentiation: 1.09±0.10, 0.87±0.13, 1.24±0.15 fold change respectively). We also examined total protein levels of FAK as well as its phosphorylation at sites 397 and 576 during proliferation, but found no change under these conditions (1.18±0.11 and 1.13±0.17 fold change respectively).

Interestingly, however, preliminary data indicate that the cyclin dependent kinase inhibitor p27 may be regulated by dystroglycan signaling in SVZ cells. Dystroglycan has the potential ability to regulate p27 protein levels and phosphorylation through a variety of means. For example, laminin binding to dystroglycan enhances phosphorylation at its tyrosine 890 site [293], which in turn regulates dystroglycan's ability to bind other partners such as utrophin through its WW domain. [294-296] Dystroglycan has been shown to bind the E3 ubiquitin protein ligases WWP1 and WWP2 through its WW domain. [297] Both WWP1 and 2 are known to target p27 for degradation as a mechanism involved in the physiological delaying of cellular senescence. Additionally, dystroglycan binds protein phosphatase 1 and Src family kinases [298, 299], enzymes involved in regulating p27 phosphorylation and expression. [300, 301]

We therefore hypothesized that interrupting dystroglycan-laminin interactions may alter p27 levels at the protein level through degradation or dephosphorylation. Treatment of SVZ cultures with IIH6 blocking antibody under proliferation conditions results in increased total p27 protein levels (1.26±0.08 fold control), but with the concomitant disappearance of one of the two protein bands normally detected by western blot under denaturing conditions (Fig. 6C). This regulation of p27 likely occurs at the protein level, as transcription of p27 is unchanged during proliferation, as well as at days 3 and 5 in differentiation medium (0.94±0.11, 0.82±0.15, 0.85±0.14 fold change respectively) (Fig. 6D). (A similar pattern occurs during proliferation, and on PDL substrate (data not shown). While we have not yet confirmed the identity of the upper band, this band has been reported to be a phosphorylated moiety of p27 in the literature. [302] Depending on the site, phosphorylation of p27 can significantly reduce its stability, and is required for promotion of degradation by some E3 ligases. [303] Thus, the loss of phosphorylated p27 may reflect either increased or decreased stability (as a consequence of reduced phosphorylation or the promotion of degradation of the already-phosphorylated p27). The phosphorylation patterns of p27 and their relationship to cell cycle and cell quiescence and activation are complex [304-306], thus further studies are required before any meaningful conclusions can be made about the effect of dystroglycan blockade on p27 activity. However, these data indicate that dystroglycan regulates p27 in a laminin-binding dependent manner. Future studies include determining the identity of these two bands, localization of p27, and cell-cycle analysis in primary cells upon dystroglycan blockade. Pilot studies blocking dystroglycan binding in the U87MG glioma cell line on PDL or Laminin show no change in cell growth rates at concentrations up to 50 ug/uL IIH6. IIH6 application also does not alter cell-cycle progression in these cells as measured by propidium iodide flow cytometry analysis (data not shown).

However, the role of dystroglycan in cell-cycle progression in non-cancerous cells remains to be determined.

Another pathway that may serve as a potential effector for dystroglycan signaling is the sonic hedgehog pathway. The sonic hedgehog (Shh) signaling pathway is an important regulator of neural stem cell activation and generation of the oligodendrogenic lineage. [307, 308] Interestingly, it has recently been demonstrated that the responsiveness of neural precursor cells to Shh is enhanced by notch signaling. [309] We thus tested whether dystroglycan loss of function modulated sonic hedgehog signaling *in vitro.* Under proliferating conditions over 3 days, treatment with dystroglycan-blocking antibody reduces the expression of the Shh pathway response genes Gli1, Gli2, and Gli3 (0.26±0.10; 0.52±0.13; 0.58±0.11 fold control respectively), indicating that the sonic hedgehog pathway is less active in these cells (Fig. 7A). In these cultures, expression of Shh is unchanged, and DAPT also has no effect on Shh expression as well (Fig. 7B), suggesting that it may be the ability to respond to or secrete Shh and not Shh production itself that is modulated by dystroglycan blockade.

Interestingly, these changes depend on the temporal context – acute treatment with dystroglycan blocking antibody does not abrogate Gli1 expression. Under these conditions, DAPT also does not have a significant effect on Gli1 expression, but joint treatment with IIH6 and DAPT may potentiate the effects of each as co-treatment leads to a trend towards reduced Gli1 expression. (0.79±0.11, 0.84±0.06, 0.69±0.07 fold respectively; p-values of 0.25, 0.17, 0.07 respectively; Fig. 7C). The effect of dystroglycan alone on this signaling pathway may therefore be masked in the short run by increased Notch activation which eventually gives way to suppressed sonic hedgehog activity over time as Notch effector activity returns to normal over several days. Furthermore, the effects of dystroglycan blockade on Gli activation is also cell-type

dependent. While IIH6 antibody suppresses Gli1 expression in proliferating cultures, Gli1 expression is unchanged by blockade during differentiation conditions in ependymal cell culture and in cultured primary OPCs (data not shown).

We next conducted pilot studies in induced P3 SVZs to determine whether Shh expression was changed in the *in vivo* environment after loss of dystroglycan. While there was very high variability in this cohort, there are indications that Shh expression may increase significantly upon dystroglycan loss (Fig. 7D). These results cannot be replicated by treatment with dystroglycan blockade in neurospheres (Fig. 7E, F) indicating that either Shh upregulation upon dystroglycan loss is a phenomenon that is niche-dependent, or that it is not dystroglycan binding, but some constitutive activity of the dystroglycan protein itself that regulates Shh expression in this model. We next examined the effect of dystroglycan blockade on the expression of Glypican3, a heparin-sulfate proteoglycan that functions as a co-receptor for Shh, inhibiting the activation of Shh, reasoning that perhaps an upregulation Glyp3 might be responsible for inhibition of Gli in the ECC experiments. Surprisingly, in ECCs, dystroglycan blockade actually has a small inhibitory effect on the expression of Glyp3 (Fig. 7G). In the induced P3 SVZ, however, preliminary results indicate that there may be a significant increase in Glyp3 expression, though again, these data are rather variable (Fig. 7H), potentially due to variability in SVZ dissection or in induction efficiency. Interestingly, however, dystroglycan blockade has no effect on neurosphere expression of Glyp3 at 6 or 24 hours during proliferation (1.04±0.04, 0.98±0.05 fold control respectively) or differentiation (1.06±0.10, 1.12±0.11 fold control respectively). Taken together these results suggest that dystroglycan may regulate the Shh pathway in the SVZ in a niche-dependent manner. In particular, dystroglycan may potentiate Shh signaling in mixed populations of neural stem cells and developing ependymal cells. *In vivo*,

but not *in vitro,* dystroglycan may also regulate SVZ expression of sonic hedgehog as well as its co-receptor glypican 3. Additional studies are underway in our lab to understand the role of dystroglycan in modulating the sonic hedgehog pathway in the SVZ.

Conclusions and Discussion

These results show that dystroglycan regulates notch signaling in the mammalian SVZ. These results are novel in that they highlight dystroglycan as a regulator of Notch signaling for the first time. They also pose an interesting contrast to two recent studies linking dystroglycan and notch signaling in *Xenopus*, [310] and C. elegans [311]. In these models, Notch signaling functions upstream of dystroglycan, regulating its transcription and trafficking in epithelial morphogenesis and uterine-vulval attachment, respectively. It will be interesting to determine whether notch activation alters dystroglycan localization or availability in the context of SVZ cells.

While the specific details of how dystroglycan regulates notch activation in the SVZ remain unclear, the loss of dystroglycan leads to an increase in levels of the active notch Intracellular Domain (NICD) fragment. Prevention of the generation of this fragment by the γ-secretase inhibitor DAPT or prevention of the formation of the Notch-RBPJ-MAML1 transcriptional activator complex once the fragment has been generated rescues the effects of dystroglycan blockade. Dystroglycan may also have the ability to regulate the pathway downstream of FoxJ1 directly, though it is unclear how. One possibility is by directly regulating expression of multicillin and/or c-myb. Another potential target is p73, a transcription factor important for multicilliogenesis recently described as downstream of notch and upstream of

multicillin. [312, 313] Finally, dystroglycan may regulate a miRNA to exert pleiotropic effects on the multicilliogenic pathway.[314]

As both neural stem cells and ependymal cells express dystroglycan, it remains unclear if dystroglycan acts in cis or trans (or both) to regulate Notch activity. Given that the expression of dystroglycan appears to be higher in ependymal cells compared to NSCs during early development, and that notch activity is higher in NSCs relative to that in ependymal cells, an attractive hypothesis is that ependymal cell dystroglycan acts in trans to regulate Notch activation status in adjacent NSCs. Dystroglycan has recently been linked to regulating the endocytosis, and therefore the surface availability, of water channels in astrocytic endfeet, and several years ago was shown to modulate the turnover of laminin on cell surfaces. [246, 315] Thus the turnover of Notch ligand, or Notch itself, present an intriguing avenue to investigate in the quest to understand how dystroglycan regulates Notch activation. Further studies are needed to answer these and other open mechanistic questions regarding dystroglycan-Notch interactions.

At the cell surface, dystroglycan is found as part of a larger complex known as the dystrophin-glycoprotein complex, which plays a role in several forms of muscular dystrophy. The loss of dystrophin itself results in Duchenne muscular dystrophy, an X-linked disease that is the most common form of muscular dystrophy. Intriguingly, it was recently reported that an escaper mutation, which caused muscle cells to upregulate the Notch ligand Jagged1, could rescue muscular dystrophy phenotypes in two separate animal models of Duchenne muscular dystrophy. [316] Furthermore, NSCs from mice with dystrophin defects express less Notch than control NSCs, and display a range of structural and functional abnormalities [317]. The link between dystroglycan, its associated proteins and signaling pathways, and Notch signaling may therefore prove fruitful as an avenue of study not only for the understanding of ECM-mediated

regulation of cell dynamics, but also as a starting point for therapeutic options for patients with any of the plethora of muscular dystrophies resulting from disruptions in the dystrophin-glycoprotein complex.

While many of its effects in governing SVZ maturation appear to be related to its suppression of Notch signaling, at least some of dystroglycan's regulatory effects are mediated through other, non-Notch related signaling. Dystroglycan's direct signaling capabilities are complex – beyond functioning as a physical link between the extra- and intracellular environments, it can interact with the ERK signaling pathway, and the Ezrin/Radixin/Moesin family of proteins among others. Additionally, dystroglycan contains SH2, SH3, and WW domains, and has recently been shown to have an intracellular domain that translocates to the nucleus (though its function there remains poorly understood). (Reviewed in [154]) It will be interesting to see which of these pathways are active downstream of dystroglycan in the SVZ and whether their activity is modulated by laminin hubs.

Figure III-1

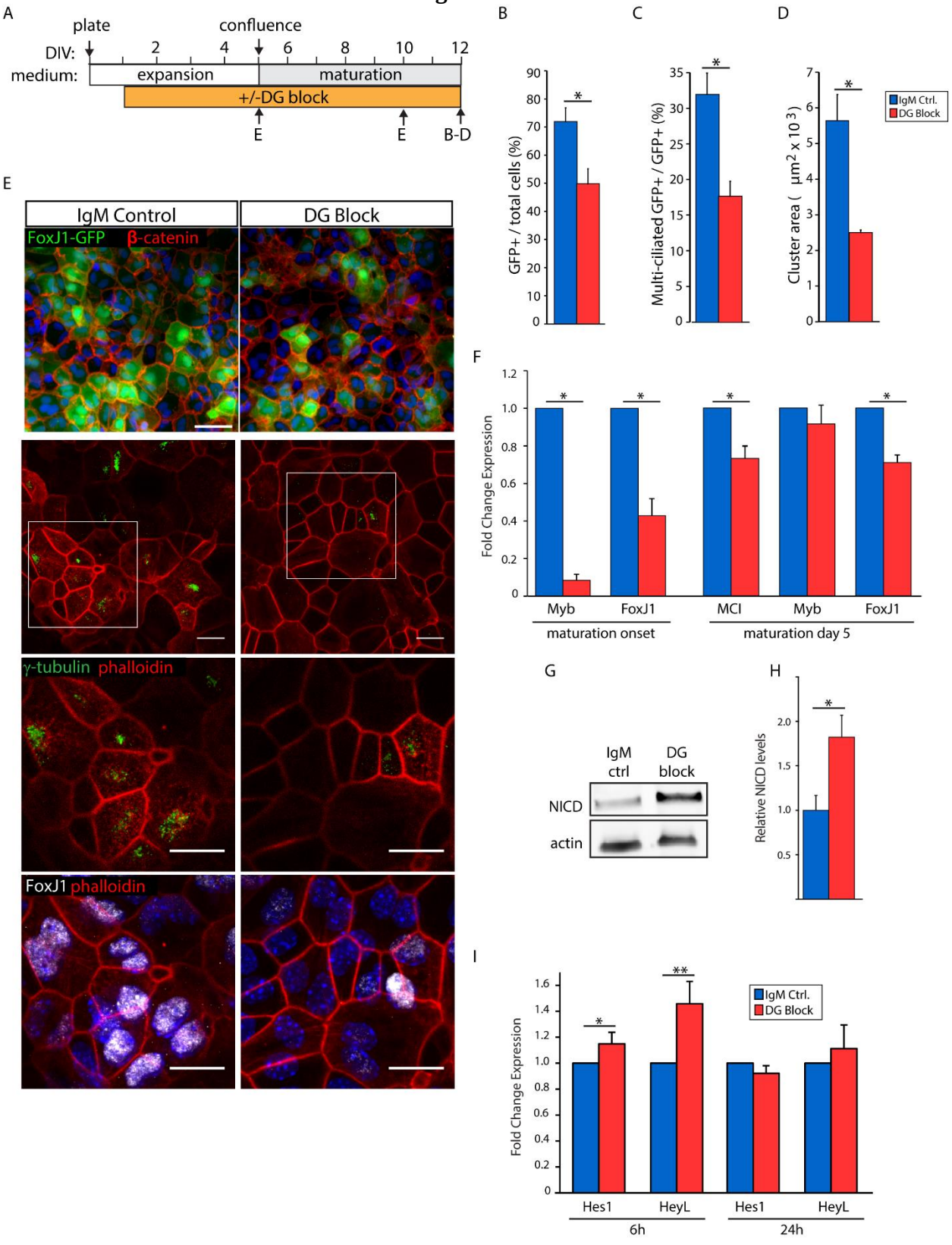
A
plate
confluence
DIV:
2
4
6
8
10
12
medium:
expansion
maturation
+/-DG block
E
E
B-D
B
C
D
GFP+ / total cells (%)
Multi-ciliated GFP+ / GFP+ (%)
Cluster area (µm2 x 10 3)
IgM Ctrl.
DG Block
E
IgM Control
DG Block
FoxJ1-GFP
β-catenin
γ-tubulin
phalloidin
FoxJ1
phalloidin
F
Fold Change Expression
Myb
FoxJ1
MCI
Myb
FoxJ1
maturation onset
maturation day 5
G
IgM ctrl
DG block
NICD
actin
H
Relative NICD levels
I
Fold Change Expression
IgM Ctrl.
DG Block
Hes1
HeyL
Hes1
HeyL
6h
24h

Figure III-1: Dystroglycan Regulates Transcriptional Control of Ependymal Cell Maturation

(A) Schematic timeline of SVZ cultures; timepoints for experiments depicted in panels are shown along the bottom.
(B) Quantification of GFP+ ependymal cells following differentiation with control or DG-blocking antibodies (*$p < 0.05$, Student's t test).
(C) Quantification of multiciliated GFP+ cells after differentiation with control or DG-blocking antibodies (*$p < 0.05$, Student's t test).
(D) Quantification of ependymal cell/RGC cluster area in control or DG-blocked cultures (*$p < 0.05$, Student's t test).
(E) IHC to detect GFP and β-catenin (upper panel) or γ-tubulin, FoxJ1, and phalloidin (middle and lower panels) in differentiating FoxJ1-GFP SVZ ependymal cultures in the presence of control or dystroglycan (DG)-blocking antibodies. Dystroglycan block reduces the number of cells that become FoxJ1+ and multicilliated. Multicilliated cells tend to arise in clusters, and are only present on cells that are FoxJ1+.
(F) Fold change in mRNA levels of multiciliogenic program genes at maturation onset or after 5 days in medium to promote ependymal cell maturation (*$p < 0.05$,Student's t test).
(G) NICD western blots of protein lysates obtained from neonatal SVZ ependymal cultures after 3 days in medium to promote ependymal cell differentiation.
(H) Cultures with dystroglycan (DG)-blocking antibodies had increased levels of NICD protein relative to actin, compared to cultures treated with control antibodies (*$p<0.05$, Student's t-test.
(I) Fold change in mRNA levels of Hes1 and HeyL in SVZ ependymal cultures at 6 and 24 hr after switch to maturation medium in the presence or absence of DG-blocking antibodies. Note that in this set of experiments, DG-blocking antibodies were only added upon confluence. (*$p < 0.05$, **$p < 0.01$, Student's t test).

Figure III-2

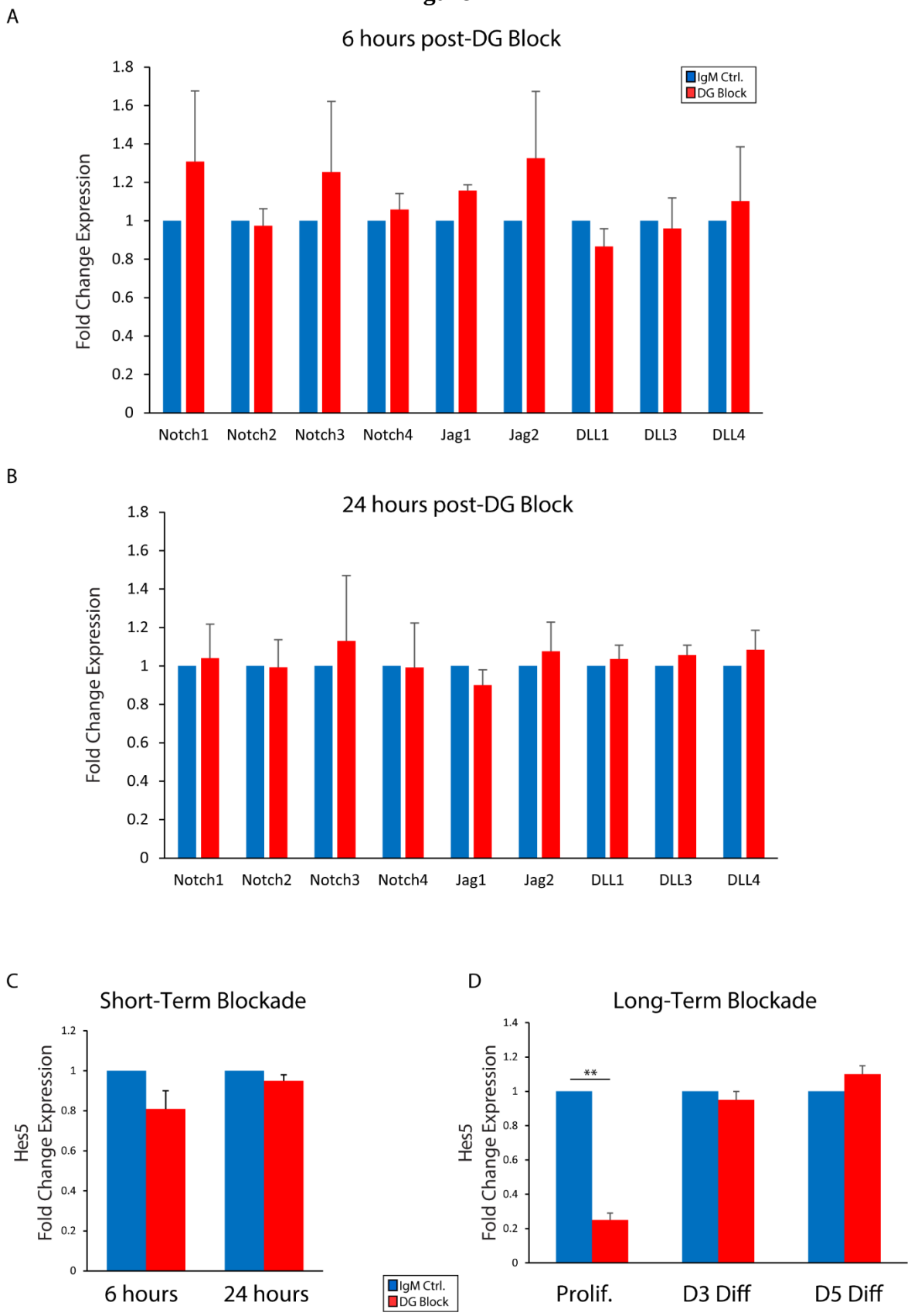
A
6 hours post-DG Block
IgM Ctrl.
DG Block
Fold Change Expression
1.8
1.6
1.4
1.2
1
0.8
0.6
0.4
0.2
0
Notch1
Notch2
Notch3
Notch4
Jag1
Jag2
DLL1
DLL3
DLL4
B
24 hours post-DG Block
Fold Change Expression
1.8
1.6
1.4
1.2
1
0.8
0.6
0.4
0.2
0
Notch1
Notch2
Notch3
Notch4
Jag1
Jag2
DLL1
DLL3
DLL4
C
Short-Term Blockade
Hes5
Fold Change Expression
1.2
1
0.8
0.6
0.4
0.2
0
6 hours
24 hours
IgM Ctrl.
DG Block
D
Long-Term Blockade
Hes5
Fold Change Expression
1.4
1.2
1
0.8
0.6
0.4
0.2
0
**
Prolif.
D3 Diff
D5 Diff

Figure III-2: Dystroglycan Blockade Does Not Regulate Notch or Notch Ligand Expression but Suppresses Hes5 in Proliferating SVZ Cultures

(A) Quantification of mRNA levels of Notch receptor and ligands in SVZ ependymal cultures at 6 hours after switch to maturation medium in the presence or absence of DG-blocking antibodies.
(B) Quantification of mRNA levels of Notch receptor and ligands in SVZ ependymal cultures at 24 hours after switch to maturation medium in the presence of absence of DG-blocking antibodies.
(C) Quantification of mRNA levels of Hes5 in SVZ ependymal cultures at 6 and 24 hours after switch to maturation medium in presence or absence of DG-blocking antibodies
(D) Quantification of mRNA levels of Hes5 in SVZ ependymal cultures at longer timepoints in differentiation medium.

Figure III-3

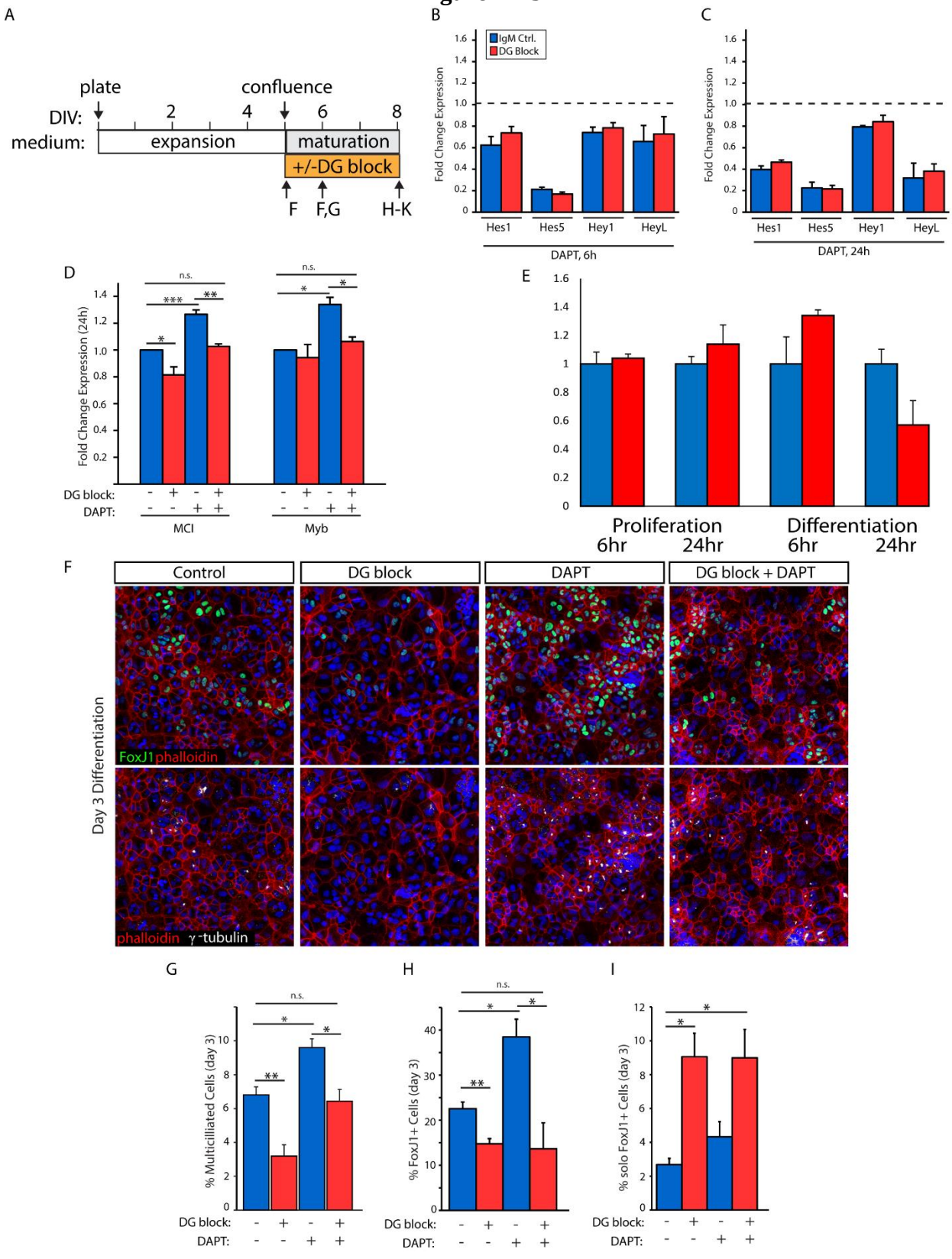
A
plate
confluence
DIV:
2
4
6
8
medium:
expansion
maturation
+/-DG block
F
F,G
H-K
B
IgM Ctrl.
DG Block
Fold Change Expression
Hes1
Hes5
Hey1
HeyL
DAPT, 6h
C
Fold Change Expression
Hes1
Hes5
Hey1
HeyL
DAPT, 24h
D
Fold Change Expression (24h)
n.s.
DG block:
DAPT:
MCI
Myb
E
Proliferation
Differentiation
6hr
24hr
6hr
24hr
F
Control
DG block
DAPT
DG block + DAPT
Day 3 Differentiation
FoxJ1 phalloidin
phalloidin γ-tubulin
G
% Multiciliated Cells (day 3)
DG block:
DAPT:
H
% FoxJ1+ Cells (day 3)
DG block:
DAPT:
I
% solo FoxJ1+ Cells (day 3)
DG block:
DAPT:

Figure III-3: Dystroglycan Suppresses Notch Signaling to Promote Ependymal Cell Differentiation

(A) Schematic timeline of SVZ cultures; timepoints for experiments depicted in panels are shown along the bottom.
(B) Fold change in mRNA levels of *Hes1*, *Hes5*, *Hey1*, and *HeyL* in confluent SVZ ependymal cultures at 6 hours post-switch to maturation medium, in the presence or absence of the g-secretase inhibitor, DAPT, or dystroglycan (DG)-blocking antibodies.
(C) Experiment as in (A) but mRNA was analyzed at 24 hours post-treatment
(D) Fold change in mRNA levels of MCI and Myb following 24 hr in DG-blocking antibodies, the g-secretase inhibitor DAPT, or a combination of both (*$p < 0.05$, **$p < 0.01$, ***$p < 0.001$, Student's t test).
(E) Fold change in mRNA levels of dystroglycan (DAG1) under proliferating and differentiating conditions 6 and 24 hours after DAPT or vehicle administration.
(F) Ependymal cell cultures at day 3 of differentiation, with IHC to detect either FoxJ1 and cortical actin (phalloidin; upper panels), or FoxJ1 and g-tubulin (lower panels) in cultures treated with DAPT, DG-blocking antibodies (DG block), or a combination thereof.
(G) Quantification of the percentage of SVZ cells acquiring a multiciliated phenotype in SVZ ependymal cultures treated as in (H). Multicilliated cells detected by IHC for γ-tubulin showing patches of basal bodies on the cell surface. (*$p < 0.05$, **$p < 0.01$, Student's t test).
(H) Quantification of the percentage of FoxJ1+ cells in SVZ ependymal cultures treated as in (H) (*$p < 0.05$, **$p < 0.01$, Student's t test).
(I) Analysis of solo and clustered FoxJ1+ cells in SVZ ependymal cultures treated as in (H) Counts indicate percentage of all FoxJ1+ cells that did not contact another FoxJ1+ cell (*$p < 0.05$, Student's t test).

Figure III-4

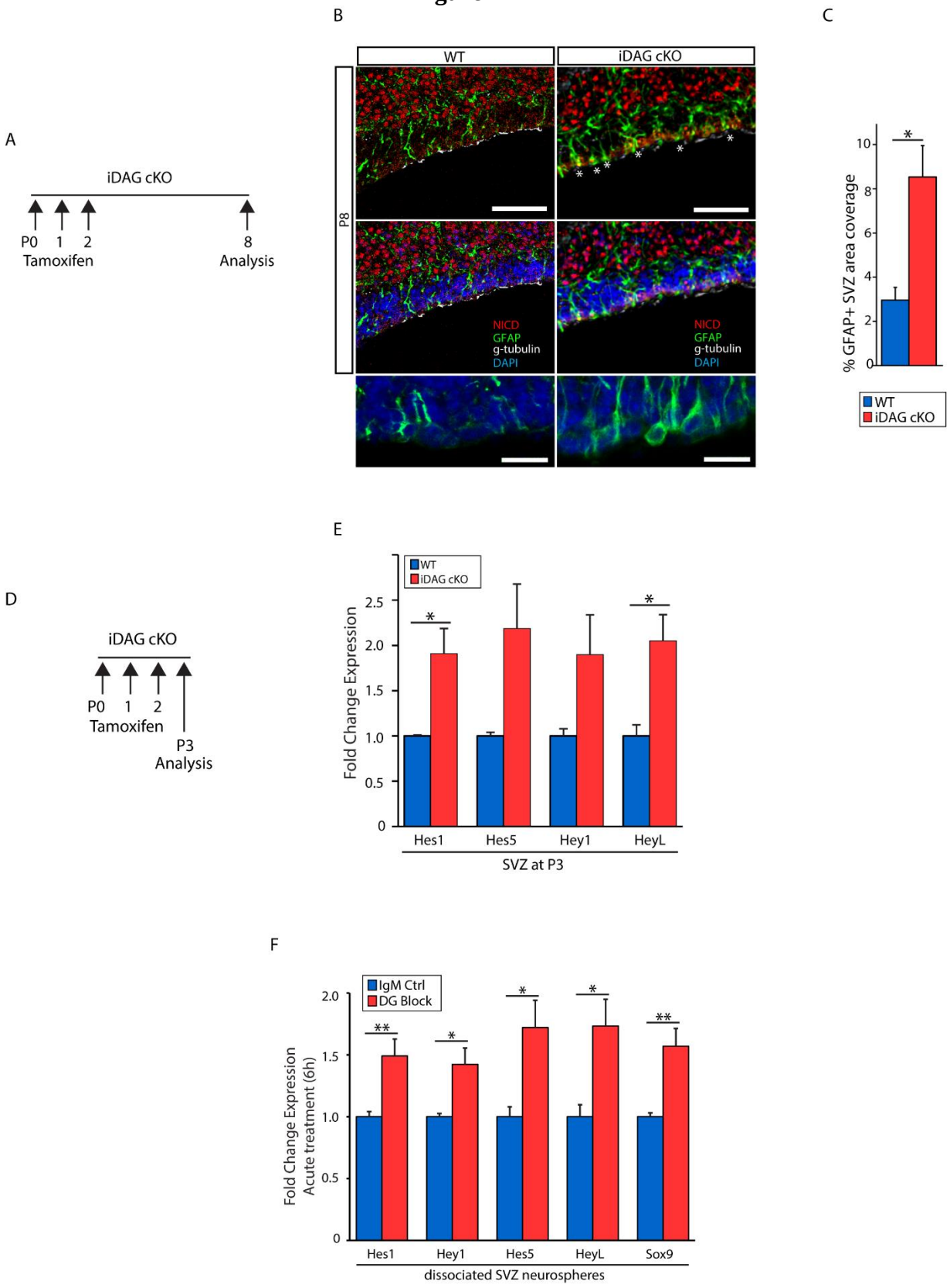
A
iDAG cKO
P0 1 2
Tamoxifen
8
Analysis
B
WT
iDAG cKO
P8
NICD
GFAP
g-tubulin
DAPI
C
% GFAP+ SVZ area coverage
WT
iDAG cKO
D
iDAG cKO
P0 1 2
Tamoxifen
P3
Analysis
E
Fold Change Expression
Hes1
Hes5
Hey1
HeyL
SVZ at P3
F
IgM Ctrl
DG Block
Fold Change Expression
Acute treatment (6h)
Hes1
Hey1
Hes5
HeyL
Sox9
dissociated SVZ neurospheres

Figure III-4: Dystroglycan Regulates Notch Signaling in Neural Stem Cells *in vivo* and in *ex vivo* Neurospheres.

(A) Time line of tamoxifen injections and cellular analysis for iDAG cKO mice data in panels (B) and (C)
(B) IHC to detect Notch Intracellular Domain (NICD), GFAP, and γ-tubulin in coronal sections from P8 WT and iDAG cKO SVZ. GFAP+ radial glial endfeet are indicated by white asterisks. Regions of maturing ependymal cells are indicated by apical surface γ-tubulin immunoreactivity. Lower panels depict highermagnification views of GFAP+ radial glial endfeet.
(C) Quantification of the percent area coverage by GFAP immunoreactivity in the WT and iDAG cKO SVZ at P8 (*$p < 0.05$, Student's t test).
(D) Time line of tamoxifen injections and gene expression analysis for iDAG cKO mice data in panel (E)
(E) Quantification of mRNA levels of Notch-regulated genes, Hes1, Hes5, Hey1, and HeyL, in the WT and iDAG cKO SVZ (*$p < 0.05$, Student's t test).
(F) Dissociated neurospheres from WT SVZ were plated in the presence of control or dystroglycan-blocking antibodies (DG Block) and evaluated at 6 hr to determine mRNA levels of Notch-regulated genes Hes1, Hey1, Hes5, HeyL, and Sox9 (*$p < 0.05$, **$p < 0.01$, Student's t test).

Figure III-5

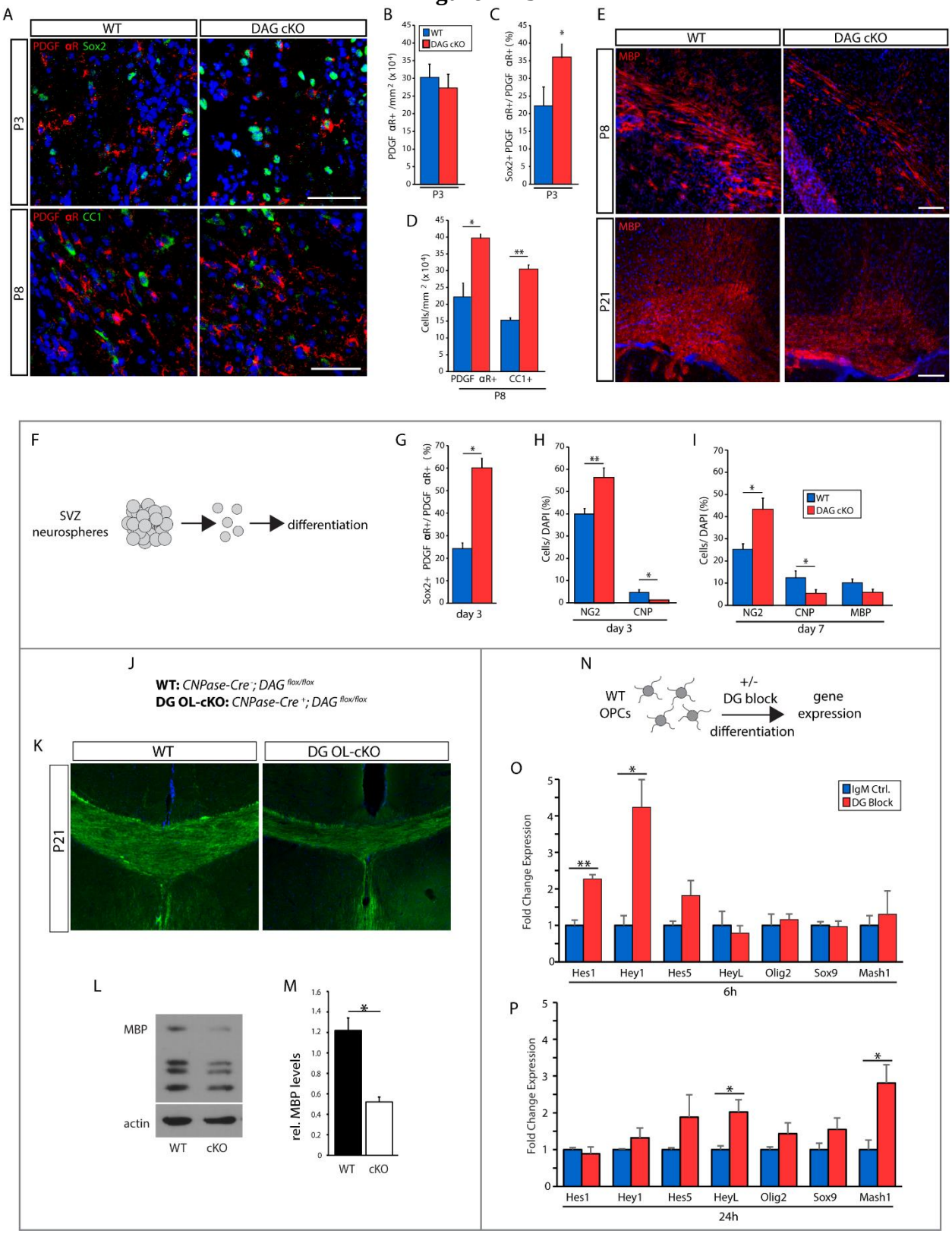
A
WT
DAG cKO
PDGF αR Sox2
P3
PDGF αR CC1
P8
B
WT
DAG cKO
PDGF αR+ /mm² (x10⁴)
P3
C
Sox2+ PDGF αR+/ PDGF αR+ (%)
P3
D
Cells/mm ² (x10⁴)
PDGF αR+
CC1+
P8
E
WT
DAG cKO
MBP
P8
P21
F
SVZ
neurospheres
differentiation
G
Sox2+ PDGF αR+/ PDGF αR+ (%)
day 3
H
Cells/ DAPI (%)
NG2
CNP
day 3
I
Cells/ DAPI (%)
WT
DAG cKO
NG2
CNP
MBP
day 7
J
WT: CNPase-Cre⁻; DAG flox/flox
DG OL-cKO: CNPase-Cre ¹; DAG flox/flox
K
WT
DG OL-cKO
P21
L
MBP
actin
WT
cKO
M
rel. MBP levels
WT
cKO
N
WT
OPCs
+/-
DG block
differentiation
gene
expression
O
IgM Ctrl.
DG Block
Fold Change Expression
Hes1
Hey1
Hes5
HeyL
Olig2
Sox9
Mash1
6h
P
Fold Change Expression
Hes1
Hey1
Hes5
HeyL
Olig2
Sox9
Mash1
24h

Figure III-5: Dystroglycan Regulates Notch Signaling In Oligodendrogenic Lineage Cells to Promote Their Maturation

(A) IHC to detect PDGFRα, Sox2, and CC1 in the corpus callosum in coronal sections from P3 and P8 wild-type (WT) and DAG cKO mice.
(B) Quantification of PDGFRa+ OPC densities in the P3 corpus callosum.
(C) Quantification of Sox2+ cells within PDGFRa+ cell population in the P3 corpus callosum (*$p < 0.05$, Student's t test).
(D) Quantification of PDGFRa+ and CC1+ cell densities in the P8 corpus callosum (*$p < 0.05$, **$p < 0.01$, Student's t test).
(E) IHC to detect myelin basic protein (MBP) in the corpus callosum in coronal sections from P8 and P21 WT and DAG cKO mice.
(F) Schematic depicting isolation of cells for analysis from neurospheres
(G) Quantification of Sox2+ cells within the PDGFRa+ cell population at day 3 in differentiation medium (*$p < 0.05$, Student's t test).
(H) Quantification of OPCs (NG2+) and OLs (CNP+) at day 3 in differentiation medium (*$p < 0.05$, **$p < 0.01$, Student's t test).
(I) Quantification of OPCs (NG2+), OLs (CNP+) and myelin-competent OLs (MBP+) at day 7 in differentiation medium (*$p < 0.05$, Student's t test).
(J) Breeding scheme used generate DG OL cKO mice
(K) IHC to detect myelin basic protein (MBP) in the corpus callosum in coronal sections from P21 WT and DAG OL-cKO mice. MBP immunoreactivity is decreased in DAG OL cKO mice.
(L) Western blot analyses of MBP protein levels in cortical lysates from WT and DAG OL-cKO mice at P21
(M) Quantification of relative MBP protein levels in cortical lysates from WT and DAG OL-cKO mice at P21 (*$p<0.05$; Student's t-test).
(N) Schematic depicting isolation of OPCs for panels O and P
(O) WT OPCs were plated on PDL in differentiation-permissive medium in the presence of dystroglycan-blocking (DG block) or control antibodies and evaluated 6 hr later for mRNA levels of Notch-regulated genes, Hes1 and Hey1 (*$p < 0.05$, **$p < 0.01$, Student's t test).
(P) Treatment of OPCs as in (L) but analyzed at 24 hr (*$p < 0.05$, Student's t test).

Figure III-6

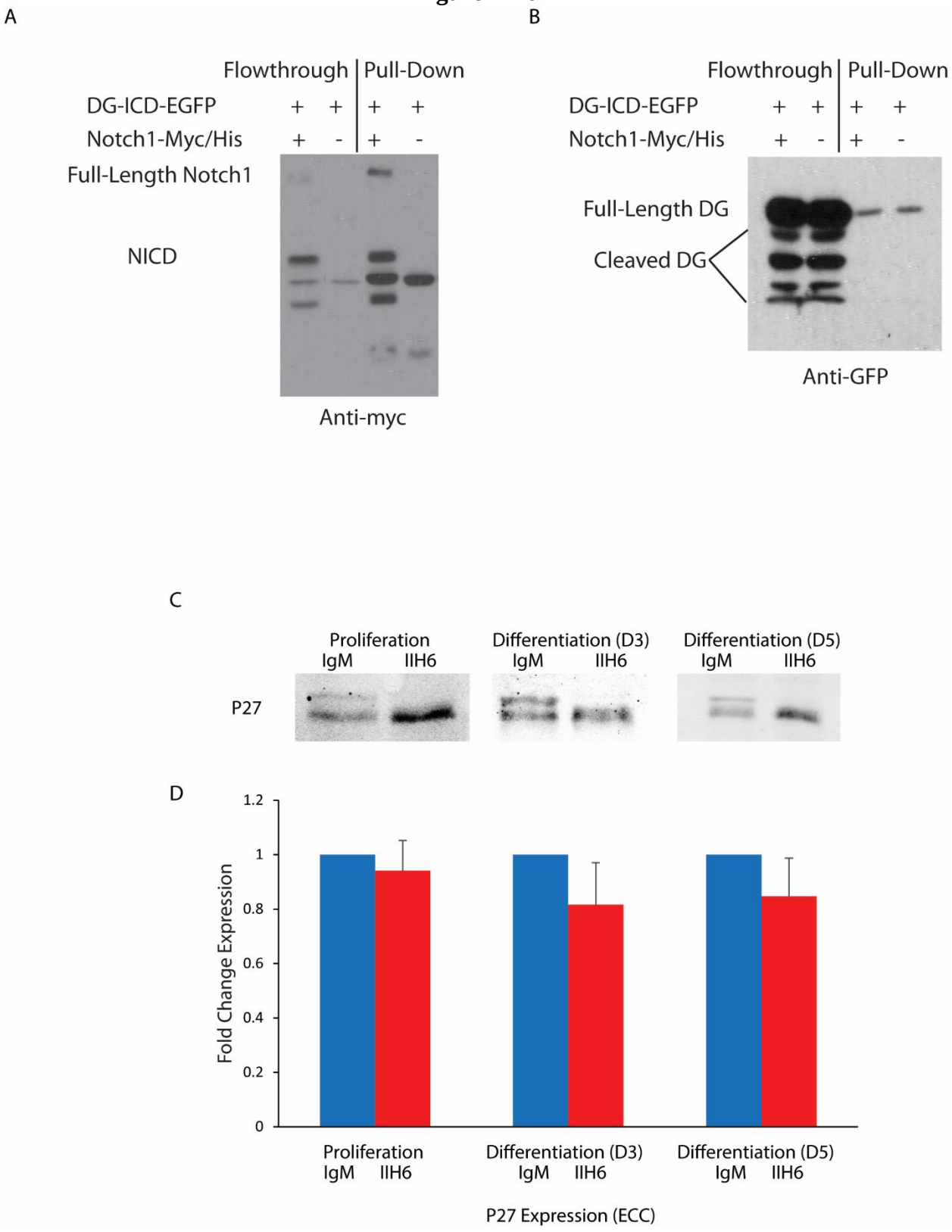
A
Flowthrough
Pull-Down
DG-ICD-EGFP + + + +
Notch1-Myc/His + - + -
Full-Length Notch1
NICD
Anti-myc
B
Flowthrough
Pull-Down
DG-ICD-EGFP + + + +
Notch1-Myc/His + - + -
Full-Length DG
Cleaved DG
Anti-GFP
C
Proliferation
IgM IIH6
Differentiation (D3)
IgM IIH6
Differentiation (D5)
IgM IIH6
P27
D
Fold Change Expression
1.2
1
0.8
0.6
0.4
0.2
0
Proliferation
IgM IIH6
Differentiation (D3)
IgM IIH6
Differentiation (D5)
IgM IIH6
P27 Expression (ECC)

Figure III-6: Dystroglycan Binding Regulates P27 in Proliferating and Differentiating SVZ Cultures

(A) Western Blot of pulldown experiments conducted in HEK293T cells. Notch1 was pulled down by nickel column affinity chromatography for the poly-His tag, and blots were visualized by anti-Myc antibody. Empty vector with a myc/his tag was used as control.
(B) Western Blot of pulldown experiments conducted in HEK293T cells. Upon pull down, the gel was probed with anti-GFP antibody to the visualize dystroglycan intracellular domain. Despite some off-target GFP visualization, no changes were seen in cells with Notch overexpression.
(C) Western blots of SVZ cultures on PDL treated with either IIH6 DG-blocking antibody or IgM control for long-term culture and lysed at proliferation, differentiation day 3, or differentiation day 5 timepoints. Blots were probed with anti-P27 antibody.
(D) Quantification of mRNA levels of p27 transcripts under conditions in (C).

Figure III-7

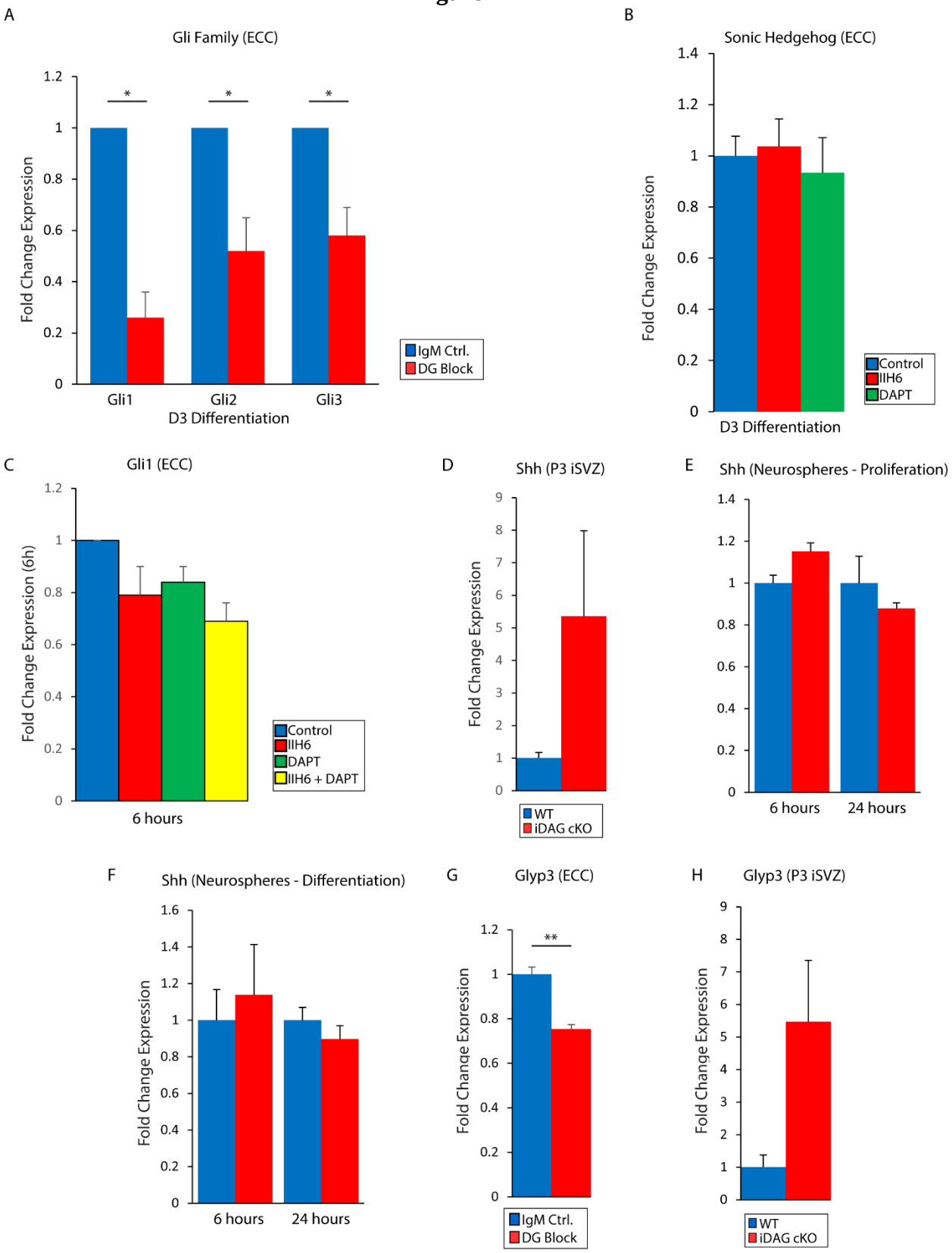
A
Gli Family (ECC)
Fold Change Expression
1.2
1
0.8
0.6
0.4
0.2
0
*
*
*
Gli1
Gli2
Gli3
D3 Differentiation
IgM Ctrl.
DG Block
B
Sonic Hedgehog (ECC)
Fold Change Expression
1.4
1.2
1
0.8
0.6
0.4
0.2
0
D3 Differentiation
Control
IIH6
DAPT
C
Gli1 (ECC)
Fold Change Expression (6h)
1.2
1
0.8
0.6
0.4
0.2
0
6 hours
Control
IIH6
DAPT
IIH6 + DAPT
D
Shh (P3 iSVZ)
Fold Change Expression
9
8
7
6
5
4
3
2
1
0
WT
iDAG cKO
E
Shh (Neurospheres - Proliferation)
1.4
1.2
1
0.8
0.6
0.4
0.2
0
6 hours
24 hours
F
Shh (Neurospheres - Differentiation)
Fold Change Expression
1.6
1.4
1.2
1
0.8
0.6
0.4
0.2
0
6 hours
24 hours
G
Glyp3 (ECC)
Fold Change Expression
1.2
1
0.8
0.6
0.4
0.2
0
**
IgM Ctrl.
DG Block
H
Glyp3 (P3 iSVZ)
Fold Change Expression
9
8
7
6
5
4
3
2
1
0
WT
iDAG cKO

Figure III-7: Dystroglycan Regulates Sonic Hedgehog Signaling in a Niche-Dependent Manner

(A) Quantification of mRNA levels of Shh-regulated transcription factors upon DG blockade for 3 days in SVZ culture under proliferating conditions. ECC = Ependymal Cell Culture (*$p < 0.05$, Student's t test).
(B) Quantification of mRNA levels of Shh expression upon DG blockade or DAPT treatment for 3 days in SVZ culture under proliferating conditions
(C) Quantification of Gli1 mRNA levels after 6 hours of DG blockade, DAPT treatment, or both in SVZ culture under proliferating conditions.
(D) Quantification of mRNA levels of Shh in the P3 SVZ of iDAG cKO mice after tamoxifen-induced recombination.
(E) Quantification of mRNA levels of Shh in dissociated neurospheres after 6 or 24 hours of DG blockade under proliferating conditions.
(F) Quantification of mRNA levels of Shh in dissociated neurospheres after 6 or 24 hours of DG blockade under differentiating conditions.
(G) Quantification of mRNA levels of Glyp3 in SVZ cultures upon DG blockade for 3 days in SVZ culture under proliferating conditions (**$p < 0.01$, Student's t test).
(H) Quantification of mRNA levels of Shh in the P3 SVZ of iDAG cKO mice after tamoxifen-induced recombination.

Chapter 4: Ependymal Cell Dystroglycan Continues to Regulate SVZ Function after FoxJ1 Expression

As discussed earlier, the phenotypic effects of dystroglycan loss in the brain spans several cell types including two of the major permanent cell types of the SVZ (ECs and NSCs). While our studies in the DG-CNS-KO indicated that dystroglycan loss delays expression of FoxJ1 in developing ependymal cells, it remained unknown whether dystroglycan plays any further role in maturing and/or mature ECs (i.e. ependymal cells that are lineage committed and already express the FoxJ1 transcription factor). One hint that dystroglycan may have such a role came from closer examination of the effects of dystroglycan loss in the ependymal cell population. During the postnatal period, after the onset of FoxJ1 expression, ependymal cells continue to mature, arrange themselves into pinwheels, and reorganize surface laminin. As all of these processes are disrupted in the DG-CNS-KO SVZ, we hypothesized that dystroglycan may indeed have further roles to play in EC function after controlling the onset of FoxJ1 expression.

In order to test this hypothesis, we generated a conditional knockout to eliminate dystroglycan expression only in multiciliated cells by driving expression of Cre recombinase under the control of the FoxJ1 promoter, and crossing these mice to dystroglycan floxed mice (DG-EC-KO) (Fig. 1A). This strategy allowed us to examine the effects of dystroglycan in ependymal cells after the expression of FoxJ1. Additionally, by observing whether this strategy resulted in phenotypic changes in neural stem cells, we hoped that this strategy could provide some insight as to if and how ependymal cell function regulates the form and function of NSCs in the developing SVZ, a topic that very little is currently known about.

As results in developing wildtype mice suggested that the laminin hubs that form during the immediate postnatal period are primarily generated and assembled by developing ependymal cells, we sought first to ask whether DG-EC-KO SVZs had the same characteristic laminin hubs at the end of EC maturation, (i.e. around the end of the third week of postnatal life). Recall that in the DG-CNS-KO SVZ, the loss of dystroglycan led to thirty-fold fewer laminin hubs by this time point, and those hubs that remained were only a third the size of wildtype hubs at P21. The ependymal cell specific strategy, by virtue of the timing of FoxJ1 expression, involved removing dystroglycan after initial laminin was present on the VZ surface. Furthermore, dystroglycan appears to be a relatively long-lived protein species *in vivo*, requiring several days before genetic loss of the DAG1 gene results in total loss of protein at the tissue level (Kevin Wright, personal communication). As such, we expected that if EC-specific dystroglycan loss had an effect on the laminin hubs, this effect would not be as severe. In this case, initial laminin cluster formation would proceed normally for at least the first few days of postnatal life before the effects of loss of the dystroglycan protein could manifest themselves. Indeed, at P3, there did not appear to be significant differences in the amount of laminin on the ventricular surface of the DG-EC-KO SVZ compared to their WT littermate controls.

However, by P21, the DG-EC-KO SVZ displays a two-fold reduction in hubs per square micron (3.54 ± 0.09 vs. 1.83 ± 0.19 hubs per 1,000 μm^2) and the individual hubs are about 40% smaller in these animals (5.19 ± 0.07 vs. 3.21 ± 0.44 μm^2). (Fig. 1B-D) This indicated that dystroglycan does play a role in the organization and/or maintenance of hubs after the expression of FoxJ1 in ependymal cells. It was not clear, however, how this might occur in the framework of what was already known about the role of dystroglycan in regulating EC maturation and function. One clue, however, appeared when we plotted the laminin hub size distribution in these

animals. In the wildtype, a local maximum occurred at about 5 μm^2 (Fig. 1E) In the DG-EC-KO, there was a small bump at this size bin, but it was much reduced (Fig. 1F). In fact, a comparative size distribution indicated that the size of hubs in the knockouts were shifted to the left, demonstrative of an inability to generate larger hub sizes in these animals (Fig. 1G).

Thus, in order to understand the developmental timeline of these effects on surface laminin and to probe whether the loss of EC dystroglycan engendered a failure of laminin clustering, we decided to look at the laminin clusters at the end of the first postnatal week (P8). At this time point, dystroglycan would have only been absent for a period of several days, and the acute effects of its loss might be more visible, providing information as to how the process leading to fewer and smaller laminin hubs began. At P8, while there did not appear to be a significant change in total laminin coverage (197.39 ± 16.69 vs. 158.69 ± 31.92 μm^2 of laminin+ area per HPF), the average laminin cluster size was almost two-fold smaller (0.60 ± 0.06 vs. 0.35 ± 0.01) in the knockouts (Fig. 2A – C). The number of clusters per field was highly variable in the DG-EC-KO, and trended higher, but did not reach significance (Fig. 2D). Indeed, examination of the VZ surface by IHC for laminin showed that the morphology of laminin clusters in the DG-EC-KO appeared more fragmented than in the WT, indicating that dystroglycan may play a role in the putative merging of laminin hub structures that occurs over the first three weeks of postnatal life to promote laminin hub formation (Fig. 2A).

Another major change in EC maturation that occurs during this period is the generation and organization of cilia into polarized patches on the apical surfaces of the ependymal cells. This process is largely complete by P21, and many of the drivers of the ciliogenenic program are part of a transcriptional cascade that culminates in FoxJ1 expression, prior to the functional multiciliated phenotype (reviewed in [318]). As this transcriptional cascade is upstream of

FoxJ1, we expected that loss of dystroglycan in FoxJ1+ ECs would not have an effect on the generation of ciliary patches. Surprisingly, however, at P21, there are changes in the fractional basal body patch displacement in the DG-EC-KO, with the knockout ECs displaying more eccentrically displaced patches (0.33 ± 0.018 vs. 0.42 ± 0.002). The knockout patches also trended towards a smaller patch area, though this trend did not reach statistical significance (0.28 ± 0.007 vs. 0.24 ± 0.012; P = 0.068). (Fig. 2F)

We also wanted to understand whether the role of dystroglycan in the development of multiciliated cells after FoxJ1 expression was generalizable to other systems, so we examined the maturation of DG-EC-KO airway multiciliated cells in the mammalian tracheal epithelial cell *in vitro* model. In this system, however, we found no striking differences in ciliogenesis either during development or at maturity of these cells. (Fig. 3A) These results show that dystroglycan plays a role after the onset of FoxJ1 expression in driving ciliogenesis and/or organization of basal body patches specifically in ependymal cells. Whether this is by continuing to support the activation of the transcriptional cascade upstream of FoxJ1 in these cells or through some other mechanism impacting the generation and organization of cilia remains to be determined. Continued FoxJ1 expression is required for the maintenance of ependymal cells, so this is one possibility, but as dystroglycan plays a role in organizing cytoskeletal structures that interact with microtubules, the loss of dystroglycan may also dysregulate basal body organization.

As structural aspects of ependymal cells and laminin hubs were clearly altered by P21, though not to the same extent as seen in the whole brain knockout, we next sought to examine whether changes in ependymal cell function through loss of dystroglycan in this cell type had any effect on the type B1 neural stem cells at this stage. We conducted immunostaining for GFAP to observe the density of these adult neural stem cells by wholemount (WM) at P21, and

were surprised to find stark differences in the presence of GFAP+ processes in the central regions of the SVZ at this time. There were clearly fewer GFAP+ cells in the knockout, (Fig. 4A) though the filamentous nature of the staining made it difficult to accurately count GFAP+ population sizes. We were instead able to quantify the volume of the SVZ that was occupied by GFAP+ processes, finding an extreme reduction (3.33 ± .40 vs. 0.09 ± 0.05 percent of GFAP+ SVZ volume) (Fig. 4B). Furthermore, the intensity of the processes that were GFAP+ was reduced in the DG-EC-KO (0.0047 ± 0.0004 vs. 0.0015 ± 0.0006 AU) (Fig. 4C), and these results of reduced GFAP processes in the SVZ were mirrored (though somewhat variable) in coronal sections in P8 and P21 tissue (data not shown). These results are of particular note, as they indicate a non-cell autonomous effect of dystroglycan function, wherein changes in ependymal cell function lead to alterations in neural stem cell morphology and potentially, function.

We therefore then examined the P21 SVZ by coronal sections to observe whether niche proliferation was altered at this time in the DG-EC-KO. It became rapidly apparent that one of the interesting aspects of the phenotype in these mice was that the DG-EC-KO SVZ displayed region-specific effects of ependymal dystroglycan loss. As a result, we separated our analysis of niche proliferation into three segments, encompassing the dorsal, middle, and ventral regions of the SVZ. One intriguing finding was that at P21, some EC-DG-KO mice appeared to have adhesions between the lateral and medial walls, extending as far dorsal as the top of the ventricle. Lateral pressure applied to these sections resulted in separation, not between the ventricular walls, but between the ependymal and SVZ layer, suggesting either relatively strong adhesive forces between the ventricular walls, or a disruption of adhesion between the ependymal layer and the underlying cells of the SVZ. (Fig. 4D)

We next examined the proliferation in the P21 SVZ by IHC for Ki67 to test whether the overall proliferative profile was affected by ependymal dystroglycan loss. (Fig. 5A) The dorsal SVZ at P21 displayed a trend towards an increase in proliferation, though this did not reach statistical significance (0.134 ± 0.002 vs. 0.190 ± 0.016 cells/μm^2; p = 0.06) (Fig. 5B), while the middle (0.076 ± 0.011 vs. 0.095 ± 0.006) region's proliferation rate was not affected by the loss of ependymal dystroglycan. (Fig. 5C, D) We also examined the average distance of proliferating cells from the ventricular surface as this is normally tightly regulated in the wildtype SVZ. At P21, there was no apparent difference in the distance of proliferating cells from the ventricular surface in the dorsal and middle regions (Fig. 5E, F). When we examined the ventral region of the SVZ, however, despite no change in the overall proliferation rate (0.095 ± 0.019 vs. 0.081 ± 0.011) (Fig. 5A, B), proliferating cells were mislocalized in the SVZ, being found on average much closer to the ventricular wall in the DG-EC-KO SVZ (13.24 ± 0.18 vs. 9.99 ± 0.19 μm from the VZ surface) (Fig. 6C). These results pose an interesting contrast to our findings in the whole-brain knockout (DG-CNS-KO) where proliferating cells tended to be mislocalized further from the ventricular surface at P0, but then closer at P3. Also of note in this model, is the fact that the mislocalization effect is regional, as the middle and dorsal regions do not show the same effect.

As some changes in the surface laminin were apparent as early as the end of the first postnatal week, we decided to quantify SVZ proliferation at this time point as well. At P8, the dorsal proliferation was already elevated in the DG-EC-KO mice almost twofold (0.224 ± 0.014 vs. 0.371 ± 0.030 μm^2) (Fig. 7A, B) however there was no apparent change in proliferation in the middle (0.153 ± 0.014 vs. 0.172 ± 0.004 μm^2) region once again. (Fig. 7C, D) Additionally, there was no change in the average distance of proliferating cells in the dorsal and middle regions of

the SVZ in DG-EC-KO mice compared with their wildtype littermates at this time (16.05 ± 1.45 vs. 15.37 ± 1.03 μm and 10.43 ± 0.64 vs. 10.67 ± 1.03 μm respectively). (Fig. 7E, F) The identity of the proliferating cells in the dorsal region is still unclear however; although pilot studies indicate generally increased low level Olig2 expression and increased PDGFRα+/PCNA+ immunoreactivity in the SVZ of DG-EC-KO mice (data not shown), the increased proliferation of PDGFRα+ cells alone does not appear to be of a magnitude sufficient to account for the entire increase in SVZ proliferation in these mice. One future direction is the acquisition of nuclear-localized GFAP-GFP reporter mice which, when crossed onto the DG-EC-KO line will enable not only FACS of stem cells for examination of the intracellular signaling status of these cells, but also accurate quantification of NSC proliferation in the SVZ.

In the ventral region of the SVZ, there was no significant difference in proliferation density at P8, but there was a trend towards increased proliferation in the DG-EC-KO mice (0.163 ± 0.023 vs. 0.234 ± 0.014 μm^2). (Fig. 8A, B) Interestingly, at P8 the average distance of proliferating cells in the knockout was significantly *increased* in the DG-EC-KO mice (15.46 ± 0.94 vs. 27.31 ± 1.14 μm) (Fig. 8C, D) in contrast to the decreased proliferation distance seen at P21. Furthermore, knockout SVZs sometimes also displayed a "zone of exclusion" in the ventral region sampled slightly more caudally wherein proliferating cells were excluded from the areas closest to the ventricular surface. (Fig. 8C) This even culminated in some more posterior sections of the SVZ showing a complete lack of proliferation in the ventral region where proliferation only occurred very close to the ventricular surface in the wildtype mice. (Fig. 8D)

These results show that ependymal dystroglycan in particular is required for the proper formation of laminin hubs on the ventricular surface, but that loss of dystroglycan upon FoxJ1 expression does not ablate the hubs to the same level as seen in the nestin-driven knockout. The

formation of the laminin hubs, therefore is a process that begins before the emergence of ependymal cells, but as expected, continues to require dystroglycan during the maturation of ependymal cells over the first weeks of postnatal life. In addition, dystroglycan plays a major role in helping laminin clusters to merge during early postnatal life as well as maintain the laminin hubs during this period.

The results showing alterations in NSC morphology and proliferation by P8 in these animals are striking not only because they show that dystroglycan has cell-type specific effects, but they are also some of the first results to show how crucial proper signaling within ependymal cells is to the function of NSCs. While other studies have demonstrated that ablation of ependymal cells or gross alterations in their ability to function [319, 320] predictably disrupt the SVZ niche, the ependymal cells in this set of studies show only minor structural changes. Nonetheless, either the timing of ependymal maturation or the signaling status of these cells (e.g. expression of notch and/or its ligands) is clearly very important for the regulation of proliferation in the developing niche. Additionally, this effect appears to be related to spatial location within the SVZ, demonstrating yet another level of spatial heterogeneity within the developing SVZ, and expanding on recent discoveries indicating that spatial localization along the surface of the SVZ is a key regulator of stem cell function and fate. (Reviewed in ([321])

Figure IV-1

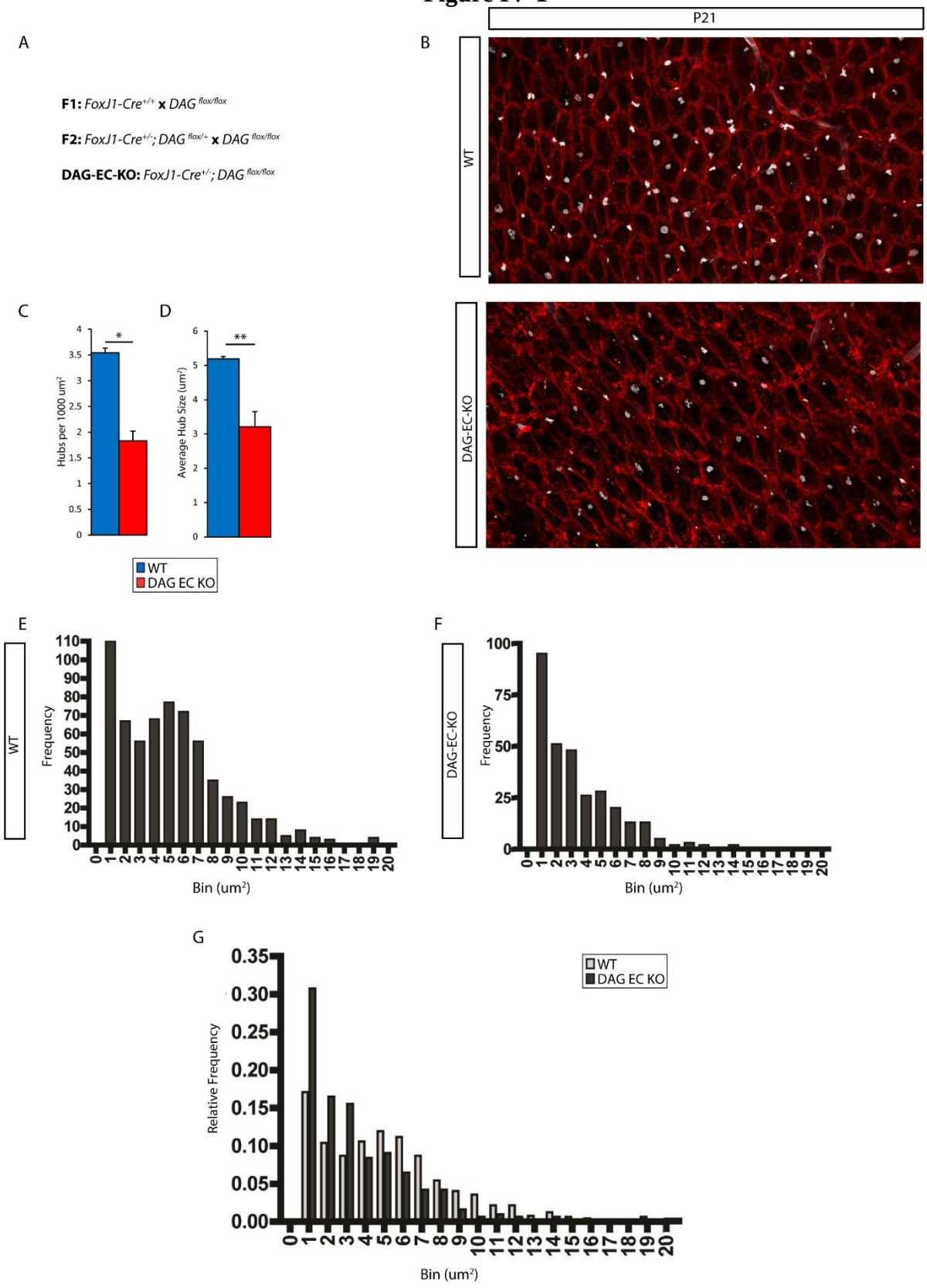
A
F1: FoxJ1-Cre+/+ x DAG flox/flox
F2: FoxJ1-Cre+/-; DAG flox/+ x DAG flox/flox
DAG-EC-KO: FoxJ1-Cre+/-; DAG flox/flox
B
P21
WT
DAG-EC-KO
C
Hubs per 1000 um2
*
D
Average Hub Size (um2)
**
WT
DAG EC KO
E
WT
Frequency
Bin (um2)
F
DAG-EC-KO
Frequency
Bin (um2)
G
WT
DAG EC KO
Relative Frequency
Bin (um2)

Figure IV-1: Ependymal Cell Dystroglycan Continues to Regulate Laminin Hub Formation After FoxJ1 Expression

(A) Breeding scheme used to generate DAG-EC-KO mice
(B) En face view of laminin and β-catenin IHC in WT and DAG-EC-KO P21 SVZ whole mounts to detect laminin+ ECM hubs.
(C) Quantification of laminin hubs per 1,000 mm^2. *$p < 0.05$, Student's t test.
(D) Quantification of mean hub size. **$p < 0.01$, Student's t test.
(E) Histogram of laminin hub frequency by surface area size in WT SVZ wholemounts (n = 3)
(F) Histogram of laminin hub frequency by surface area size in DAG-EC-KO SVZ wholemounts (n = 3)
(G) Histogram of relative laminin hub frequency as a fraction of total hubs by surface area size

Figure IV-2

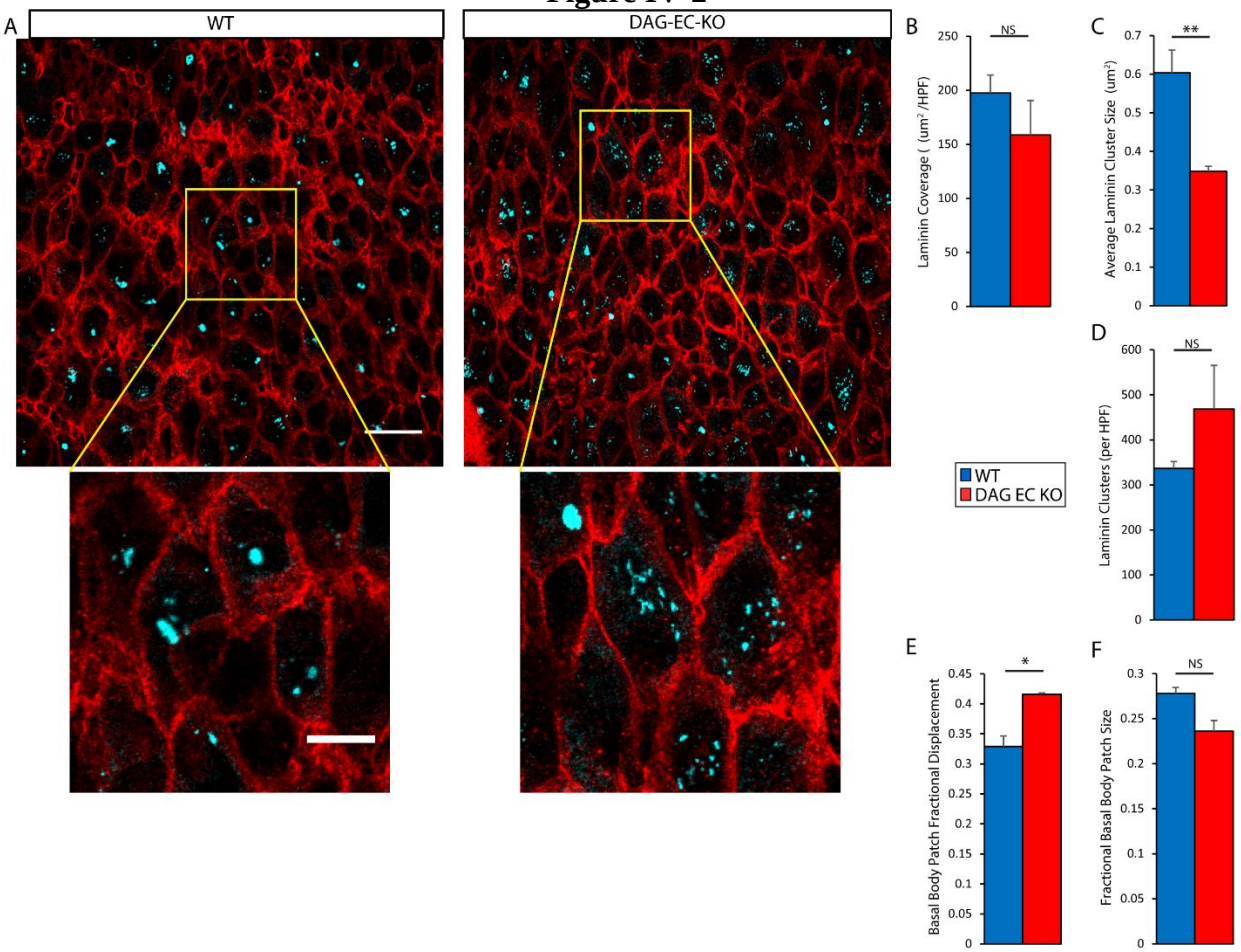

Figure IV-2: Ependymal Cell Dystroglycan Regulates Laminin Hub Cluster Formation

(A) En face view of laminin and β-catenin IHC in WT and DAG-EC-KO P8 SVZ whole mounts to detect laminin+ ECM hubs. Insets are higher magnification view of boxed area.
(B) Quantification of laminin coverage per high power field (HPF) in DAG-EC-KO SVZs (n=3)
(C) Quantification of average size of laminin cluster in WT and DAG-EC-KO SVZs (**$p<0.01$) (n=3)
(D) Quantification of number of laminin clusters per high power field (HPF) in DAG-EC-KO SVZs (n=3)
(E) Quantification of basal body patch displacement as a fraction of apical radius in WT and DAG-EC-KO SVZs as described in Chapter 2, Figure 5 (*$p<0.05$)
(F) Quantification of basal body patch size as a fraction of apical surface area in WT and DAG-EC-KO SVZs

Figure IV-3

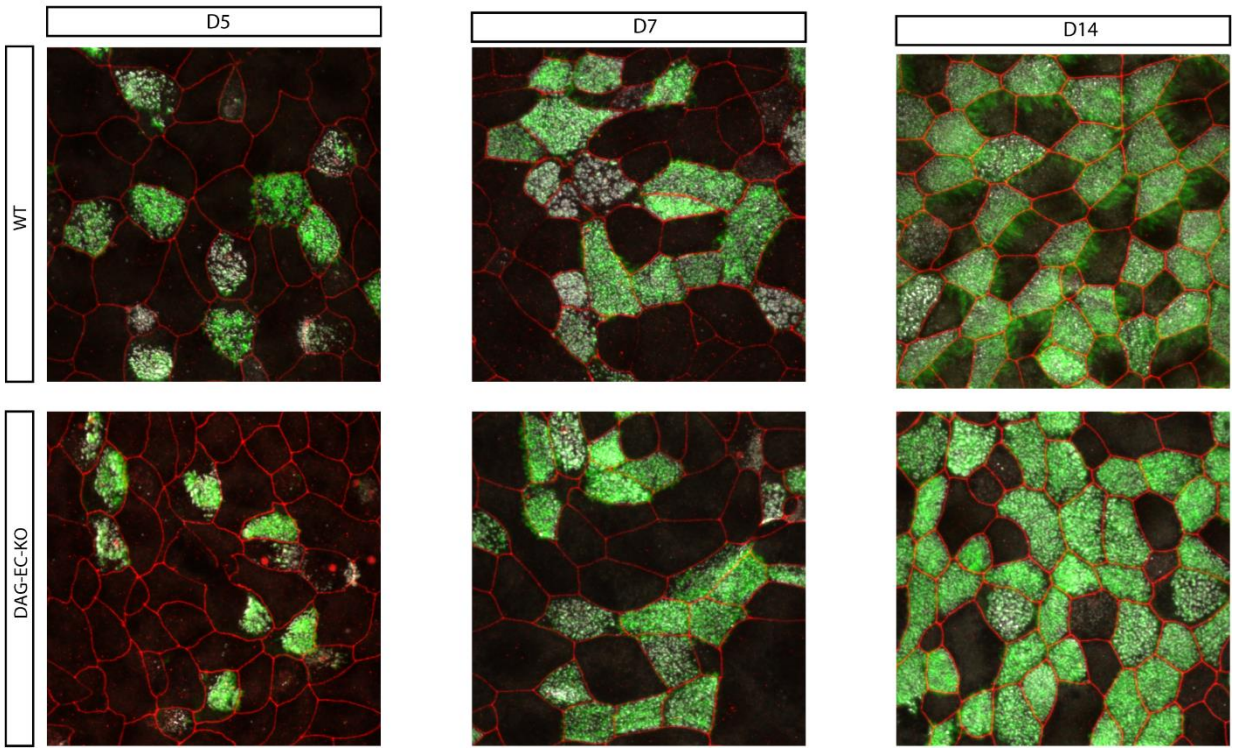

Figure IV-3: Dystroglycan Likely Does Not Regulate Maturation of Airway Epithelial Cells After FoxJ1 Expression

IHC for ZO-1 (red), acetylated α-Tub (green), and γ-tub (white) in mammalian tracheal epithelial preparations from WT and DAG-EC-KO mice at Day 5, 7, and 14 after induction of air-liquid interface.

Figure IV-4

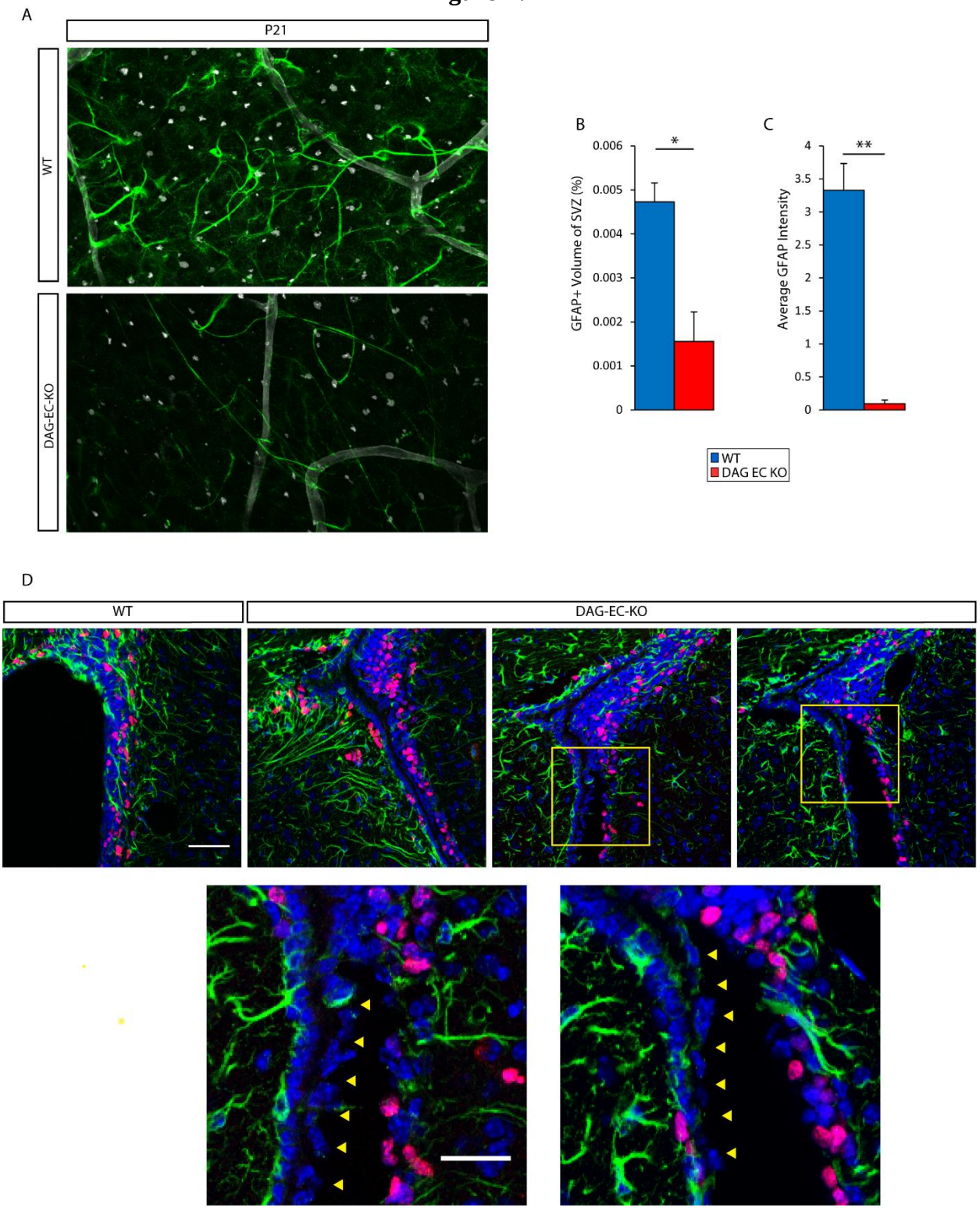
A
P21
WT
DAG-EC-KO
B
GFAP+ Volume of SVZ (%)
0.006
0.005
0.004
0.003
0.002
0.001
0
*
C
Average GFAP Intensity
4
3.5
3
2.5
2
1.5
1
0.5
0
**
WT
DAG EC KO
D
WT
DAG-EC-KO

Figure IV-4: Ependymal Dystroglycan Regulates GFAP Expression and VZ-SVZ Adhesion

(A) En face view of WT and DAG-EC-KO SVZ wholemounts at P21 immunostained for GFAP+ neural stem cells (green), and laminin (white). Representative pictures taken from the anterior central region of the SVZ.
(B) Quantification of the volume of the SVZ taken up by GFAP+ processes analyzed from 3D reconstructions of the SVZ from confocal stacks of WT and DAG-EC-KO SVZs. (*$p<0.05$, n=3)
(C) Average intensity of GFAP+ processes in arbitrary units in WT and DAG-EC-KO SVZs (**$P<0.01$, n=3)
(D) IHC for GFAP (green), Ki67 (red), and DAPI (blue) in coronal sections of WT and DAG-EC-KO SVZs at P21. Right panels: 3 representative DAG-EC-KO sections with increasing separation between the ependymal layer (ventricular zone) and subjacent SVZ. Bottom panels: high magnification of regions indicated by yellow boxes. Arrowheads show separated ependymal layer seen as a row of DAPI+ nuclei. Dorsal regions pictured and analyzed.

Figure IV-5

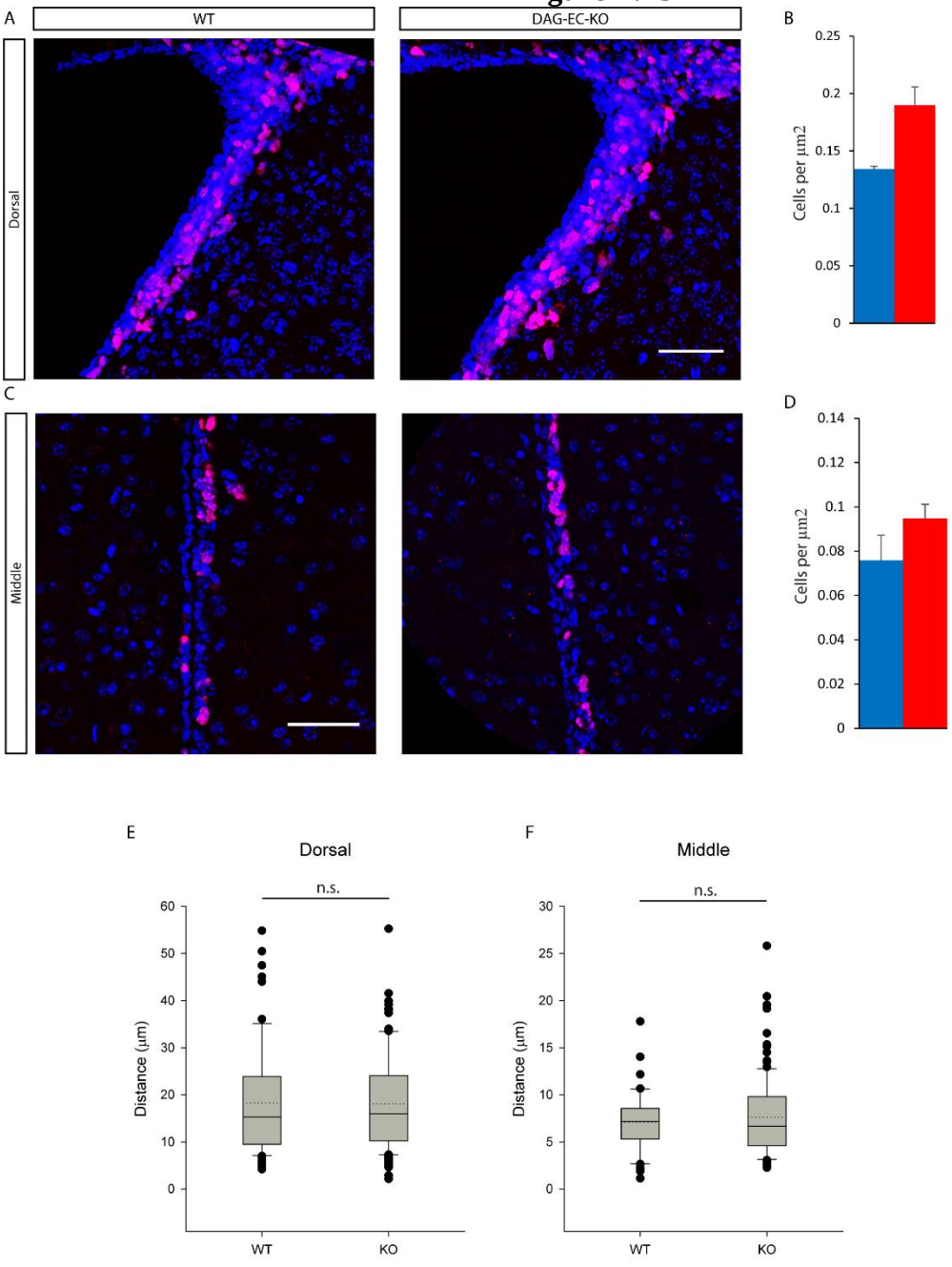
A
WT
DAG-EC-KO
Dorsal
B
Cells per µm2
0.25
0.2
0.15
0.1
0.05
0
C
Middle
D
Cells per µm2
0.14
0.12
0.1
0.08
0.06
0.04
0.02
0
E
Dorsal
n.s.
Distance (µm)
60
50
40
30
20
10
0
WT
KO
F
Middle
n.s.
Distance (µm)
30
25
20
15
10
5
0
WT
KO

Figure IV-5: Ependymal Dystroglycan Loss Does Not Significantly Change Dorsal and Middle Proliferation in the P21 SVZ

(A) IHC for Ki67 (red) and DAPI (blue) in the dorsal region of coronal sections of WT and DAG-EC-KO SVZs at P21
(B) Quantification of proliferation in WT and DAG-EC-KO dorsal SVZs at P21. (n=3)
(C) IHC for Ki67 (red) and DAPI (blue) in the middle region of coronal sections of WT and DAG-EC-KO SVZs at P21.
(D) Quantification of proliferation in WT and DAG-EC-KO middle SVZs at P21. (n=3)
(E) Boxplot of proliferating cells' distances from the ventricular wall in the dorsal region of P21 WT and DAG-EC-KO mice. Solid bar indicates median, dotted line indicates mean, and box extends from 25^{th} to 75^{th} percentiles. Whiskers delineate 10^{th} and 90^{th} percentiles. (n=3)
(F) Boxplot of proliferating cells' distances from the ventricular wall in the middle region of P21 WT and DAG-EC-KO mice. Solid bar indicates median, dotted line indicates mean, and box extends from 25^{th} to 75^{th} percentiles. Whiskers delineate 10^{th} and 90^{th} percentiles. (n=3)

Figure IV-6

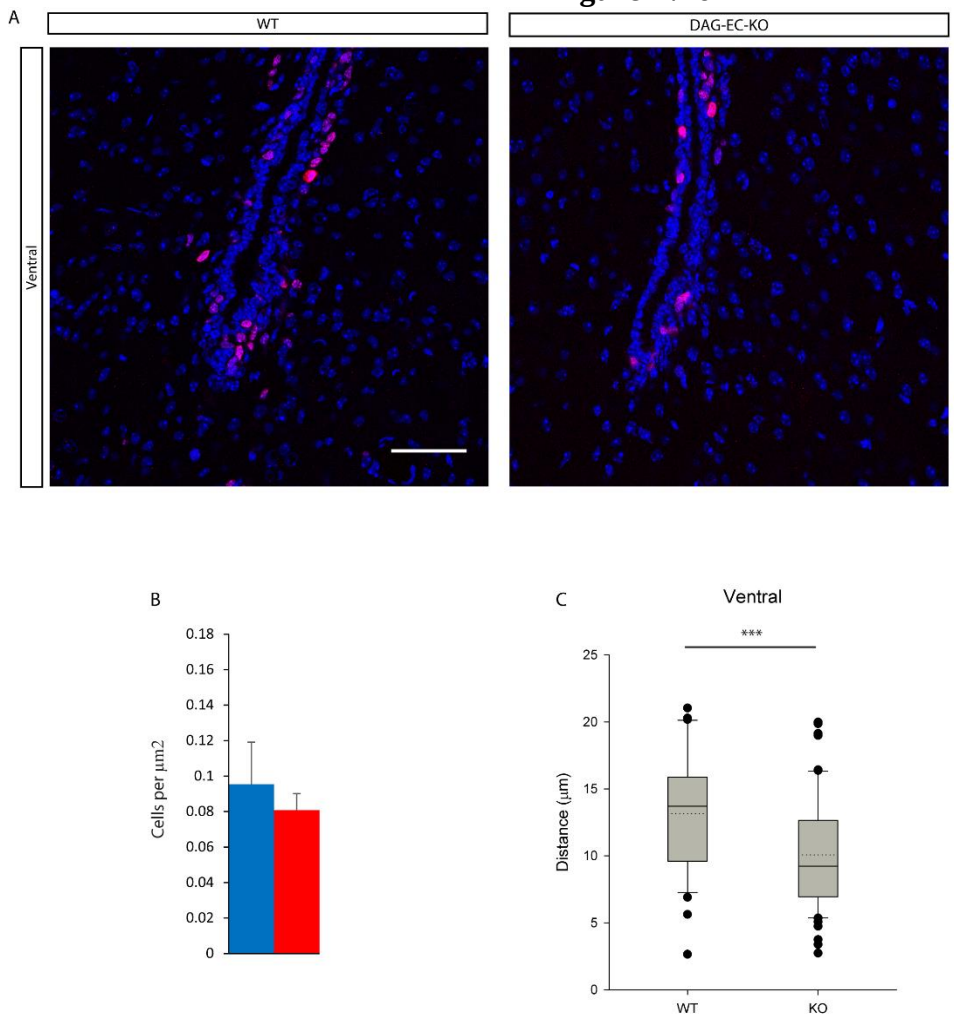

Figure IV-6: Ependymal Dystroglycan Regulates Localization of Proliferating Cells in the Ventral SVZ

(A) IHC for Ki67 (red) and DAPI (blue) in the ventral region of coronal sections of WT and DAG-EC-KO SVZs at P21

(B) Quantification of proliferation in WT and DAG-EC-KO ventral SVZs at P21. (n=3)

(C) Boxplot of proliferating cells' distances from the ventricular wall in the ventral region of P21 WT and DAG-EC-KO mice. Solid bar indicates median, dotted line indicates mean, and box

extends from 25th to 75th percentiles. Whiskers delineate 10th and 90th percentiles. (***$p<0.001$, $n=3$)

Figure IV-7

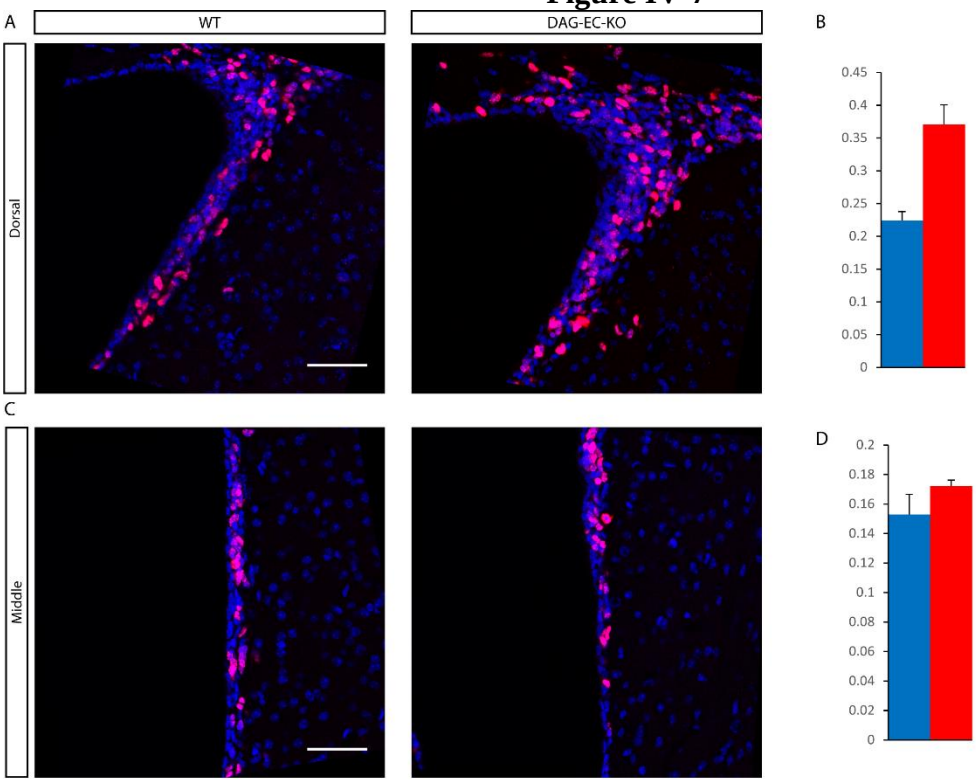
A
WT
DAG-EC-KO
Dorsal
B
0.45
0.4
0.35
0.3
0.25
0.2
0.15
0.1
0.05
0
C
Middle
D
0.2
0.18
0.16
0.14
0.12
0.1
0.08
0.06
0.04
0.02
0

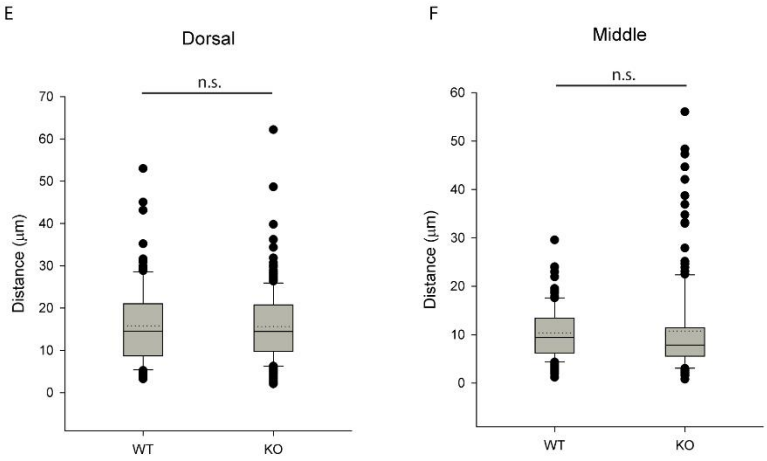
E
Dorsal
n.s.
Distance (μm)
70
60
50
40
30
20
10
0
WT
KO
F
Middle
n.s.
Distance (μm)
60
50
40
30
20
10
0
WT
KO

Figure IV-7: Ependymal Dystroglycan Regulates Dorsal Proliferation in the P8 SVZ

(A) IHC for Ki67 (red) and DAPI (blue) in the dorsal region of coronal sections of WT and DAG-EC-KO SVZs at P8
(B) Quantification of proliferation in WT and DAG-EC-KO dorsal SVZs at P8. (n=3)
(C) IHC for Ki67 (red) and DAPI (blue) in the middle region of coronal sections of WT and DAG-EC-KO SVZs at P8
(D) Quantification of proliferation in WT and DAG-EC-KO middle SVZs at P8. (n=3)
(E) Boxplot of proliferating cells' distances from the ventricular wall in the dorsal region of P8 WT and DAG-EC-KO mice. Solid bar indicates median, dotted line indicates mean, and box extends from 25^{th} to 75^{th} percentiles. Whiskers delineate 10^{th} and 90^{th} percentiles. (n=3)
(F) Boxplot of proliferating cells' distances from the ventricular wall in the dorsal region of P8 WT and DAG-EC-KO mice. Solid bar indicates median, dotted line indicates mean, and box extends from 25^{th} to 75^{th} percentiles. Whiskers delineate 10^{th} and 90^{th} percentiles. (n=3)

Figure IV-8

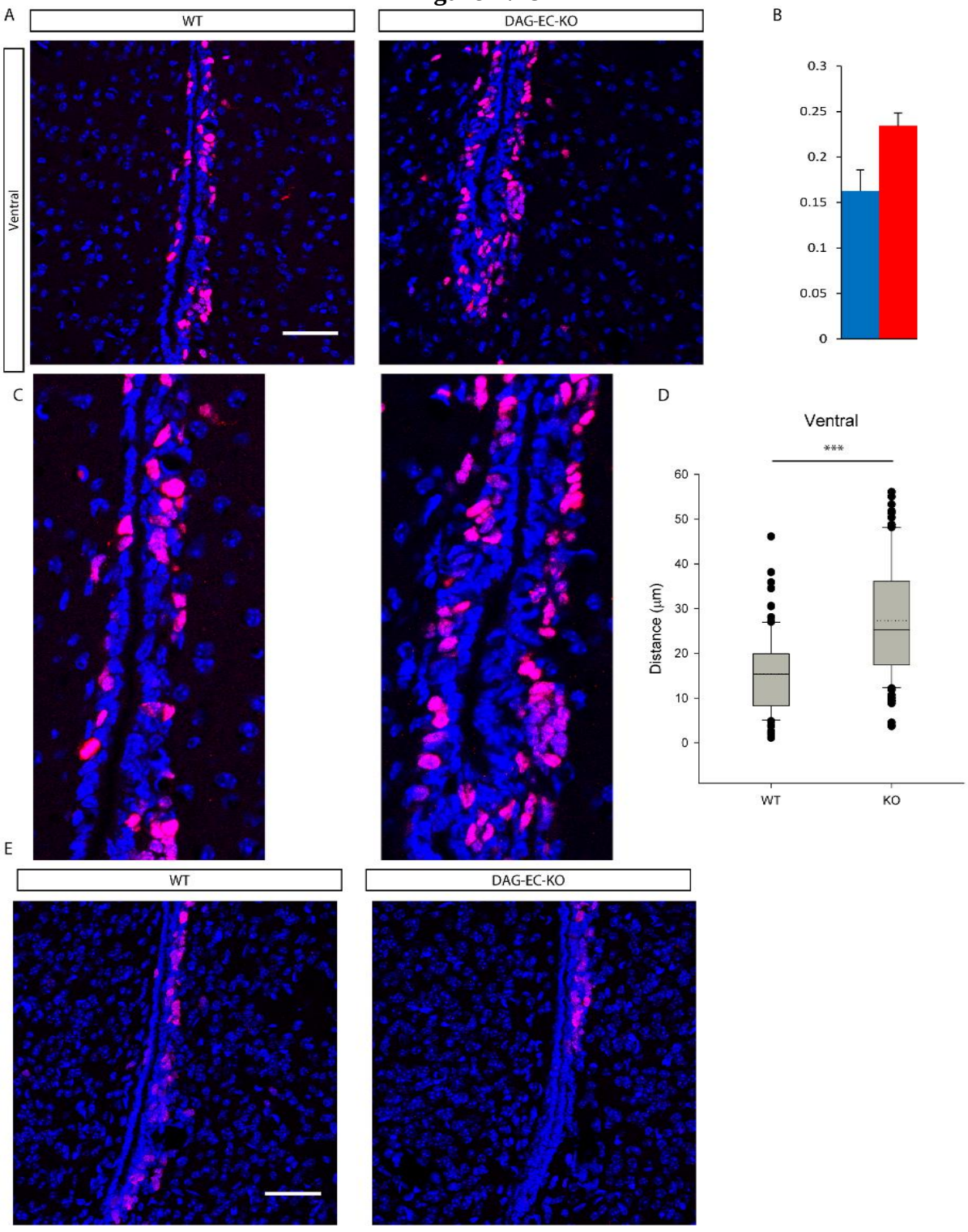
A
WT
DAG-EC-KO
Ventral
B
0.3
0.25
0.2
0.15
0.1
0.05
0
C
D
Ventral
***
60
50
40
30
20
10
0
Distance (μm)
WT
KO
E
WT
DAG-EC-KO

Figure IV-8: Ependymal Dystroglycan Regulates Proliferating Cell in the Ventral P8 SVZ

(A) IHC for Ki67 (red) and DAPI (blue) in the ventral region of coronal sections of WT and DAG-EC-KO SVZs at P8.
(B) Quantification of proliferation in WT and DAG-EC-KO dorsal SVZs at P8. (n=3)
(C) Higher magnification image illustrating proliferation-free zone near the ventricular wall
(D) Boxplot of proliferating cells' distances from the ventricular wall in the dorsal region of P8 WT and DAG-EC-KO mice. Solid bar indicates median, dotted line indicates mean, and box extends from 25^{th} to 75^{th} percentiles. Whiskers delineate 10^{th} and 90^{th} percentiles. (***$p<0.001$, n=3)
(E) IHC for Ki67 (red) and DAPI (blue) in the ventral region of coronal sections of WT and DAG-EC-KO SVZs at P8 from a region more caudal than shown in (A) illustrating absent proliferation in the ventral-most region of the SVZ in the DAG-EC-KO.

Chapter 5: Conclusions and Future Directions

Not only are the neurogenic regions of the brain (i.e. the SVZ and dentate gyrus) enriched in ECM, but the SVZ also houses unique ECM structures such as highly branched ECM fractones, [225] and laminin hubs. In the adult SVZ, the basal processes of NSCs contact the basement membrane of the local vasculature, [203, 204, 221] where α6β1 integrin receptors mediate attachment of NSCs and neural progenitors to vasculature-associated laminin. However it has remained unknown what role ECM receptors have during the phase of "niche building" in which the intricate cell-cell and cell-ECM interactions of the adult SVZ niche are first established. These recent findings establish for the first time dystroglycan as both promoting SVZ niche establishment, i.e., the development of ependymal cells and their organization into niche pinwheel structures, and regulating SVZ niche output, i.e., production of oligodendrocyte progenitors in the early postnatal period.

This new role for dystroglycan, however, raises many new questions. One such set of questions pertains to the functions of laminin hubs. A significant amount of time and cellular energy is likely devoted to generating these structures: hubs take several weeks to fully form, continue to grow throughout life, and maintain contact with GFAP+ NSC processes even in the aged animal [322]. Furthermore, they appear to be generated by cellular machinery distinct from that involved in the vascular ECM of the SVZ, as dystroglycan loss has no appreciable effect on vasculature-associated laminin or on the adhesion of NSCs to the vasculature.

Complicating matters, the nature of the dystroglycan-laminin-integrin relationship makes it difficult to perturb the hubs in isolation. By removing dystroglycan, surface laminin is altered, but this has the potential to indirectly impact laminin-triggered integrin signaling. Thus far, however, integrin signaling in the SVZ does not appear to be affected by loss of dystroglycan or

the concomitant disruption of hubs, although we cannot rule this possibility out. Preventing laminin expression specifically at hub structures, perhaps through an ependymal cell-specific promoter would be a good step forward in understanding the effects of locally produced ECM, but would also be subject to the same potential issue of altering integrin activity. One interesting possibility is to generate a mouse lacking the intracellular domain of dystroglycan, which might allow for laminin binding along the ventricular surface, but at the same time ablate intracellular transmission of dystroglycan-mediated signals.

As it stands, there are several intriguing possibilities as to the function of laminin hubs. The hubs may regulate dystroglycan signaling directly by binding to the dystroglycan receptor and activating downstream signaling cascades. Spatial localization in this context could serve to cluster receptors [169] and/or ensure that both neural stem cells and ependymal cells have access to ligand for dystroglycan activation. Temporal dynamics of dystroglycan-laminin localization are also likely to be important determinants of dystroglycan signaling. Dystroglycan and laminin are preferentially upregulated on the surface of developing ependymal cells, where they begin to form laminin clusters. After the first few weeks of postnatal life, however, these hubs localize to the centers of emerging niche pinwheel structures where they can signal to both cell-types directly. During early development therefore, dystroglycan-mediated signals are more heavily received by ependymal cells. As NSC proliferative activity is altered in the dystroglycan cKO during this time, and dystroglycan loss delays EC emergence and maturation, it is tempting to speculate that niche output disturbances during this time are due to developmentally stalled ECs being unable to provide appropriate cues to regulate NSC proliferation during development. This mechanism may also explain the alterations in niche proliferation seen in the EC-DAG-KO.

ECM hubs may also serve as a sponge to capture growth factors circulating in the CSF, thereby modulating their local concentration, stability, and/or availability. This is one of the functions attributed to a separate set of ECM structures deeper within the SVZ, termed fractones. Fractones have been shown to be able to bind to and capture growth factors, increasing their concentration and potentially their availability in the local environment [226-228]. The CSF is enriched in a wide variety of signaling molecules that may bind to these hubs in this fashion, and the presence and concentration of these factors can change dramatically from day to day during development, which may explain how the dysregulation of NSC dynamics in the dystroglycan-deficient SVZ varies so dramatically over the first few weeks of postnatal life. [323, 324]

Another question prompted by this study is whether dystroglycan signaling modulates only gliogenic NSCs in the SVZ. Judging from levels of Pax6+ neuronal progenitors, we did not observe any changes in neuronal progenitor densities, but more detailed studies are required to definitely rule out changes in the generation of neuronal lineage cells. If, as the evidence suggests, however, dystroglycan regulates gliogenesis without significantly impacting neurogenesis, several potential explanations arise. One straightforward possibility is that this phenomenon is due to timing, i.e. that the early postnatal SVZ is weighted towards gliogenic output, so global disturbances in output result primarily in disrupted gliogenesis. Another possibility is that dystroglycan and/or surface laminin mediate responsiveness to primarily gliogenic cues present in the environment at this time, and so loss of dystroglycan only abrogates the ability of NSCs to properly interpret gliogenic cues. A third possibility, however, is that only NSCs primed to generate oligodendrogenic lineage progeny are competent to receive and/or respond to dystroglycan-mediated signals. This possibility could indicate that dystroglycan signaling is somehow intrinsically related to gliogenesis in the SVZ. It would be interesting to

identify the progeny cells that arise from NSCs characterized by high levels of dystroglycan to see if dystroglycan expression either marks or biases NSC lineage commitment.

Additionally, acute antibody blockade of dystroglycan leads to increases in OPC densities (as measured by PDGFRα+ IHC) within the SVZ with remarkable rapidity (6 hours post-injection). This speed suggests that the loss of dystroglycan binding may in effect remove the "brakes" on the differentiation of NSCs that are already either somehow primed or committed to becoming oligodendrogenic intermediate precursor cells. How this might occur and what those brakes may be pose an exciting area of future exploration. It would, in particular, be interesting to observe the chromatin and expression landscapes of NSC genomes before and after exposure to dystroglycan blocking antibody.

In humans, primary mutations in dystroglycan are exceedingly rare, as dystroglycan is required for proper embryonic attachment to the placenta [173]. However, human pathologies related to dystroglycan occur when mutations arise in a group of enzymes that function to glycosylate dystroglycan thereby modulating its ability to bind extracellular substrates. These mutations lead to a wide variety of diseases collectively termed secondary dystroglycanopathies characterized by muscular dystrophy and a wide range of ocular and cognitive deficits. However, the role of dystroglycan in the development of the CNS is still poorly understood. Dystroglycan at the basal endfeet of radial glia helps mediate attachment to the pial surface during embryonic development, and a reduction of dystroglycan's ability to bind its extracellular partners leads to detachment of these processes and concomitant disorganization of radial neuronal migration [188, 192]. Additionally, neuronal (as opposed to glial) dystroglycan appears to play a role in hippocampal long-term potentiation, though its actions at the synapse remain poorly understood. [146, 188] Recent work has shown that during development, dystroglycan binds to the axon

guidance molecule Slit (which contains the laminin-like globular, or LG, domain) and as such, regulates axon pathfinding in the developing CNS [325]. These studies along with the results discussed here [290] make it clear that dystroglycan plays a major role in the development of the CNS, both embryonically and postnatally, and explain how even mild alterations in dystroglycan's ability to bind its extracellular partners can lead to significant pathologies.

By examining the ECM-dystroglycan signaling axis in postnatal brain development, this set of studies has revealed a new role for dystroglycan in both building the SVZ neural stem cell niche and in regulating the output of this niche. The details of how dystroglycan and the laminin hubs it engenders regulate NSC development and activity remain to be fully understood, though the Notch pathway appears to be a key mediator of dystroglycan function in this context. The role of p27, Shh, and other signaling mediators however, remain exciting avenues of future inquiry. Futhermore, while dystroglycan clearly plays a role in the postnatal development of the V/SVZ, it remains unknown whether it has a role in the maintenance of the adult niche, or upon reactivation of the niche in response to injury. Our lab is currently in the process of setting up experimental models to be able to probe these questions.

The findings that ependymal cell dystroglycan loss dysregulates NSC and progenitor function in the SVZ make understanding the niche support functions that ependymal cells provide more important to if we are to gain a better picture of endogenous neural stem cell function. The results of those studies would also be likely to have a major impact on the burgeoning field of *in vitro* stem cell production and maintenance for therapeutic strategies. These results also present the possibility that laminin hubs, by virtue of their location at the interface of ependymal cells and NSCs and accessible via the CSF, may serve as a new target for therapeutic strategies for early development. For example, either modulating the hubs, or

designing therapeutics that can bind directly to these structures, could locally and transiently affect NSC activation and dynamics. While the studies described here have demonstrated a role for dystroglycan-ECM interactions in the SVZ, it is clear that we have only begun to scratch the surface of understanding the role these interactions play in the SVZ in development, health, and disease.

Chapter 6: Materials and Methods

Mice

Generation of conditional *DAG1* mutant mice (*nestin-Cre*$^{+}$*:DAG1*$^{fl/fl}$) was achieved using *DAG1*$^{fl/fl}$ mice [188], and *nestin-Cre* mice [326]. Generation of conditional DAG1 mutant mice (*CNP-Cre+:DAG1*$^{fl/fl}$) was achieved using *CNP-Cre* mice [327]. Generation of inducible conditional DAG1 mutant mice (*nestin-Cre*ER^{T2+}*;DAG1*$^{fl/fl}$) was achieved using *nestin-Cre*ER^{T2} mice [328]. Generation of conditional FoxJ1 mutant mice was achieved using FoxJ1-Cre mice [329]. For induction, tamoxifen was dissolved in corn oil at 1 μg/uL and delivered by intragastric injection for a final dose of 50 μg on three consecutive days beginning at birth. All rodent experiments were conducted with the approval by the Institutional Animal Care and Use Committee of Stony Brook University and conform to National Institutes of Health guidelines.

SVZ Wholemount Dissection and Immunohistochemistry

SVZ wholemounts were dissected as previously described [330]. Briefly, a 2-3 mm thick strip of the striatal wall of the lateral ventricle parallel to the ventricular wall itself was dissected from underneath the corpus callosum to the top of the midbrain at the ventral tip of the lateral ventricle from mice at various postnatal ages as indicated, fixed with cold 4% paraformaldehyde in 0.1 M PBS for 12 hours at 4°C and washed with PBS prior to staining. For laminin immunohistochemistry, wholemounts were fixed with cold 4% paraformaldehyde for 30 minutes on ice, followed by 100% methanol on ice. To visualize antigens at the ventricular surface, wholemounts were blocked in 10% donkey serum with 0.2% Triton-X100 and incubated with primary and secondary antibodies for 24 hours at 4°C. For deeper structures, wholemounts were

blocked with 10% donkey serum with 0.5% or 2% Triton-X100 and incubated in primary and secondary antibodies for 48 hours.

Frozen Tissue Processing and Immunohistochemistry

Mice were first deeply anesthetized with isofluorane and intra-cardially perfused and brains post-fixed with 4% paraformaldehyde (PFA) in 0.1M PBS. Brains from mice younger than P14 were immersion-fixed in 4% PFA at 4°C. Tissue was cryo-protected with 30% sucrose in PBS, embedded in OCT medium and frozen in dry ice cooled with isopentane. 18 - 40 µm sections were prepared on a cryostat, blocked in 10% donkey serum with 0.1% Triton X-100, incubated with primary antibodies diluted in blocking solution overnight at 4°C and incubated with appropriate fluorophore-conjugated secondary antibodies (Jackson) in blocking solution at room temperature for 2 hours. Sections less than 20 µm in thickness were stained on glass slides, while sections greater than 20 µm were stained in wells as floating sections. Selected antigens were visualized by antigen retrieval with citrate buffer target retrieval solution (Dako) performed at 95°C for 25 minutes prior to washing in 0.1M PBS and blocking.

Cell Culture

For neurosphere and ependymal cell culture experiments, the lateral ventricular wall was dissected from P0/1 mice and mechanically dissociated in MEM with 25mM HEPES (Lonza) with 1% Pen/Strep (Mediatech). For neurosphere differentiation assays, cells isolated from Nestin-Cre/DAG$^{fl/fl}$ mice and their wild-type littermates were grown in suspension in DMEM/F12 (Thermo) with B27 (GIBCO) and 20 ng/mL EGF and FGF (Peprotech). Neurospheres were passaged at 5 and 10 days in vitro. Following the second passage, cells were

resuspended in the same media without growth factors, plated at 15,000 cells/cm^2 on PDL-coated chamber slides and differentiated for timepoints as indicated in the text. Cells were fixed with 4% PFA in PBS for 15 minutes at room temperature and washed with PBS prior to staining. Ependymal cell cultures were performed as previously described [331]. Briefly, cells isolated from wildtype or FoxJ1-GFP mice were resuspended in DMEM-High Glucose (Mediatech) with 10% FBS and 1% Pen/Strep and plated at 100,000 cells/cm^2 on PDL-coated chamber slides. Each SVZ was dissected and plated separately as a biological replicate. For ependymal cell differentiation experiments, cells were incubated under normal cell culture conditions until confluent (3-5 days), then media was switched to 2% FBS and cells were incubated for time periods as indicated, up to 7 days. Dystroglycan-blocking (IIH6C4, Millipore) or IgM control antibodies (Biolegend) were added to culture media at 10 μg/ml and refreshed every 3 days for long term experiments. DAPT and SAHM1 were used at 10 μM and 20 μM, respectively, in DMSO. Control cells were treated with equivalent volume of vehicle (DMSO). For all experiments, cells were fixed with 4% PFA in PBS. For oligodendrocyte progenitor cell (OPC) experiments, OPCs were isolated as previously described [285]. Briefly, cerebral cortices dissected from neonatal rats were dissociated using papain and trituration, then resuspended in DMEM supplemented with 10% FBS and seeded onto PDL-coated flasks. Medium was changed every 3 days, and after 10 days, OPCs were isolated by mechanical agitation and differential adhesion [332]. Isolated OPCs were resuspended in SATO with T3 to induce differentiation and plated on PDL-coated dishes. For cell transfection experiments, 1.5 μg of plasmid was mixed with 18 μL PEI and 300 μL optiMEM. Transfection was conducted in 10 cm dishes at 70% confluence, and cells were washed after 4.5 hours in media. 293T cells were washed and grown

in DMEM + 10% Bovine Calf Serum + 1% Pen/Strep, while C2C12 cells were washed and grown in DMEM + 10% Fetal Bovine Serum + 1% Pen/Strep.

In Vivo Antibody Injections

Postnatal day 2 Sprague-Dawley rats were anaesthetized on ice, positioned in a stereotaxic device and given a single 2.5 µL injection of IIH6 antibody or mouse IgM control at 1 mg/mL into the lateral ventricle (1.4 lateral, 2.2 ventral to bregma).

qRT-PCR

Total RNA was isolated using Qiazol and cleaned up with RNAeasy Kit (Qiagen), with DNase being used to eliminate DNA contamination. Synthesis of cDNA was carried out using the ProtoScript First Strand kit (New England Biolabs). qPCR was performed on a StepOnePlus system (Applied Biosystems) in a 20-µL reaction mixture using SYBR Green Fast PCR master mix or SYBR Green PowerUp master mix. Cycle parameters were 3s at 95ºC and 30s at 60ºC, or 1s at 95ºC and 30s at 60ºC respectively. Amplification data were normalized to GAPDH.

Image Acquisition and Analysis

Coronal sections and SVZ wholemounts were imaged with a Zeiss LSM 510, a Leica SP5, or Leica SP8X confocal laser-scanning microscope. SVZ wholemount fields were random fields were selected from anterior dorsal areas. Images from selected cell culture preparations were acquired on a Zeiss Axiovert 200M epifluorescent microscope. All images were processed and quantified using ImageJ software. For in vivo ependymal cell pinwheel analysis and in vitro cluster analysis, pinwheels/clusters were defined as 4 or more ependymal cells immediately

adjacent to each other and one or more monociliated cells. Clusters of basal bodies, visualized using γ-tubulin immunohistochemistry, in conjunction with apical cell area, were used to define multiciliated ependymal cells, whereas NSCs were defined by the presence of a single primary cilium and a smaller apical surface area. Where pinwheels overlapped, the larger of the two was measured. For *in vitro* analysis of FoxJ1+ cells and multicilliated cells via IHC, cells were plated in 8-well glass bottomed chamberslides. 9 images were taken from each well in a 3 x 3 box pattern for analysis.

Basal Body Patch Analysis

Cell outlines and basal body (BB) patches were manually outlined using ImageJ software. Absolute areas were directly calculated and reported while fractional areas were calculated by dividing the area of the BB patch by the apical cell surface area. The center of each area was calculated in ImageJ and the vector from the center of the cell and center of the BB patch was calculated. The angle of this vector was termed the BB patch angle, which was normalized to the average of all angles within a given field (set at 180 degrees). The percent distribution of patch angles was plotted in a histogram with a 15 degree bin. BB patch displacement was calculated by taking the magnitude of this vector. Fractional displacement was calculated by dividing the magnitude of the vector running from the center of the cell to the center of the BB patch by the magnitude of a manually drawn vector running from the center of the cell through the center of the BB and terminating at the cell border.

Statistics

All data are expressed as mean +/- SEM. Student's t-tests and ANOVA analyses were performed using Excel and SigmaPlot software. Patch angle distributions were analyzed using the Watson's U^2 test (MatLab). P values of <0.05 were defined as statistically significant.

Primary Antibodies

Rabbit anti-γ-tubulin (Sigma-Aldrich T5192, 1:500), mouse anti-β-catenin (BD Transduction 610153, 1:500), mouse IgM anti-α-Dystroglycan, clone IIH6C4 (Upstate Cell Signaling 05-593, 1:50- 1:100), mouse anti-PCNA (Cell Signaling Technology, 1:200), rabbit anti-Sox2 (Millipore AB5603, 1:100), chicken anti-Nestin (Aves Labs NES, 1:500), mouse anti-Nestin (Developmental Studies Hybridoma Bank Rat-401, 1:5), rat anti-MBP (Serotec MCA409S, 1:100), mouse anti-CNPase (Sigma C5922, 1:100), rabbit anti-NG2 (Chemicon International AB5320, 1:200), mouse anti-APC (CC-1) (Calbiochem OP80, 1:100), rabbit anti-GFAP (DakoCytomation Z0334, 1:500), rat anti-PDGFRα (CD140a) (BD Pharmingen 558774, 1:100), rabbit anti-PDGFRα (Santa Cruz SC-338, 1:150), rabbit anti-Laminin (Sigma L9393, 1:100), chicken anti-GFP(Aves GFP, 1:500), rat anti-CD24 (BD Biosciences 557436, 1:100-1:200), rabbit anti-notch ICD for IHC (Abcam), mouse anti-notch ICD for western (Developmental Studies Hybridoma Bank).

Primers

Myb: 5'-AGC AGG CAT TAC CAA CAC AGA-3' and 5'-CTG CTG AGA TCA CAC CAC GA-3'; *FoxJ1*: 5'-CTT CCG CCA TGC AGA CCC CA-3' and 5'-CGG GCA AAG GCA GGG TGG AT-3'; *Notch1*: 5'-AGT GCA ACC CCC TGT ATG AC-3' and 5'-TCT AGG CCA TCC CAC TCA CA-3'; *Numb*: 5'-GGC TTC TTT GGA AAA ACG GGA-3' and 5'-CTC AGT CTT

TCC CCC GTG TC3’; *MCIDAS*: 5’GGC CTC AGT GCT GGA TAA GC-3' and 5'-TAG GGT CAC GAT TGT GCA GG-3'; *Jagged1*: 5’- ATA CAC GTG GCC ATC TCT GC-3’ and 5’-CCG CTT CCT TAC ACA CCA GT-3’; *Jagged2*: 5’- TGC CTC TAA CCC ATG TGC AG – 3’ and 5’- TCA CAC TCA TTG GCG TCC AG-3’; *Dll1*: 5’- ACC AAG TGC CAG TCA CAG AG-3’ and 5’- TCC ATC TTA CAC CTC AGT CGC – 3’; *Dll3*: 5’ - GGG CAG CTG TAG TGA AAC CT-3’ and 5’- CTT CAC CGC CAA CAC ACA AG-3’; *Dll4*: 5’ - GTG GCA GCT GTA AGG ACC A – 3’ and 5’- CGC GCA GGT CAA GGT ACT AT-3’; *Olig2*: 5’ - TTA CAG ACC GAG CCA ACA CC – 3’ and 5’- TCA ACC TTC CGA ATG TGA ATT AGA -3’; *Mash1*: 5’ - GAA TGG ACT TTG GAA GCA GGA TG-3’ and 5’- CAT TTG ACG TCG TTG GCG AG- 3’; *Sox9*: 5’ - CAC AAG AAA GAC CAC CCC GA – 3’ and 5’- GGA CCC TGA GAT TGC CCA GA-3’; *Hes5*: 5’ - CAA GGA GAA AAA CCG ACT GCG – 3’ and 5’ - GCG AAG GCT TTG CTG TGT TT – 3’; *HeyL*: 5’ - GAA GAA GCG CAG AGG GAT CA – 3’ and 5’ - AGG CAT TCC CGA AAC CCA AT – 3’; 5’-*Hes1*: CTA CCC CAG CCA GTG TCA AC-3’ and 5’-ATG CCG GGA GCT ATC TTT CT-3’; *Hey1*: 5’- TAC CCA GTG CCT TTG AGA AG-3’ and 5’- AAC CCC AAA CTC CGA TAG TC-3’

Genotyping Primers: Dag Forward: GGA GAG GAT CAA TCA TGG; Reverse: CAA CTG CTG CAT CTC TAC

Chapter 7: References

1. Weissman, I.L., *Stem Cells: Units of Development, Units of Regeneration, and Units in Evolution.* Cell, 2000. **100**(1): p. 157-168.
2. Fuchs, E. and T. Chen, *A matter of life and death: Self-renewal in stem cells.* EMBO Reports, 2013. **14**(1): p. 39-48.
3. Morrison, S.J. and J. Kimble, *Asymmetric and symmetric stem-cell divisions in development and cancer.* Nature, 2006. **441**(7097): p. 1068-1074.
4. Cheung, T.H. and T.A. Rando, *Molecular regulation of stem cell quiescence.* Nat Rev Mol Cell Biol, 2013. **14**(6): p. 329-340.
5. Terzi, M.Y., M. Izmirli, and B. Gogebakan, *The cell fate: senescence or quiescence.* Molecular Biology Reports, 2016. **43**(11): p. 1213-1220.
6. Baserga, R., *BIOCHEMISTRY OF THE CELL CYCLE: A REVIEW.* Cell Proliferation, 1968. **1**(2): p. 167-191.
7. Patt, H.M. and H. Quastler, *Radiation effects on cell renewal and related systems.* Physiol Rev, 1963. **43**: p. 357-96.
8. Pardee, A.B., *A Restriction Point for Control of Normal Animal Cell Proliferation.* Proceedings of the National Academy of Sciences, 1974. **71**(4): p. 1286-1290.
9. Zetterberg, A. and O. Larsson, *Kinetic analysis of regulatory events in G1 leading to proliferation or quiescence of Swiss 3T3 cells.* Proceedings of the National Academy of Sciences, 1985. **82**(16): p. 5365-5369.
10. Orford, K.W. and D.T. Scadden, *Deconstructing stem cell self-renewal: genetic insights into cell-cycle regulation.* Nat Rev Genet, 2008. **9**(2): p. 115-128.
11. Tothova, Z. and D.G. Gilliland, *FoxO Transcription Factors and Stem Cell Homeostasis: Insights from the Hematopoietic System.* Cell Stem Cell, 2007. **1**(2): p. 140-152.
12. Tothova, Z., et al., *FoxOs Are Critical Mediators of Hematopoietic Stem Cell Resistance to Physiologic Oxidative Stress.* Cell, 2007. **128**(2): p. 325-339.
13. Renault, V.M., et al., *FoxO3 Regulates Neural Stem Cell Homeostasis.* Cell Stem Cell, 2009. **5**(5): p. 527-539.
14. Takubo, K., et al., *Regulation of the HIF-1α Level Is Essential for Hematopoietic Stem Cells.* Cell Stem Cell, 2010. **7**(3): p. 391-402.
15. Gurumurthy, S., et al., *The Lkb1 metabolic sensor maintains haematopoietic stem cell survival.* Nature, 2010. **468**(7324): p. 659-663.
16. Gan, B., et al., *Lkb1 regulates quiescence and metabolic homeostasis of haematopoietic stem cells.* Nature, 2010. **468**(7324): p. 701-704.
17. Latil, M., et al., *Skeletal muscle stem cells adopt a dormant cell state post mortem and retain regenerative capacity.* Nature Communications, 2012. **3**: p. 903.
18. Narbonne, P. and R. Roy, *Inhibition of germline proliferation during C. elegans dauer development requires PTEN, LKB1 and AMPK signalling.* Development, 2006. **133**(4): p. 611-619.
19. Li, L. and H. Clevers, *Coexistence of Quiescent and Active Adult Stem Cells in Mammals.* Science (New York, N.Y.), 2010. **327**(5965): p. 542-545.
20. Hüttmann, A., et al., *Functional heterogeneity within rhodamine123lo Hoechst33342lo/sp primitive hemopoietic stem cells revealed by pyronin Y.* Experimental Hematology, 2001. **29**(9): p. 1109-1116.
21. Fukada, S.-i., et al., *Molecular Signature of Quiescent Satellite Cells in Adult Skeletal Muscle.* STEM CELLS, 2007. **25**(10): p. 2448-2459.
22. Conboy, M.J., A.O. Karasov, and T.A. Rando, *High Incidence of Non-Random Template Strand Segregation and Asymmetric Fate Determination In Dividing Stem Cells and their Progeny.* PLOS Biology, 2007. **5**(5): p. e102.

23. Shinin, V., et al., *Asymmetric division and cosegregation of template DNA strands in adult muscle satellite cells.* Nat Cell Biol, 2006. **8**(7): p. 677-682.
24. Cotsarelis, G., T.-T. Sun, and R.M. Lavker, *Label-retaining cells reside in the bulge area of pilosebaceous unit: Implications for follicular stem cells, hair cycle, and skin carcinogenesis.* Cell, 1990. **61**(7): p. 1329-1337.
25. Potten, C.S., et al., *The segregation of DNA in epithelial stem cells.* Cell, 1978. **15**(3): p. 899-906.
26. Wilson, A., et al., *Hematopoietic Stem Cells Reversibly Switch from Dormancy to Self-Renewal during Homeostasis and Repair.* Cell, 2008. **135**(6): p. 1118-1129.
27. Buczacki, S.J.A., et al., *Intestinal label-retaining cells are secretory precursors expressing Lgr5.* Nature, 2013. **495**(7439): p. 65-69.
28. Van Keymeulen, A., et al., *Distinct stem cells contribute to mammary gland development and maintenance.* Nature, 2011. **479**(7372): p. 189-193.
29. Shackleton, M., et al., *Generation of a functional mammary gland from a single stem cell.* Nature, 2006. **439**(7072): p. 84-88.
30. Ousset, M., et al., *Multipotent and unipotent progenitors contribute to prostate postnatal development.* Nat Cell Biol, 2012. **14**(11): p. 1131-1138.
31. Forsberg, E.C., et al., *Molecular Signatures of Quiescent, Mobilized and Leukemia-Initiating Hematopoietic Stem Cells.* PLOS ONE, 2010. **5**(1): p. e8785.
32. Blanpain, C., et al., *Self-Renewal, Multipotency, and the Existence of Two Cell Populations within an Epithelial Stem Cell Niche.* Cell, 2004. **118**(5): p. 635-648.
33. Lien, W.-H., et al., *Genome-wide Maps of Histone Modifications Unwind In Vivo Chromatin States of the Hair Follicle Lineage.* Cell Stem Cell, 2011. **9**(3): p. 219-232.
34. Liu, Y., et al., *p53 Regulates Hematopoietic Stem Cell Quiescence.* Cell Stem Cell, 2009. **4**(1): p. 37-48.
35. Cheng, T., et al., *Hematopoietic Stem Cell Quiescence Maintained by p21^{cip1/waf1}.* Science, 2000. **287**(5459): p. 1804-1808.
36. Zou, P., et al., *p57Kip2 and p27Kip1 Cooperate to Maintain Hematopoietic Stem Cell Quiescence through Interactions with Hsc70.* Cell Stem Cell, 2011. **9**(3): p. 247-261.
37. Bjornson, C.R.R., et al., *Notch Signaling Is Necessary to Maintain Quiescence in Adult Muscle Stem Cells.* STEM CELLS, 2012. **30**(2): p. 232-242.
38. Mourikis, P., et al., *A Critical Requirement for Notch Signaling in Maintenance of the Quiescent Skeletal Muscle Stem Cell State.* STEM CELLS, 2012. **30**(2): p. 243-252.
39. Chapouton, P., et al., *Notch Activity Levels Control the Balance between Quiescence and Recruitment of Adult Neural Stem Cells.* The Journal of Neuroscience, 2010. **30**(23): p. 7961-7974.
40. He, H., et al., *p53 and p73 Regulate Apoptosis but Not Cell-Cycle Progression in Mouse Embryonic Stem Cells upon DNA Damage and Differentiation.* Stem Cell Reports, 2016. **7**(6): p. 1087-1098.
41. Wingert, S., et al., *DNA-damage response gene GADD45A induces differentiation in hematopoietic stem cells without inhibiting cell cycle or survival.* Stem Cells, 2016. **34**(3): p. 699-710.
42. Beerman, I., et al., *Quiescent hematopoietic stem cells accumulate DNA damage during aging that is repaired upon entry into cell cycle.* Cell Stem Cell, 2014. **15**(1): p. 37-50.
43. Drummond-Barbosa, D. and A.C. Spradling, *Stem cells and their progeny respond to nutritional changes during Drosophila oogenesis.* Dev Biol, 2001. **231**(1): p. 265-78.
44. Arvidsson, A., et al., *Neuronal replacement from endogenous precursors in the adult brain after stroke.* Nat Med, 2002. **8**(9): p. 963-70.
45. Yan, Y.P., et al., *Insulin-like growth factor-1 is an endogenous mediator of focal ischemia-induced neural progenitor proliferation.* Eur J Neurosci, 2006. **24**(1): p. 45-54.
46. Suzuki, S., et al., *Estradiol enhances neurogenesis following ischemic stroke through estrogen receptors alpha and beta.* J Comp Neurol, 2007. **500**(6): p. 1064-75.

47. van Es, J.H., et al., *Dll1+ secretory progenitor cells revert to stem cells upon crypt damage.* Nat Cell Biol, 2012. **14**(10): p. 1099-1104.
48. Sato, T., et al., *Paneth cells constitute the niche for Lgr5 stem cells in intestinal crypts.* Nature, 2011. **469**(7330): p. 415-418.
49. Srinivasan, S., A.P. Mahowald, and M.T. Fuller, *The receptor tyrosine phosphatase Lar regulates adhesion between Drosophila male germline stem cells and the niche.* Development, 2012. **139**(8): p. 1381-1390.
50. Winkler, I.G., et al., *Vascular niche E-selectin regulates hematopoietic stem cell dormancy, self renewal and chemoresistance.* Nat Med, 2012. **18**(11): p. 1651-1657.
51. Swift, J., et al., *Nuclear Lamin-A Scales with Tissue Stiffness and Enhances Matrix-Directed Differentiation.* Science, 2013. **341**(6149).
52. Forristal, C.E., et al., *Pharmacologic stabilization of HIF-1α increases hematopoietic stem cell quiescence in vivo and accelerates blood recovery after severe irradiation.* Blood, 2013. **121**(5): p. 759-769.
53. Trappmann, B., et al., *Extracellular-matrix tethering regulates stem-cell fate.* Nat Mater, 2012. **11**(7): p. 642-649.
54. Rahul Jandial, A.L.H., Michael L Levy, Evan Y Snyder, *Stem Cell Therapy for Brain Tumors*, in *CNS Regeneration: Basic Science and Clinical Advances*, M.H.T. Jeffrey H Kordower, Editor. 2008, Elsevier: New York. p. 147.
55. Buchholtz, A., *Ueber das Vorkommen von Karyokinesen in Zellen des Centralnervensystems von neugeborenen und jungen Hunden.* Neur. Centralblatt, 1890. **9**: p. 140-142.
56. Sclavunos, G., *Ueber Keimzellen in d. weissen Substanz d. Ruckenmarks von alteren Embryonen und Neugeborenen.* Anat. Anzeiger, 1899. **16**: p. 467 - 473.
57. Allen, E., *The cessation of mitosis in the central nervous system of the albino rat.* Journal of Comparative Neurology, 1912. **22**: p. 547-568.
58. Bryans, W.A., *Mitotic activity in the brain of the adult rat.* Anat. Rec., 1959. **133**: p. 65-71.
59. Taylor, J.H., P.S. Woods, and W.L. Hughes, *THE ORGANIZATION AND DUPLICATION OF CHROMOSOMES AS REVEALED BY AUTORADIOGRAPHIC STUDIES USING TRITIUM-LABELED THYMIDINEE.* Proceedings of the National Academy of Sciences of the United States of America, 1957. **43**(1): p. 122-128.
60. Altman, J., *Are new neurons formed in the brains of adult mammals?* Science, 1962. **135**(3509): p. 1127-8.
61. Altman, J. and G.D. Das, *Autoradiographic and histological evidence of postnatal hippocampal neurogenesis in rats.* J Comp Neurol, 1965. **124**(3): p. 319-35.
62. Altman, J. and G.D. Das, *Post-natal origin of microneurones in the rat brain.* Nature, 1965. **207**(5000): p. 953-6.
63. Korr, H., *Proliferation of different cell types in the brain.* Adv Anat Embryol Cell Biol, 1980. **61**: p. 1-72.
64. Goldman, S.A. and F. Nottebohm, *Neuronal production, migration, and differentiation in a vocal control nucleus of the adult female canary brain.* Proc Natl Acad Sci U S A, 1983. **80**(8): p. 2390-4.
65. Paton, J.A. and F.N. Nottebohm, *Neurons generated in the adult brain are recruited into functional circuits.* Science, 1984. **225**(4666): p. 1046-8.
66. Bayer, S.A., J.W. Yackel, and P.S. Puri, *Neurons in the rat dentate gyrus granular layer substantially increase during juvenile and adult life.* Science, 1982. **216**(4548): p. 890-2.
67. Boss, B.D., G.M. Peterson, and W.M. Cowan, *On the number of neurons in the dentate gyrus of the rat.* Brain Res, 1985. **338**(1): p. 144-50.
68. Das, G.D. and J. Altman, *Postnatal neurogenesis in the cerebellum of the cat and tritiated thymidine autoradiography.* Brain Res, 1971. **30**(2): p. 323-30.
69. Bayer, S.A., *3H-thymidine-radiographic studies of neurogenesis in the rat olfactory bulb.* Exp Brain Res, 1983. **50**(2-3): p. 329-40.

70. Kaplan, M.S. and J.W. Hinds, *Neurogenesis in the adult rat: electron microscopic analysis of light radioautographs.* Science, 1977. **197**(4308): p. 1092-4.
71. Temple, S., *Division and differentiation of isolated CNS blast cells in microculture.* Nature, 1989. **340**(6233): p. 471-3.
72. Reynolds, B.A. and S. Weiss, *Generation of neurons and astrocytes from isolated cells of the adult mammalian central nervous system.* Science, 1992. **255**(5052): p. 1707-10.
73. Lois, C. and A. Alvarez-Buylla, *Long-distance neuronal migration in the adult mammalian brain.* Science, 1994. **264**(5162): p. 1145-8.
74. Lois, C. and A. Alvarez-Buylla, *Proliferating subventricular zone cells in the adult mammalian forebrain can differentiate into neurons and glia.* Proc Natl Acad Sci U S A, 1993. **90**(5): p. 2074-7.
75. Eriksson, P.S., et al., *Neurogenesis in the adult human hippocampus.* Nat Med, 1998. **4**(11): p. 1313-7.
76. Ahlenius, H., et al., *Neural stem and progenitor cells retain their potential for proliferation and differentiation into functional neurons despite lower number in aged brain.* J Neurosci, 2009. **29**(14): p. 4408-19.
77. Piccin, D., A. Tufford, and C.M. Morshead, *Neural stem and progenitor cells in the aged subependyma are activated by the young niche.* Neurobiology of Aging, 2014. **35**(7): p. 1669-1679.
78. Schofield, R., *The relationship between the spleen colony-forming cell and the haemopoietic stem cell.* Blood Cells, 1978. **4**(1-2): p. 7-25.
79. Fujisaki, J., et al., *In vivo imaging of Treg cells providing immune privilege to the haematopoietic stem-cell niche.* Nature, 2011. **474**(7350): p. 216-219.
80. Winkler, I.G., et al., *Bone marrow macrophages maintain hematopoietic stem cell (HSC) niches and their depletion mobilizes HSCs.* Blood, 2010. **116**(23): p. 4815-4828.
81. Katayama, Y., et al., *Signals from the Sympathetic Nervous System Regulate Hematopoietic Stem Cell Egress from Bone Marrow.* Cell, 2006. **124**(2): p. 407-421.
82. Lo Celso, C., et al., *Live-animal tracking of individual haematopoietic stem/progenitor cells in their niche.* Nature, 2009. **457**(7225): p. 92-96.
83. Kiel, M.J., et al., *SLAM Family Receptors Distinguish Hematopoietic Stem and Progenitor Cells and Reveal Endothelial Niches for Stem Cells.* Cell, 2005. **121**(7): p. 1109-1121.
84. Kunisaki, Y., et al., *Arteriolar niches maintain haematopoietic stem cell quiescence.* Nature, 2013. **502**(7473): p. 637-643.
85. Olson, T.S., et al., *Megakaryocytes promote murine osteoblastic HSC niche expansion and stem cell engraftment after radioablative conditioning.* Blood, 2013. **121**(26): p. 5238-5249.
86. Holst, J., et al., *Substrate elasticity provides mechanical signals for the expansion of hemopoietic stem and progenitor cells.* Nat Biotech, 2010. **28**(10): p. 1123-1128.
87. Gilbert, P.M., et al., *Substrate Elasticity Regulates Skeletal Muscle Stem Cell Self-Renewal in Culture.* Science, 2010. **329**(5995): p. 1078-1081.
88. North, T.E., et al., *Hematopoietic Stem Cell Development Is Dependent on Blood Flow.* Cell, 2009. **137**(4): p. 736-748.
89. Shin, J.-W., et al., *Contractile Forces Sustain and Polarize Hematopoiesis from Stem and Progenitor Cells.* Cell Stem Cell, 2014. **14**(1): p. 81-93.
90. McBeath, R., et al., *Cell Shape, Cytoskeletal Tension, and RhoA Regulate Stem Cell Lineage Commitment.* Developmental Cell, 2004. **6**(4): p. 483-495.
91. Kilian, K.A., et al., *Geometric cues for directing the differentiation of mesenchymal stem cells.* Proceedings of the National Academy of Sciences, 2010. **107**(11): p. 4872-4877.
92. Lanotte, M., S. Schor, and T.M. Dexter, *Collagen gels as a matrix for haemopoiesis.* Journal of Cellular Physiology, 1981. **106**(2): p. 269-277.
93. Özbek, S., et al., *The Evolution of Extracellular Matrix.* Molecular Biology of the Cell, 2010. **21**(24): p. 4300-4305.

94. Watt, F.M. and W.T.S. Huck, *Role of the extracellular matrix in regulating stem cell fate.* Nat Rev Mol Cell Biol, 2013. **14**(8): p. 467-473.
95. Hynes, R.O., *The Extracellular Matrix: Not Just Pretty Fibrils.* Science, 2009. **326**(5957): p. 1216-1219.
96. Page-McCaw, A., A.J. Ewald, and Z. Werb, *Matrix metalloproteinases and the regulation of tissue remodelling.* Nat Rev Mol Cell Biol, 2007. **8**(3): p. 221-233.
97. Lu, P., V.M. Weaver, and Z. Werb, *The extracellular matrix: A dynamic niche in cancer progression.* The Journal of Cell Biology, 2012. **196**(4): p. 395-406.
98. Yurchenco, P.D., *Basement membranes: cell scaffoldings and signaling platforms.* Cold Spring Harb Perspect Biol, 2011. **3**(2).
99. Timpl, R. and J.C. Brown, *Supramolecular assembly of basement membranes.* Bioessays, 1996. **18**(2): p. 123-32.
100. Smyth, N., et al., *The targeted deletion of the LAMC1 gene.* Ann N Y Acad Sci, 1998. **857**: p. 283-6.
101. Li, S., et al., *Matrix assembly, regulation, and survival functions of laminin and its receptors in embryonic stem cell differentiation.* J Cell Biol, 2002. **157**(7): p. 1279-90.
102. Li, S., et al., *Laminin-sulfatide binding initiates basement membrane assembly and enables receptor signaling in Schwann cells and fibroblasts.* J Cell Biol, 2005. **169**(1): p. 179-89.
103. McKee, K.K., et al., *Role of laminin terminal globular domains in basement membrane assembly.* J Biol Chem, 2007. **282**(29): p. 21437-47.
104. McKee, K.K., S. Capizzi, and P.D. Yurchenco, *Scaffold-forming and Adhesive Contributions of Synthetic Laminin-binding Proteins to Basement Membrane Assembly.* J Biol Chem, 2009. **284**(13): p. 8984-94.
105. Colognato, H., D.A. Winkelmann, and P.D. Yurchenco, *Laminin Polymerization Induces a Receptor–Cytoskeleton Network.* The Journal of Cell Biology, 1999. **145**(3): p. 619-631.
106. Yurchenco, P.D., *Basement Membranes: Cell Scaffoldings and Signaling Platforms.* Cold Spring Harbor Perspectives in Biology, 2011. **3**(2).
107. Aumailley, M., et al., *A simplified laminin nomenclature.* Matrix Biol, 2005. **24**(5): p. 326-32.
108. Kanninen, L.K., et al., *Laminin-511 and laminin-521-based matrices for efficient hepatic specification of human pluripotent stem cells.* Biomaterials, 2016. **103**: p. 86-100.
109. Takayama, K., et al., *Laminin 411 and 511 promote the cholangiocyte differentiation of human induced pluripotent stem cells.* Biochem Biophys Res Commun, 2016. **474**(1): p. 91-6.
110. Flanagan, L.A., et al., *Regulation of human neural precursor cells by laminin and integrins.* J Neurosci Res, 2006. **83**(5): p. 845-56.
111. Roberts, R., et al., *Heparan sulphate bound growth factors: a mechanism for stromal cell mediated haemopoiesis.* Nature, 1988. **332**(6162): p. 376-8.
112. Gordon, M.Y., et al., *Compartmentalization of a haematopoietic growth factor (GM-CSF) by glycosaminoglycans in the bone marrow microenvironment.* Nature, 1987. **326**(6111): p. 403-405.
113. Uygun, B.E., et al., *Organ reengineering through development of a transplantable recellularized liver graft using decellularized liver matrix.* Nat Med, 2010. **16**(7): p. 814-820.
114. Ott, H.C., et al., *Perfusion-decellularized matrix: using nature's platform to engineer a bioartificial heart.* Nat Med, 2008. **14**(2): p. 213-221.
115. Higuchi, Y., et al., *Synthesized basement membranes direct the differentiation of mouse embryonic stem cells into pancreatic lineages.* Journal of Cell Science, 2010. **123**(16): p. 2733-2742.
116. Murphy, S.V. and A. Atala, *3D bioprinting of tissues and organs.* Nat Biotech, 2014. **32**(8): p. 773-785.
117. Gu, J., et al., *Laminin-10/11 and Fibronectin Differentially Prevent Apoptosis Induced by Serum Removal via Phosphatidylinositol 3-Kinase/Akt- and MEK1/ERK-dependent Pathways.* Journal of Biological Chemistry, 2002. **277**(22): p. 19922-19928.

118. Baeg, G.H., et al., *Heparan sulfate proteoglycans are critical for the organization of the extracellular distribution of Wingless.* Development, 2001. **128**(1): p. 87-94.
119. Moreno, M., et al., *Biglycan is a new extracellular component of the Chordin–BMP4 signaling pathway.* The EMBO Journal, 2005. **24**(7): p. 1397-1405.
120. Hynes, R.O., *Integrins: Bidirectional, Allosteric Signaling Machines.* Cell, 2002. **110**(6): p. 673-687.
121. Connelly, J.T., et al., *Actin and serum response factor transduce physical cues from the microenvironment to regulate epidermal stem cell fate decisions.* Nat Cell Biol, 2010. **12**(7): p. 711-718.
122. Stoykova, A., et al., *Pax6-dependent regulation of adhesive patterning, R-cadherin expression and boundary formation in developing forebrain.* Development, 1997. **124**(19): p. 3765-3777.
123. Yuasa, S., *Development of Astrocytes in the Mouse Hippocampus as Tracked by Tenascin-C Gene Expression.* Archives of Histology and Cytology, 2001. **64**(2): p. 149-158.
124. Garcion, E., et al., *Generation of an environmental niche for neural stem cell development by the extracellular matrix molecule tenascin C.* Development, 2004. **131**(14): p. 3423-3432.
125. Karus, M., et al., *The extracellular matrix molecule tenascin C modulates expression levels and territories of key patterning genes during spinal cord astrocyte specification.* Development, 2011. **138**(24): p. 5321-5331.
126. Kazanis, I., et al., *The Adult Mouse Subependymal Zone Regenerates Efficiently in the Absence of Tenascin-C.* The Journal of Neuroscience, 2007. **27**(51): p. 13991-13996.
127. Richards, L.J., T.J. Kilpatrick, and P.F. Bartlett, *De novo generation of neuronal cells from the adult mouse brain.* Proceedings of the National Academy of Sciences, 1992. **89**(18): p. 8591-8595.
128. Vescovi, A.L., et al., *bFGF regulates the proliferative fate of unipotent (neuronal) and bipotent (neuronal/astroglial) EGF-generated CNS progenitor cells.* Neuron, 1993. **11**(5): p. 951-66.
129. Palmer, T.D., J. Ray, and F.H. Gage, *FGF-2-responsive neuronal progenitors reside in proliferative and quiescent regions of the adult rodent brain.* Mol Cell Neurosci, 1995. **6**(5): p. 474-86.
130. Gritti, A., et al., *Multipotential stem cells from the adult mouse brain proliferate and self-renew in response to basic fibroblast growth factor.* The Journal of Neuroscience, 1996. **16**(3): p. 1091-1100.
131. Sirko, S., et al., *Chondroitin sulfates are required for fibroblast growth factor-2-dependent proliferation and maintenance in neural stem cells and for epidermal growth factor-dependent migration of their progeny.* Stem Cells, 2010. **28**(4): p. 775-87.
132. Sirko, S., et al., *Chondroitin sulfate glycosaminoglycans control proliferation, radial glia cell differentiation and neurogenesis in neural stem/progenitor cells.* Development, 2007. **134**(15): p. 2727-38.
133. Kerever, A., et al., *Perlecan is required for FGF-2 signaling in the neural stem cell niche.* Stem Cell Res, 2014. **12**(2): p. 492-505.
134. Endo, Y., H. Ishiwata-Endo, and K.M. Yamada, *Extracellular matrix protein anosmin promotes neural crest formation and regulates FGF, BMP, and WNT activities.* Dev Cell, 2012. **23**(2): p. 305-16.
135. Barresi, R. and K.P. Campbell, *Dystroglycan: from biosynthesis to pathogenesis of human disease.* Journal of Cell Science, 2006. **119**(2): p. 199-207.
136. Smalheiser, N.R. and N.B. Schwartz, *Cranin: a laminin-binding protein of cell membranes.* Proc Natl Acad Sci U S A, 1987. **84**(18): p. 6457-61.
137. Ibraghimov-Beskrovnaya, O., et al., *Primary structure of dystrophin-associated glycoproteins linking dystrophin to the extracellular matrix.* Nature, 1992. **355**(6362): p. 696-702.
138. Smalheiser, N.R. and E. Kim, *Purification of cranin, a laminin binding membrane protein. Identity with dystroglycan and reassessment of its carbohydrate moieties.* J Biol Chem, 1995. **270**(25): p. 15425-33.

139. Gee, S.H., et al., *Laminin-binding protein 120 from brain is closely related to the dystrophin-associated glycoprotein, dystroglycan, and binds with high affinity to the major heparin binding domain of laminin.* J Biol Chem, 1993. **268**(20): p. 14972-80.
140. Holt, K.H., et al., *Biosynthesis of dystroglycan: processing of a precursor propeptide.* FEBS Lett, 2000. **468**(1): p. 79-83.
141. Ervasti, J.M. and K.P. Campbell, *A role for the dystrophin-glycoprotein complex as a transmembrane linker between laminin and actin.* J Cell Biol, 1993. **122**(4): p. 809-23.
142. Ervasti, J. and K. Campbell, *A role for the dystrophin-glycoprotein complex as a transmembrane linker between laminin and actin.* The Journal of Cell Biology, 1993. **122**(4): p. 809-823.
143. Ervasti, J.M., A.L. Burwell, and A.L. Geissler, *Tissue-specific heterogeneity in alpha-dystroglycan sialoglycosylation. Skeletal muscle alpha-dystroglycan is a latent receptor for Vicia villosa agglutinin b4 masked by sialic acid modification.* J Biol Chem, 1997. **272**(35): p. 22315-21.
144. Oak, S.A., Y.W. Zhou, and H.W. Jarrett, *Skeletal muscle signaling pathway through the dystrophin glycoprotein complex and Rac1.* J Biol Chem, 2003. **278**(41): p. 39287-95.
145. McDearmon, E.L., A.C. Combs, and J.M. Ervasti, *Differential Vicia villosa agglutinin reactivity identifies three distinct dystroglycan complexes in skeletal muscle.* J Biol Chem, 2001. **276**(37): p. 35078-86.
146. Satz, J.S., et al., *Distinct functions of glial and neuronal dystroglycan in the developing and adult mouse brain.* J Neurosci, 2010. **30**(43): p. 14560-72.
147. Ervasti, J.M. and K.P. Campbell, *Membrane organization of the dystrophin-glycoprotein complex.* Cell, 1991. **66**(6): p. 1121-31.
148. Briggs, D.C., et al., *Structural basis of laminin binding to the LARGE glycans on dystroglycan.* Nat Chem Biol, 2016. **12**(10): p. 810-4.
149. Inamori, K.I., et al., *LARGE2-dependent glycosylation confers laminin-binding ability on proteoglycans.* Glycobiology, 2016. **26**(12): p. 1284-1296.
150. Kuwabara, N., et al., *Carbohydrate-binding domain of the POMGnT1 stem region modulates O-mannosylation sites of alpha-dystroglycan.* Proc Natl Acad Sci U S A, 2016. **113**(33): p. 9280-5.
151. Gerin, I., et al., *ISPD produces CDP-ribitol used by FKTN and FKRP to transfer ribitol phosphate onto alpha-dystroglycan.* Nat Commun, 2016. **7**: p. 11534.
152. Praissman, J.L., et al., *The functional O-mannose glycan on alpha-dystroglycan contains a phospho-ribitol primed for matriglycan addition.* Elife, 2016. **5**.
153. Chen, Y.J., et al., *Direct interaction of beta-dystroglycan with F-actin.* Biochem J, 2003. **375**(Pt 2): p. 329-37.
154. Moore, C.J. and S.J. Winder, *Dystroglycan versatility in cell adhesion: a tale of multiple motifs.* Cell Commun Signal, 2010. **8**: p. 3.
155. Lai, Y., et al., *Dystrophins carrying spectrin-like repeats 16 and 17 anchor nNOS to the sarcolemma and enhance exercise performance in a mouse model of muscular dystrophy.* J Clin Invest, 2009. **119**(3): p. 624-35.
156. Xiong, Y., Y. Zhou, and H.W. Jarrett, *Dystrophin glycoprotein complex-associated Gβγ subunits activate phosphatidylinositol-3-kinase/Akt signaling in skeletal muscle in a laminin-dependent manner.* Journal of Cellular Physiology, 2009. **219**(2): p. 402-414.
157. Zhou, Y.W., et al., *Laminin-α₁ globular domains 3 and 4 induce heterotrimeric G protein binding to α-syntrophin's PDZ domain and alter intracellular Ca²⁺ in muscle.* American Journal of Physiology - Cell Physiology, 2005. **288**(2): p. C377-C388.
158. Gould, C.M., et al., *ELM: the status of the 2010 eukaryotic linear motif resource.* Nucleic acids research, 2009: p. gkp1016.
159. Spence, H.J., et al., *Dystroglycan, a scaffold for the ERK-MAP kinase cascade.* EMBO Rep, 2004. **5**(5): p. 484-9.
160. Russo, K., et al., *Characterization of the β-Dystroglycan–Growth Factor Receptor 2 (Grb2) Interaction.* Biochemical and Biophysical Research Communications, 2000. **274**(1): p. 93-98.

161. Sotgia, F., et al., *Caveolin-3 Directly Interacts with the C-terminal Tail of β-Dystroglycan: IDENTIFICATION OF A CENTRAL WW-LIKE DOMAIN WITHIN CAVEOLIN FAMILY MEMBERS.* Journal of Biological Chemistry, 2000. **275**(48): p. 38048-38058.
162. Zhan, Y., et al., *Evidence that dystroglycan is associated with dynamin and regulates endocytosis.* J Biol Chem, 2005. **280**(18): p. 18015-24.
163. Langenbach, K.J. and T.A. Rando, *Inhibition of dystroglycan binding to laminin disrupts the PI3K/AKT pathway and survival signaling in muscle cells.* Muscle Nerve, 2002. **26**(5): p. 644-53.
164. Lara-Chacon, B., et al., *Characterization of an Importin alpha/beta-recognized nuclear localization signal in beta-dystroglycan.* J Cell Biochem, 2010. **110**(3): p. 706-17.
165. Martinez-Vieyra, I.A., et al., *A role for beta-dystroglycan in the organization and structure of the nucleus in myoblasts.* Biochim Biophys Acta, 2013. **1833**(3): p. 698-711.
166. Mathew, G., et al., *Nuclear targeting of dystroglycan promotes the expression of androgen regulated transcription factors in prostate cancer.* Sci Rep, 2013. **3**: p. 2792.
167. Henry, M.D. and K.P. Campbell, *A role for dystroglycan in basement membrane assembly.* Cell, 1998. **95**(6): p. 859-70.
168. Henry, M.D., et al., *Distinct roles for dystroglycan, beta1 integrin and perlecan in cell surface laminin organization.* J Cell Sci, 2001. **114**(Pt 6): p. 1137-44.
169. Cohen, M.W., et al., *Laminin-induced clustering of dystroglycan on embryonic muscle cells: comparison with agrin-induced clustering.* J Cell Biol, 1997. **136**(5): p. 1047-58.
170. Tsiper, M.V. and P.D. Yurchenco, *Laminin assembles into separate basement membrane and fibrillar matrices in Schwann cells.* J Cell Sci, 2002. **115**(Pt 5): p. 1005-15.
171. Campanelli, J.T., et al., *A role for dystrophin-associated glycoproteins and utrophin in agrin-induced AChR clustering.* Cell, 1994. **77**(5): p. 663-74.
172. Noell, S., et al., *Evidence for a role of dystroglycan regulating the membrane architecture of astroglial endfeet.* Eur J Neurosci, 2011. **33**(12): p. 2179-86.
173. Williamson, R.A., et al., *Dystroglycan is essential for early embryonic development: disruption of Reichert's membrane in Dag1-null mice.* Hum Mol Genet, 1997. **6**(6): p. 831-41.
174. Barresi, R. and K.P. Campbell, *Dystroglycan: from biosynthesis to pathogenesis of human disease.* J Cell Sci, 2006. **119**(Pt 2): p. 199-207.
175. Bindu, P.S., et al., *Pattern recognition on brain magnetic resonance imaging in alpha dystroglycanopathies.* Neurol India, 2010. **58**(3): p. 460-5.
176. Waite, A., S.C. Brown, and D.J. Blake, *The dystrophin-glycoprotein complex in brain development and disease.* Trends Neurosci, 2012. **35**(8): p. 487-96.
177. de Bernabe, D.B., et al., *Loss of alpha-dystroglycan laminin binding in epithelium-derived cancers is caused by silencing of LARGE.* J Biol Chem, 2009. **284**(17): p. 11279-84.
178. Calogero, A., et al., *Altered expression of alpha-dystroglycan subunit in human gliomas.* Cancer Biol Ther, 2006. **5**(4): p. 441-8.
179. Mitchell, A., et al., *Dystroglycan function is a novel determinant of tumor growth and behavior in prostate cancer.* Prostate, 2013. **73**(4): p. 398-408.
180. Bao, X., et al., *Tumor suppressor function of laminin-binding alpha-dystroglycan requires a distinct beta3-N-acetylglucosaminyltransferase.* Proc Natl Acad Sci U S A, 2009. **106**(29): p. 12109-14.
181. Hockfield, S. and R.D. McKay, *Identification of major cell classes in the developing mammalian nervous system.* J Neurosci, 1985. **5**(12): p. 3310-28.
182. Feng, L., M.E. Hatten, and N. Heintz, *Brain lipid-binding protein (BLBP): a novel signaling system in the developing mammalian CNS.* Neuron, 1994. **12**(4): p. 895-908.
183. Shibata, T., et al., *Glutamate transporter GLAST is expressed in the radial glia-astrocyte lineage of developing mouse spinal cord.* J Neurosci, 1997. **17**(23): p. 9212-9.
184. Pixley, S.K. and J. de Vellis, *Transition between immature radial glia and mature astrocytes studied with a monoclonal antibody to vimentin.* Brain Res, 1984. **317**(2): p. 201-9.

185. Malatesta, P., E. Hartfuss, and M. Gotz, *Isolation of radial glial cells by fluorescent-activated cell sorting reveals a neuronal lineage.* Development, 2000. **127**(24): p. 5253-63.
186. Hartfuss, E., et al., *Characterization of CNS precursor subtypes and radial glia.* Dev Biol, 2001. **229**(1): p. 15-30.
187. Noctor, S.C., et al., *Neurons derived from radial glial cells establish radial units in neocortex.* Nature, 2001. **409**(6821): p. 714-20.
188. Moore, S.A., et al., *Deletion of brain dystroglycan recapitulates aspects of congenital muscular dystrophy.* Nature, 2002. **418**(6896): p. 422-5.
189. Ohtsuka-Tsurumi, E., et al., *Co-localization of fukutin and alpha-dystroglycan in the mouse central nervous system.* Brain Res Dev Brain Res, 2004. **152**(2): p. 121-7.
190. Lathia, J.D., et al., *Patterns of laminins and integrins in the embryonic ventricular zone of the CNS.* J Comp Neurol, 2007. **505**(6): p. 630-43.
191. Pawlisz, A.S. and Y. Feng, *Three-dimensional regulation of radial glial functions by Lis1-Nde1 and dystrophin glycoprotein complexes.* PLoS Biol, 2011. **9**(10): p. e1001172.
192. Myshrall, T.D., et al., *Dystroglycan on radial glia end feet is required for pial basement membrane integrity and columnar organization of the developing cerebral cortex.* J Neuropathol Exp Neurol, 2012. **71**(12): p. 1047-63.
193. Zaccaria, M.L., et al., *Dystroglycan distribution in adult mouse brain: a light and electron microscopy study.* Neuroscience, 2001. **104**(2): p. 311-24.
194. Hawkins, B.T., et al., *Disruption of dystroglycan-laminin interactions modulates water uptake by astrocytes.* Brain Res, 2013. **1503**: p. 89-96.
195. Menezes, M.J., et al., *The extracellular matrix protein laminin alpha2 regulates the maturation and function of the blood-brain barrier.* J Neurosci, 2014. **34**(46): p. 15260-80.
196. Schmechel, D.E. and P. Rakic, *A golgi study of radial glial cells in developing monkey telencephalon: Morphogenesis and transformation into astrocytes.* Anatomy and Embryology, 1979. **156**(2): p. 115-152.
197. Voigt, T., *Development of glial cells in the cerebral wall of ferrets: Direct tracing of their transformation from radial glia into astrocytes.* The Journal of Comparative Neurology, 1989. **289**(1): p. 74-88.
198. Doetsch, F., J.M. García-Verdugo, and A. Alvarez-Buylla, *Cellular composition and three-dimensional organization of the subventricular germinal zone in the adult mammalian brain.* Journal of Neuroscience, 1997. **17**(13): p. 5046-5061.
199. Doetsch, F., et al., *Subventricular Zone Astrocytes Are Neural Stem Cells in the Adult Mammalian Brain.* Cell, 1999. **97**(6): p. 703-716.
200. Liu, X., et al., *GFAP-expressing cells in the postnatal subventricular zone display a unique glial phenotype intermediate between radial glia and astrocytes.* Glia, 2006. **54**(5): p. 394-410.
201. Bonfanti, L. and P. Peretto, *Adult neurogenesis in mammals – a theme with many variations.* European Journal of Neuroscience, 2011. **34**(6): p. 930-950.
202. Kriegstein, A. and A. Alvarez-Buylla, *The glial nature of embryonic and adult neural stem cells.* Annu Rev Neurosci, 2009. **32**: p. 149-84.
203. Tavazoie, M., et al., *A specialized vascular niche for adult neural stem cells.* Cell Stem Cell, 2008. **3**(3): p. 279-88.
204. Shen, Q., et al., *Adult SVZ stem cells lie in a vascular niche: a quantitative analysis of niche cell-cell interactions.* Cell Stem Cell, 2008. **3**(3): p. 289-300.
205. Mirzadeh, Z., et al., *Neural Stem Cells Confer Unique Pinwheel Architecture to the Ventricular Surface in Neurogenic Regions of the Adult Brain.* Cell Stem Cell, 2008. **3**(3): p. 265-278.
206. Lacar, B., et al., *Gap junction-mediated calcium waves define communication networks among murine postnatal neural progenitor cells.* European Journal of Neuroscience, 2011. **34**(12): p. 1895-1905.
207. Spassky, N., et al., *Adult ependymal cells are postmitotic and are derived from radial glial cells during embryogenesis.* J Neurosci, 2005. **25**(1): p. 10-8.

208. Rakic, P. and R.L. Sidman, *Subcommissural organ and adjacent ependyma: autoradiographic study of their origin in the mouse brain.* Am J Anat, 1968. **122**(2): p. 317-35.
209. Brightman, M.W. and T.S. Reese, *Junctions between intimately apposed cell membranes in the vertebrate brain.* J Cell Biol, 1969. **40**(3): p. 648-77.
210. Danilov, A.I., et al., *Ultrastructural and antigenic properties of neural stem cells and their progeny in adult rat subventricular zone.* Glia, 2009. **57**(2): p. 136-52.
211. Del Bigio, M.R., *Ependymal cells: biology and pathology.* Acta Neuropathol, 2010. **119**(1): p. 55-73.
212. Mirzadeh, Z., et al., *Cilia Organize Ependymal Planar Polarity.* The Journal of Neuroscience, 2010. **30**(7): p. 2600-2610.
213. Guirao, B., et al., *Coupling between hydrodynamic forces and planar cell polarity orients mammalian motile cilia.* Nature Cell Biology, 2010. **12**(4): p. 341-350.
214. Boutin, C., et al., *A dual role for planar cell polarity genes in ciliated cells.* Proceedings of the National Academy of Sciences, 2014. **111**(30): p. E3129-E3138.
215. Ohata, S., et al., *Loss of Dishevelleds Disrupts Planar Polarity in Ependymal Motile Cilia and Results in Hydrocephalus.* Neuron, 2014. **83**(3): p. 558-571.
216. Herranz-Pérez, V., et al., *Mechanosensory Genes Pkd1 and Pkd2 Contribute to the Planar Polarization of Brain Ventricular Epithelium.* The Journal of Neuroscience, 2015. **35**(31): p. 11153-11168.
217. Sawamoto, K., et al., *New neurons follow the flow of cerebrospinal fluid in the adult brain.* Science, 2006. **311**(5761): p. 629-32.
218. Kessaris, N., et al., *Competing waves of oligodendrocytes in the forebrain and postnatal elimination of an embryonic lineage.* Nat Neurosci, 2006. **9**(2): p. 173-9.
219. Sakamoto, M., et al., *Continuous Postnatal Neurogenesis Contributes to Formation of the Olfactory Bulb Neural Circuits and Flexible Olfactory Associative Learning.* The Journal of Neuroscience, 2014. **34**(17): p. 5788-5799.
220. Luskin, M.B., *Restricted proliferation and migration of postnatally generated neurons derived from the forebrain subventricular zone.* Neuron, 1993. **11**(1): p. 173-189.
221. Mirzadeh, Z., et al., *Neural stem cells confer unique pinwheel architecture to the ventricular surface in neurogenic regions of the adult brain.* Cell Stem Cell, 2008. **3**(3): p. 265-78.
222. Kokovay, E., et al., *Adult SVZ lineage cells home to and leave the vascular niche via differential responses to SDF1/CXCR4 signaling.* Cell Stem Cell, 2010. **7**(2): p. 163-73.
223. Kazanis, I., et al., *Quiescence and activation of stem and precursor cell populations in the subependymal zone of the mammalian brain are associated with distinct cellular and extracellular matrix signals.* J Neurosci, 2010. **30**(29): p. 9771-81.
224. Rosa, A.I., et al., *Heterocellular Contacts with Mouse Brain Endothelial Cells Via Laminin and alpha6beta1 Integrin Sustain Subventricular Zone (SVZ) Stem/Progenitor Cells Properties.* Front Cell Neurosci, 2016. **10**: p. 284.
225. Mercier, F., J.T. Kitasako, and G.I. Hatton, *Anatomy of the brain neurogenic zones revisited: fractones and the fibroblast/macrophage network.* J Comp Neurol, 2002. **451**(2): p. 170-88.
226. Kerever, A., et al., *Novel extracellular matrix structures in the neural stem cell niche capture the neurogenic factor fibroblast growth factor 2 from the extracellular milieu.* Stem Cells, 2007. **25**(9): p. 2146-57.
227. Douet, V., et al., *Fractone-heparan sulphates mediate FGF-2 stimulation of cell proliferation in the adult subventricular zone.* Cell Prolif, 2013. **46**(2): p. 137-45.
228. Douet, V., E. Arikawa-Hirasawa, and F. Mercier, *Fractone-heparan sulfates mediate BMP-7 inhibition of cell proliferation in the adult subventricular zone.* Neurosci Lett, 2012. **528**(2): p. 120-5.
229. Mercier, F. and V. Douet, *Bone morphogenetic protein-4 inhibits adult neurogenesis and is regulated by fractone-associated heparan sulfates in the subventricular zone.* J Chem Neuroanat, 2014. **57-58**: p. 54-61.

230. Lim, D.A., et al., *Noggin antagonizes BMP signaling to create a niche for adult neurogenesis.* Neuron, 2000. **28**(3): p. 713-26.
231. Colak, D., et al., *Adult neurogenesis requires Smad4-mediated bone morphogenic protein signaling in stem cells.* J Neurosci, 2008. **28**(2): p. 434-46.
232. Peretto, P., et al., *Expression of the secreted factors noggin and bone morphogenetic proteins in the subependymal layer and olfactory bulb of the adult mouse brain.* Neuroscience, 2004. **128**(4): p. 685-96.
233. Kerever, A., et al., *Fractone aging in the subventricular zone of the lateral ventricle.* Journal of Chemical Neuroanatomy, 2015. **66–67**: p. 52-60.
234. Enwere, E., et al., *Aging Results in Reduced Epidermal Growth Factor Receptor Signaling, Diminished Olfactory Neurogenesis, and Deficits in Fine Olfactory Discrimination.* The Journal of Neuroscience, 2004. **24**(38): p. 8354-8365.
235. Maslov, A.Y., et al., *Neural Stem Cell Detection, Characterization, and Age-Related Changes in the Subventricular Zone of Mice.* The Journal of Neuroscience, 2004. **24**(7): p. 1726-1733.
236. Tropepe, V., et al., *Transforming Growth Factor-α Null and Senescent Mice Show Decreased Neural Progenitor Cell Proliferation in the Forebrain Subependyma.* The Journal of Neuroscience, 1997. **17**(20): p. 7850-7859.
237. Pearson, B.L., et al., *Heparan sulfate deficiency in autistic postmortem brain tissue from the subventricular zone of the lateral ventricles.* Behav Brain Res, 2013. **243**: p. 138-45.
238. Meyza, K.Z., et al., *Fractone-associated N-sulfated heparan sulfate shows reduced quantity in BTBR T+tf/J mice: a strong model of autism.* Behav Brain Res, 2012. **228**(2): p. 247-53.
239. Mercier, F., Y.C. Kwon, and V. Douet, *Hippocampus/amygdala alterations, loss of heparan sulfates, fractones and ventricle wall reduction in adult BTBR T+ tf/J mice, animal model for autism.* Neuroscience Letters, 2012. **506**(2): p. 208-213.
240. Campos-Ordonez, T., et al., *Long-term hydrocephalus alters the cytoarchitecture of the adult subventricular zone.* Exp Neurol, 2014. **261**: p. 236-44.
241. Hallmann, R., et al., *Expression and Function of Laminins in the Embryonic and Mature Vasculature.* Physiological Reviews, 2005. **85**(3): p. 979-1000.
242. Hongisto, H., et al., *Laminin-511 expression is associated with the functionality of feeder cells in human embryonic stem cell culture.* Stem Cell Res, 2012. **8**(1): p. 97-108.
243. Nakagawa, M., et al., *A novel efficient feeder-free culture system for the derivation of human induced pluripotent stem cells.* Sci Rep, 2014. **4**: p. 3594.
244. Chen, Z.L., J.A. Indyk, and S. Strickland, *The hippocampal laminin matrix is dynamic and critical for neuronal survival.* Mol Biol Cell, 2003. **14**(7): p. 2665-76.
245. Adams, J.C. and A. Brancaccio, *The evolution of the dystroglycan complex, a major mediator of muscle integrity.* Biol Open, 2015. **4**(9): p. 1163-79.
246. Leonoudakis, D., et al., *Endocytic trafficking of laminin is controlled by dystroglycan and is disrupted in cancers.* J Cell Sci, 2014. **127**(Pt 22): p. 4894-903.
247. Colognato, H., D.A. Winkelmann, and P.D. Yurchenco, *Laminin polymerization induces a receptor-cytoskeleton network.* J Cell Biol, 1999. **145**(3): p. 619-31.
248. Godfrey, C., et al., *Dystroglycanopathies: coming into focus.* Curr Opin Genet Dev, 2011. **21**(3): p. 278-85.
249. Montanaro, F., M. Lindenbaum, and S. Carbonetto, *alpha-Dystroglycan is a laminin receptor involved in extracellular matrix assembly on myotubes and muscle cell viability.* J Cell Biol, 1999. **145**(6): p. 1325-40.
250. Weir, M.L., et al., *Dystroglycan loss disrupts polarity and beta-casein induction in mammary epithelial cells by perturbing laminin anchoring.* J Cell Sci, 2006. **119**(Pt 19): p. 4047-58.
251. Satz, J.S., et al., *Visual impairment in the absence of dystroglycan.* J Neurosci, 2009. **29**(42): p. 13136-46.
252. Merkle, F.T., et al., *Radial glia give rise to adult neural stem cells in the subventricular zone.* Proc Natl Acad Sci U S A, 2004. **101**(50): p. 17528-32.

253. Delgehyr, N., et al., *Ependymal cell differentiation, from monociliated to multiciliated cells.* Methods Cell Biol, 2015. **127**: p. 19-35.
254. Hirota, Y., et al., *Planar polarity of multiciliated ependymal cells involves the anterior migration of basal bodies regulated by non-muscle myosin II.* Development, 2010. **137**(18): p. 3037-46.
255. Heins, N., et al., *Glial cells generate neurons: the role of the transcription factor Pax6.* Nat Neurosci, 2002. **5**(4): p. 308-15.
256. Jang, E.S. and J.E. Goldman, *Pax6 expression is sufficient to induce a neurogenic fate in glial progenitors of the neonatal subventricular zone.* PLoS One, 2011. **6**(6): p. e20894.
257. Cruz-Molina, S., et al., *PRC2 Facilitates the Regulatory Topology Required for Poised Enhancer Function during Pluripotent Stem Cell Differentiation.* Cell Stem Cell, 2017.
258. Rada-Iglesias, A., et al., *A unique chromatin signature uncovers early developmental enhancers in humans.* Nature, 2011. **470**(7333): p. 279-83.
259. Park, D.H., et al., *Activation of neuronal gene expression by the JMJD3 demethylase is required for postnatal and adult brain neurogenesis.* Cell Rep, 2014. **8**(5): p. 1290-9.
260. Kyrousi, C., et al., *Mcidas and GemC1 are key regulators for the generation of multiciliated ependymal cells in the adult neurogenic niche.* Development, 2015. **142**(21): p. 3661-74.
261. Brody, S.L., et al., *Ciliogenesis and left-right axis defects in forkhead factor HFH-4-null mice.* Am J Respir Cell Mol Biol, 2000. **23**(1): p. 45-51.
262. Jacquet, B.V., et al., *FoxJ1-dependent gene expression is required for differentiation of radial glia into ependymal cells and a subset of astrocytes in the postnatal brain.* Development, 2009. **136**(23): p. 4021-31.
263. Yu, X., et al., *Foxj1 transcription factors are master regulators of the motile ciliogenic program.* Nat Genet, 2008. **40**(12): p. 1445-53.
264. Stubbs, J.L., et al., *The forkhead protein Foxj1 specifies node-like cilia in Xenopus and zebrafish embryos.* Nat Genet, 2008. **40**(12): p. 1454-60.
265. Tan, F.E., et al., *Myb promotes centriole amplification and later steps of the multiciliogenesis program.* Development, 2013. **140**(20): p. 4277-86.
266. Ables, J.L., et al., *Not(ch) just development: Notch signalling in the adult brain.* Nat Rev Neurosci, 2011. **12**(5): p. 269-83.
267. Stubbs, J.L., et al., *Multicilin promotes centriole assembly and ciliogenesis during multiciliate cell differentiation.* Nat Cell Biol, 2012. **14**(2): p. 140-7.
268. Marcet, B., et al., *Control of vertebrate multiciliogenesis by miR-449 through direct repression of the Delta/Notch pathway.* Nat Cell Biol, 2011. **13**(6): p. 693-9.
269. Morimoto, M., et al., *Canonical Notch signaling in the developing lung is required for determination of arterial smooth muscle cells and selection of Clara versus ciliated cell fate.* J Cell Sci, 2010. **123**(Pt 2): p. 213-24.
270. Tsao, P.N., et al., *Notch signaling controls the balance of ciliated and secretory cell fates in developing airways.* Development, 2009. **136**(13): p. 2297-307.
271. Liu, Y., et al., *Notch signaling controls the differentiation of transporting epithelia and multiciliated cells in the zebrafish pronephros.* Development, 2007. **134**(6): p. 1111-22.
272. Deblandre, G.A., et al., *A two-step mechanism generates the spacing pattern of the ciliated cells in the skin of Xenopus embryos.* Development, 1999. **126**(21): p. 4715-28.
273. Iso, T., L. Kedes, and Y. Hamamori, *HES and HERP families: multiple effectors of the Notch signaling pathway.* J Cell Physiol, 2003. **194**(3): p. 237-55.
274. Hirano, K. and M. Namihira, *LSD1 Mediates Neuronal Differentiation of Human Fetal Neural Stem Cells by Controlling the Expression of a Novel Target Gene, HEYL.* Stem Cells, 2016. **34**(7): p. 1872-82.
275. Jalali, A., et al., *HeyL promotes neuronal differentiation of neural progenitor cells.* J Neurosci Res, 2011. **89**(3): p. 299-309.
276. Martini, S., et al., *A critical role for Sox9 in notch-induced astrogliogenesis and stem cell maintenance.* Stem Cells, 2013. **31**(4): p. 741-51.

277. Finzsch, M., et al., *Sox9 and Sox10 influence survival and migration of oligodendrocyte precursors in the spinal cord by regulating PDGF receptor alpha expression.* Development, 2008. **135**(4): p. 637-46.
278. Eyermann, C., K. Czaplinski, and H. Colognato, *Dystroglycan promotes filopodial formation and process branching in differentiating oligodendroglia*. J Neurochem, 2012. **120**(6): p. 928-47.
279. Galvin, J., C. Eyermann, and H. Colognato, *Dystroglycan modulates the ability of insulin-like growth factor-1 to promote oligodendrocyte differentiation.* J Neurosci Res, 2010. **88**(15): p. 3295-307.
280. Colognato, H., et al., *Identification of dystroglycan as a second laminin receptor in oligodendrocytes, with a role in myelination.* Development, 2007. **134**(9): p. 1723-36.
281. Kim, H., et al., *Notch-regulated oligodendrocyte specification from radial glia in the spinal cord of zebrafish embryos.* Dev Dyn, 2008. **237**(8): p. 2081-9.
282. Park, H.C. and B. Appel, *Delta-Notch signaling regulates oligodendrocyte specification.* Development, 2003. **130**(16): p. 3747-55.
283. Wang, S., et al., *Notch receptor activation inhibits oligodendrocyte differentiation.* Neuron, 1998. **21**(1): p. 63-75.
284. Nakatani, H., et al., *Ascl1/Mash1 promotes brain oligodendrogenesis during myelination and remyelination.* J Neurosci, 2013. **33**(23): p. 9752-68.
285. Leiton, C.V., et al., *Laminin promotes metalloproteinase-mediated dystroglycan processing to regulate oligodendrocyte progenitor cell proliferation.* J Neurochem, 2015. **135**(3): p. 522-38.
286. Colognato, H., et al., *CNS integrins switch growth factor signalling to promote target-dependent survival.* Nat Cell Biol, 2002. **4**(11): p. 833-41.
287. Jones, K.J., et al., *The expanding phenotype of laminin alpha2 chain (merosin) abnormalities: case series and review.* J Med Genet, 2001. **38**(10): p. 649-57.
288. Benninger, Y., et al., *Beta1-integrin signaling mediates premyelinating oligodendrocyte survival but is not required for CNS myelination and remyelination.* J Neurosci, 2006. **26**(29): p. 7665-73.
289. Lee, K.K., et al., *Dominant-negative beta1 integrin mice have region-specific myelin defects accompanied by alterations in MAPK activity.* Glia, 2006. **53**(8): p. 836-44.
290. McClenahan, F.K., et al., *Dystroglycan Suppresses Notch to Regulate Stem Cell Niche Structure and Function in the Developing Postnatal Subventricular Zone.* Dev Cell, 2016. **38**(5): p. 548-66.
291. Rebay, I., R.G. Fehon, and S. Artavanis-Tsakonas, *Specific truncations of Drosophila Notch define dominant activated and dominant negative forms of the receptor.* Cell, 1993. **74**(2): p. 319-29.
292. Ayalon, G., et al., *An Ankyrin-Based Mechanism for Functional Organization of Dystrophin and Dystroglycan.* Cell, 2008. **135**(7): p. 1189-1200.
293. Sotgia, F., et al., *Tyrosine Phosphorylation of β-Dystroglycan at Its WW Domain Binding Motif, PPxY, Recruits SH2 Domain Containing Proteins.* Biochemistry, 2001. **40**(48): p. 14585-14592.
294. Ilsley, J.L., M. Sudol, and S.J. Winder, *The WW domain: Linking cell signalling to the membrane cytoskeleton.* Cellular Signalling, 2002. **14**(3): p. 183-189.
295. James, M., et al., *Adhesion-dependent tyrosine phosphorylation of (beta)-dystroglycan regulates its interaction with utrophin.* J Cell Sci, 2000. **113 (Pt 10)**: p. 1717-26.
296. Ilsley, J.L., M. Sudol, and S.J. Winder, *The interaction of dystrophin with β-dystroglycan is regulated by tyrosine phosphorylation.* Cellular Signalling, 2001. **13**(9): p. 625-632.
297. Pirozzi, G., et al., *Identification of novel human WW domain-containing proteins by cloning of ligand targets.* J Biol Chem, 1997. **272**(23): p. 14611-6.
298. Wan, C., et al., *Panorama of ancient metazoan macromolecular complexes.* Nature, 2015. **525**(7569): p. 339-44.
299. Sotgia, F., et al., *Tyrosine phosphorylation of beta-dystroglycan at its WW domain binding motif, PPxY, recruits SH2 domain containing proteins.* Biochemistry, 2001. **40**(48): p. 14585-92.

300. Xing, J., et al., *Src regulates cell cycle protein expression and renal epithelial cell proliferation via PI3K/Akt signaling-dependent and -independent mechanisms.* Am J Physiol Renal Physiol, 2008. **295**(1): p. F145-52.
301. Chu, I., et al., *p27 phosphorylation by Src regulates inhibition of Cyclin E-Cdk2 and p27 proteolysis.* Cell, 2007. **128**(2): p. 281-294.
302. Uchida, T., et al., *Deletion of Cdkn1b ameliorates hyperglycemia by maintaining compensatory hyperinsulinemia in diabetic mice.* Nat Med, 2005. **11**(2): p. 175-182.
303. Jäkel, H., et al., *Regulation of p27Kip1 by mitogen-induced tyrosine phosphorylation.* Cell Cycle, 2012. **11**(10): p. 1910-1917.
304. Zhang, W., et al., *Posttranslational modifications of p27kip1 determine its binding specificity to different cyclins and cyclin-dependent kinases in vivo.* Blood, 2005. **105**(9): p. 3691-8.
305. Ciarallo, S., et al., *Altered p27Kip1 Phosphorylation, Localization, and Function in Human Epithelial Cells Resistant to Transforming Growth Factor β-Mediated G1 Arrest.* Molecular and Cellular Biology, 2002. **22**(9): p. 2993-3002.
306. Coulonval, K., et al., *The cyclin D3-CDK4-p27kip1 holoenzyme in thyroid epithelial cells: activation by TSH, inhibition by TGFbeta, and phosphorylations of its subunits demonstrated by two-dimensional gel electrophoresis.* Exp Cell Res, 2003. **291**(1): p. 135-49.
307. Tong, C.K., et al., *A Dorsal SHH-Dependent Domain in the V-SVZ Produces Large Numbers of Oligodendroglial Lineage Cells in the Postnatal Brain.* Stem Cell Reports, 2015. **5**(4): p. 461-70.
308. Samanta, J., et al., *Inhibition of Gli1 mobilizes endogenous neural stem cells for remyelination.* Nature, 2015. **526**(7573): p. 448-52.
309. Kong, J.H., et al., *Notch activity modulates the responsiveness of neural progenitors to sonic hedgehog signaling.* Dev Cell, 2015. **33**(4): p. 373-87.
310. Sirour, C., et al., *Dystroglycan is involved in skin morphogenesis downstream of the Notch signaling pathway.* Mol Biol Cell, 2011. **22**(16): p. 2957-69.
311. McClatchey, S.T., et al., *Boundary cells restrict dystroglycan trafficking to control basement membrane sliding during tissue remodeling.* Elife, 2016. **5**.
312. Marshall, C.B., et al., *p73 is Required for Multiciliogenesis and Regulates the Foxj1-Associated Gene Network.* Cell reports, 2016. **14**(10): p. 2289-2300.
313. Nemajerova, A., et al., *TAp73 is a central transcriptional regulator of airway multiciliogenesis.* Genes & Development, 2016. **30**(11): p. 1300-1312.
314. Wu, J., et al., *Two miRNA clusters, miR-34b/c and miR-449, are essential for normal brain development, motile ciliogenesis, and spermatogenesis.* Proceedings of the National Academy of Sciences of the United States of America, 2014. **111**(28): p. E2851-E2857.
315. Tham, D.K., B. Joshi, and H. Moukhles, *Aquaporin-4 Cell-Surface Expression and Turnover Are Regulated by Dystroglycan, Dynamin, and the Extracellular Matrix in Astrocytes.* PLoS One, 2016. **11**(10): p. e0165439.
316. Vieira, N.M., et al., *Jagged 1 Rescues the Duchenne Muscular Dystrophy Phenotype.* Cell, 2015. **163**(5): p. 1204-13.
317. Annese, T., et al., *Isolation and characterization of neural stem cells from dystrophic mdx mouse.* Exp Cell Res, 2016. **343**(2): p. 190-207.
318. Choksi, S.P., et al., *Switching on cilia: transcriptional networks regulating ciliogenesis.* Development, 2014. **141**(7): p. 1427-41.
319. Paez-Gonzalez, P., et al., *Ank3-dependent SVZ niche assembly is required for the continued production of new neurons.* Neuron, 2011. **71**(1): p. 61-75.
320. Grondona, J.M., et al., *Ependymal denudation, aqueductal obliteration and hydrocephalus after a single injection of neuraminidase into the lateral ventricle of adult rats.* J Neuropathol Exp Neurol, 1996. **55**(9): p. 999-1008.
321. Chaker, Z., P. Codega, and F. Doetsch, *A mosaic world: puzzles revealed by adult neural stem cell heterogeneity.* Wiley Interdiscip Rev Dev Biol, 2016. **5**(6): p. 640-658.

322. Kerever, A., et al., *Fractone aging in the subventricular zone of the lateral ventricle.* J Chem Neuroanat, 2015. **66-67**: p. 52-60.
323. Silva-Vargas, V., et al., *Age-Dependent Niche Signals from the Choroid Plexus Regulate Adult Neural Stem Cells.* Cell Stem Cell, 2016.
324. Lehtinen, M.K., et al., *The cerebrospinal fluid provides a proliferative niche for neural progenitor cells.* Neuron, 2011. **69**(5): p. 893-905.
325. Wright, K.M., et al., *Dystroglycan organizes axon guidance cue localization and axonal pathfinding.* Neuron, 2012. **76**(5): p. 931-44.
326. Tronche, F., et al., *Disruption of the glucocorticoid receptor gene in the nervous system results in reduced anxiety.* Nat Genet, 1999. **23**(1): p. 99-103.
327. Lappe-Siefke, C., et al., *Disruption of Cnp1 uncouples oligodendroglial functions in axonal support and myelination.* Nat Genet, 2003. **33**(3): p. 366-74.
328. Lagace, D.C., et al., *Dynamic contribution of nestin-expressing stem cells to adult neurogenesis.* J Neurosci, 2007. **27**(46): p. 12623-9.
329. Zhang, Y., et al., *A transgenic FOXJ1-Cre system for gene inactivation in ciliated epithelial cells.* Am J Respir Cell Mol Biol, 2007. **36**(5): p. 515-9.
330. Doetsch, F., et al., *Subventricular zone astrocytes are neural stem cells in the adult mammalian brain.* Cell, 1999. **97**(6): p. 703-16.
331. Paez-Gonzalez, P., et al., *Ank3-dependent SVZ niche assembly is required for the continued production of new neurons.* Neuron. **71**(1): p. 61-75.
332. McCarthy, K.D. and J. de Vellis, *Preparation of separate astroglial and oligodendroglial cell cultures from rat cerebral tissue.* J Cell Biol, 1980. **85**(3): p. 890-902.